UNIVERSITY OF BELGRADE

FACULTY OF TECHNOLOGY AND METALLURGY

DOCTORAL DISSERTATION

KATARINA S. BUKARA

CONTROLLED DRUG DELIVERY SYSTEMS BASED ON MESOPOROUS SILICA AND ERYTHROCYTE MEMBRANES

BELGRADE, 2017.

UNIVERZITET U BEOGRADU

TEHNOLOŠKO-METALURŠKI FAKULTET

DOKTORSKA DISERTACIJA

KATARINA S. BUKARA

SISTEMI SA KONTROLISANIM OTPUŠTANJEM LEKOVA ZASNOVANI NA MEZOPOROZNOJ SILICI I ERITROCITNIM MEMBRANAMA

BEOGRAD, 2017.

FACULTY OF TECHNOLOGY AND METALLURGY

UNIVERSITY OF BELGRADE

DEPARTMENT FOR CHEMICAL ENGINEERING

SUPERVISORS:

_____

Dr Branko Bugarski, full professor, University of Belgrade, Faculty of Technology and Metallurgy

_____

Dr Filip Kiekens, full professor, University of Antwerp, Faculty of Pharmaceutical, Biomedical and Veterinary sciences

THE COMMITTEE MEMBERS:

_____

Dr Vesna Ilić, scientific adviser, University of Belgrade, Institute for medical research

_____

Dr Verica Đorđević, senior research associate, University of Belgrade, Faculty of Technology and Metallurgy

_____

Dr Nenad Lazarević, research associate, University of Belgrade, Institute for physics

_____

Dr Zorica Knežević-Jugović, full professor, University of Belgrade, Faculty of Technology and Metallurgy

THE DATE OF THE DEFENCE:

ABSTRACT

The main aim of this study is the development of two controlled drug delivery systems based on ordered mesoporous silica and erythrocyte membranes (in further text - ghosts) for two widely used drugs: fenofibrate and sodium diclofenac.

In the first part of the study, *in vitro* and *in vivo* performance of ordered mesoporous silica (OMS) as a carrier for the poorly water soluble compound fenofibrate was evaluated. Fenofibrate was loaded into OMS via incipient wetness impregnation to obtain a 29% drug load and formulated into capsules. Two capsule dosage forms (containing 33.5 mg and 16.75 mg fenofibrate) were compared to the commercially available forms - Lipanthyl® (fenofibrate microcrystals) and Tricor® (fenofibrate nanocrystals). *In vitro* dissolution tests showed that the amount of fenofibrate released from Lipanthyl® and Tricor® was approximately 30%, whereas ca. 66 and 60% of the drug was released from OMS capsules containing 33.5 and 16.75 mg of fenofibrate, respectively. The *in vivo* study in dogs confirmed satisfying level of safety and tolerability of fenofibrate-OMS formulation (eq. 33.5 mg) with the potential to improve the absorption of fenofibrate. Though some variability in the data, this formulation was promising to be further investigated in a clinical trial setting. Subsequent clinical trial was conducted to assess the bioavailability-enhancing potential of ordered mesoporous silica in man. In this open-label, randomized, two-way cross-over study, 12 overnight fasted healthy volunteers received a single dose of fenofibrate formulated with ordered mesoporous silica or a marketed product based on micronized fenofibrate. Plasma concentrations of fenofibric acid, the pharmacologically active metabolite of fenofibrate, were monitored up to 96 hours post-dose. The rate (C_{max}/dose increased by 77%; t_{max} reduced by 0.75 h) and extent of absorption ($AUC_{0\text{-}24h}$/dose increased by 54%) of fenofibrate were significantly enhanced following administration of the ordered mesoporous silica based formulation.

In the second part of the study controlled drug delivery system based on erythrocyte ghosts for amphiphilic compound sodium diclofenac was developed considering the differences between erythrocytes derived from two readily available materials - porcine slaughterhouse and outdated transfusion human blood. Starting erythrocytes, empty erythrocyte ghosts and diclofenac loaded ghosts were compared in terms of the encapsulation efficiency, drug releasing profiles, size

distribution, surface charge, conductivity, surface roughness and morphology. The encapsulation of sodium diclofenac was performed by an osmosis based process - gradual hemolysis. During this process sodium diclofenac exerted mild and delayed antihemolytic effect and increased potassium efflux in porcine but not in outdated human erythrocytes. FTIR spectra revealed lack of any membrane lipid disorder and chemical reaction with sodium diclofenac in encapsulated ghosts. Localization in the suspension and spatial distribution (i. e. mapping) of residual hemoglobin in erythrocyte ghosts has been resolved by two photon excitation fluorescence microscopy. Outdated human erythrocyte ghosts with detected nanoscale damages and reduced ability to shrink had encapsulation efficiency of only 8%. On the other hand, porcine erythrocyte ghosts had encapsulation efficiency of 37% and relatively slow drug release rate. More preserved structure and functional properties of porcine erythrocytes related to their superior encapsulation and release performances, define them as more appropriate for the usage in sodium diclofenac encapsulation process.

Key words: Ordered mesoporous silica, fenofibrate, poor solubility, oral bioavailability, erythrocyte membranes; encapsulation; sodium diclofenac, gradual hypotonic hemolysis, controlled drug delivery.

Scientific filed: Technological engineering

Scientific discipline: Biochemical engineering and Biotechnology

UDC number:

IZVOD

Glavni cilj ovog rada je razvoj dva sistema sa kontrolisanim otpuštanjem lekova zasnovanih na uređenoj mezoporoznoj silici i eritrocitnim membranama (u daljem tekstu duhovima) za dva leka u širokoj upotrebi: fenofibrat i natrijum diklofenak.

U prvom delu ove studije ispitivane su *in vitro* i *in vivo* performase uređene mezoporozne silike kao nosača za slabo rastvorni lek fenofibrat. Mezoporozna silika je punjena fenofibratom metodom vlažne impregnacije incipijenta dok sadržaj leka ne dostigne 29%, a potom finalno formulisana kao kapusla. Dve vrste kapsula (koje sadrže 33.5 mg i 16.75 mg fenofibrata) poređene su sa komercijalno dostupnim oblicima - Lipantil® (fenofibrat mikrokristali) i Trikor® (fenofibrat nanokristali). *In vitro* testovi rastvorljivosti pokazali su da je količina fenofibrata oslobođenog iz Lipantila® i Trikora® aproksimativno iznosila 30% dok je oko 66 i 60% leka oslobođeno iz kapsula sa mezoporoznom silikom koje su sadržale 33.5 i 16.75 mg fenofibrata, respektivno. *In vivo* studija na psima potvrdila je zadovoljavajući nivo bezbednosti i tolerantnosti formulacija sa mezoporoznom silikom i fenofibratom (33.5 mg) kao i potencijal za poboljšanje apsorpcije fenofibrata. Uprkos variabilnosti dobijenih podataka, ova formulacija je bila obećavajuća za buduća klinička ispitivanja. Sledstvena klinička studija izvedena je sa ciljem da se proceni potencijal uređene mezoporozne silike da poboljša bioraspoloživost fenofibrata kod čoveka. U ovoj otvorenoj, randomizovanoj, dvostruko ukrštenoj studiji, 12 zdravih volontera je primilo pojedinačnu dozu fenofibrata formulisanog sa uređenom mezoporoznom silikom kao i komercijalni proizvod baziran na mikroniziranom fenofibratu. Plazma koncentracije fenofibrinske kiseline, farmakološki aktivnog metabolita fenofibrata bile su praćene 96 sati nakon uzete doze. Stepen (odnos C_{max}/doza bio je povećan 77%, a t_{max} redukovano za 0,75 h) i obim apsorpcije ($PIK_{0\text{-}24\,h}$ je bila uvećana za 54%) fenofibrata su bili značajno povećani nakon administracije formulacije zasnovane na uređenoj mezoporoznoj silici.

U drugom delu studije razvijen je sistem sa kontrolisanim otpuštanjem za amfifilni lek natrijum diklofenak uz razmatranje razlika između eritrocita izolovanih iz dva lako dostupna materijala – svinjske otpadne klanične i prestarele humane krvi. Polazni eritrociti, prazni eritrocitni duhovi kao i inkapsulirani duhovi bili su poređeni u smislu efikasnosti inkapsulacije, profila oslobađanja leka, raspodele veličine, površinskog naelektrisanja, provodljivosti, hrapavosti površine i morfologije.

Inkapsulacija natrijum diklofena izvedena je procesom zasnovanim na osmozi – gradualnom hemolizom. Tokom ovog procesa natrijum diklofenak ispoljio je blag i odložen antihemolitički efekat kao i povećan efluks kalijuma kod svinjskih ali ne i kod prestarelih humanih eritrocita. FTIR spektri su otkrili odsustvo narušavanja strukture membranskih lipida kao i hemijske reakcije između natrijum diklofena i inkapsuliranih duhova. Lokalizacija rezidualnog hemoglobina u suspenziji eritrocitinih duhova i njegova prostorna distribucija određeni su primenom dvofotonske fluorescentne mikroskopije. Prestareli humani eritrocitni duhovi sa detektovanim oštećenjma na površini i smanjenom sposobnošću da se skupljaju imali su efikasnost inkapsulacije od samo 8%. Sa druge strane, svinjski eritrocitni duhovi su imali efikasnost inkapsulacije od 37% i relativno nisku brzinu oslobađanja leka. Viši stepen očuvanosti strukture i funkcije svinjskih eritrocita posmatran kroz superiornije performanse inkapsulacije i oslobađanja leka, definiše ih kao pogodniji materijal za inkapsulaciju natrijum diklofena.

Ključne reči: uređena mezoporozna silika, fenofibrat, slaba ratvorljivost, oralna bioraspoloživost, eritrocitne membrane, inkapsulacija, gradualna hipotonična hemoliza, sistemi sa kontrolisanim otpuštanjem.

Naučna oblast: Tehnološko inženjerstvo

Uža naučna oblast: Biohemijsko inženjerstvo i Biotehnologija

UDK broj:

Table of Contents

INTRODUCTION

Solubility, the phenomenon of dissolution of solute in solvent in order to obtain homogenous system, is very important parameter to achieve required concentration of the drug in systemic circulation for expected pharmacological response (***Ketan et al., 2010***). Nowadays when more than 40% of new chemical entities developed in pharmaceutical industry are practically insoluble in water the problem of solubility represent a major challenge for formulation scientist (***Sharma et al., 2009***).

Other important issues encountered by pharmaceutical scientists during the drug development are adverse effects of drugs. It is well known that pharmaceutical agents are one of the most commonly identified causes of adverse events, resulting in significant patient morbidity, mortality and excess medical care costs (***Phillips et al., 2001***). One extensive study estimated that more than 2 million hospitalized patients have severe adverse drug reactions annually in the United States even in the case of correct prescription and administration (***Phillips et al., 2001***). Also, adverse effects are ranked between the fourth and the sixth leading cause of death in the United States in 1994 (***Phillips et al., 2001***).

Since poor water-solubility of the drugs as well as their frequent adverse effects represent main problems in their development, there is a necessity for the controlled drug delivery systems which will allow better control of the drug level in plasma, less dosing frequency, decrease in adverse effects, improved efficiency and constant release. Two widely used drugs - fenofibrate and diclofenac sodium which are due to their efficacy first choice medications for the indicated pathological states, were chosen as model compounds.

Fenofibrate is a highly lipophilic drug used to normalize the plasma titer of low-density lipoproteins and cholesterol in patients with hypercholesterolemia and hypertriglyceridemia (***Guay et al., 1993, Genest et al., 2000***). As a typical Biopharmaceutical Classification System (BCS) class 2 compound (log P = 5.24), it is virtually insoluble in water and physiological fluids (***Ming-Thau et al., 1994***). Its insufficient absorption from the aqueous environment of the gastrointestinal tract results in very low systemic exposure after oral administration (***Guay et al.,***

1993). Thus, oral bioavailability of fenofibrate may be improved by increasing its aqueous solubility (***Yousaf et al. 2015***). Even though over the past few years, several conventional formulation techniques, such as micro- and nanonization (***Hens et al., 2015***), formation of liposomes (***Chen et al., 2009***), various polymeric nanoparticulated systems (***Yousaf et al., 2015***) and lipid based formulations (***Fei et al., 2013***) have been employed to enhance the oral bioavailability of fenofibrate, the number of marketed applications of these technologies remains very limited.

Ordered mesoporous silica (OMS) is a promising strategy to increase the apparent aqueous solubility and dissolution rate of poorly water-soluble entities (***Xu et al., 2013***). Mellaerts et al. were the first to correlate the increased release rate of itraconazole from OMS with an increase in bioavailability and demonstrated a performance comparable to that of the marketed product sporanox (***Mellaerts et al., 2008***). OMS with a pore size ranging from 4 to 10 nm in diameter, large specific pore volume (ca. 1 cm3/g) and surface area (ca. 1000 m2/g) (***Vialpando et al., 2012***) provides high drug load and increase in dissolution rate of active pharmaceutical ingredients (API) to the highest possible level (***Van Speybroeck et al., 2009***). The principle of the dissolution improvement is based on the adsorption of an API onto the surface of the carrier material in a molecular manner (***Mellaerts et al., 2007***). Since the deposition of an API in the mesopores of the carrier is associated with the suppression of crystallization of the entrapped molecules, mesoporous silica materials are excellent stabilizers for amorphous APIs (***Van Speybroeck et al., 2009***). When exposed to water, the adsorbed drug molecules compete for the hydrophilic silica surface and are released from the pores. Consequently, in this "dissolved" state they become available for absorption in the gastrointestinal tract (***Kiekens et al., 2011***).

The ability of mesoporous silica to improve the dissolution profile of fenofibrate in biorelevant media has already been described in literature (***Dressman et al., 2015; Fei et al., 2013; Van Speybroeck., 2010***). However, in this study, for the first time, the biopharmaceutical performance of OMS based formulations was determined in dogs by comparing the oral bioavailability of fenofibrate loaded onto OMS material with two marketed formulations Lipanthyl® (microcrystals of fenofibrate) and Tricor® (nanocrystals of fenofibrate). The results indicate that OMS could be a potential carrier to achieve enhanced oral bioavailability for fenofibrate. Moreover, it provides valuable information about formulation selection to be used

for further *in vivo* testing, in humans. Subsequent clinical trial was set up to complement these promising findings with *in vivo* data in man. To the best of our knowledge, no prior papers have reported on the oral administration of ordered mesoporous silica based formulations in man.

Sodium diclofenac (SD) is a potent non-steroidal anti-inflammatory drug with analgesic and antipyretic effects. However, due to its physicochemical action on the gastric mucous (***Odsson et al., 1990***) and inflammatory action on the small bowel and the colon (***Carson et al., 1990; Witham, 1991***), it counts for a risk factor of relatively high incidence of gastrointestinal side effects. Because of the mentioned side effects and its short biological half-life (***Todd et al., 1988***), SD is an ideal candidate for prolonged release preparations with the aim to maintain therapeutic activity, reduce toxic effects and improve patient compliance (***Krajisnik et al., 2013***). Many chemically- synthetized or naturally occurring carrier materials such as phospholipid liposomes (***Lopes et al., 2004***), sodium alginate beads (***Kulkarni et al., 1999***), PLGA-based nanoparticles (***Cooper et al., 2014***), silica-chitosan composites (***Kozakevych et al., 2013***), solid lipid nanoparticles (***Liu et al., 2014***) have been employed to design micro- or nano- sized prolonged/controlled delivery systems for SD. However, in general, the surface chemistry of the mentioned carriers differs substantially from the chemistry of the cell membrane (***Mao et al., 2011***). Studies conducted on liposomes showed that SD due to its surface-active properties can incorporate into membranes affecting the lipidic organization and leading to solubilisation of the structure (***Lopes et al., 2004***). On the other hand, erythrocyte membrane, which is more complex than liposomal membrane and also interact with SD via class of lipids found in its outer moiety (***Suwalsky et al., 2009***), but without the disruption, might be a naturally occurring alternative offering potential advantage in comparison with the liposomes as drug carriers. However, to the best authors' knowledge, literature data regarding erythrocyte based delivery systems for SD is very scarce and there hasn’t been any attempt since Jain et al. (1994) developed magnetically responsive SD loaded erythrocytes (***Jain et al., 1994***).

The majority of research groups are dealing with active substances encapsulation in small amount of autologous erythrocytes intended for personal medicine. Having in mind the ultimate goal of universal erythrocyte membrane based SD carrier production, the use of non-infectious blood material generally treated as waste, such are slaughterhouse blood and outdate transfusion human blood represent beneficial approach in the development of an added-value product. This

approach is supported by the increasing number of emerging techniques for covering antigenic determinants (***Mansouri et al., 2011***), which could allow application of these materials as carriers and the fact that these materials are available in unlimited amounts. Thus, we have recently shown that osmosis based process - gradual hemolysis can be used for loading dexamethasone sodium phosphate on large scale into erythrocytes' ghosts derived from porcine and bovine slaughterhouse blood (***Kostic et al., 2014***).

In xenotransplantation research, a pig accounts for the favoured available source of organs and tissues (***Doucet et al., 2004***). Therefore, in this study we examined the gradual hypotonic hemolysis as an osmosis based SD encapsulation process in erythrocyte membranes derived from two inexpensive, available in sufficient amount materials - porcine slaughterhouse and outdated human blood. Obtained formulations with encapsulated SD were characterized in terms of encapsulation efficiency, drug release profile, morphology, size and surface properties.

THEORETICAL PART

1. Controlled drug delivery systems

1.1. The definition and history of the development of controlled drug delivery systems

According to the definition, controlled release system represents any drug delivery system that maintains adequate and desired release of drug over an extended period of time (***Kushal et al., 2013***). The main aim of an ideal drug delivery system is to provide proper amount of the drug at regular time interval and at right site of action to maintain required therapeutic range in the blood (***Kushal et al., 2013***). The goal in the development of the controlled release drug delivery system is to decrease the frequency of the dosing, reducing the dose and provide uniform drug delivery (***Kushal et al., 2013***). So, controlled release dosage form is a dosage form that releases one or more drugs continuously in predetermined pattern for a fixed period of time, either systemically or locally to specified target organ (***John, 2002; Brahmankar, 2009; Lee, 1987***). The benefits of the controlled release dosage forms include better control of plasma drug levels, less dosage frequency, less side effects, increased efficacy and constant delivery (***Kushal et al., 2013***).

Before 1950 all drugs were formulated as a pill or capsule that released the loaded drug immediately after the contact with water without any ability to control the drug release kinetics (***Yun et al., 2015***). The first sustained release formulation developed by Smith Klein Beecham named Spansule technology, that was able to control the drug release kinetics and achieve 12-h efficacy was introduced in 1952. (***Lee, 1987***).

The historical overview of controlled drug delivery systems is represented in Table 1. Most of the fundamental understanding of the drug releasing mechanism, especially oral and transdermal dosage forms, was obtained during the first generation (1G) of the development from 1950 to 1980 (***Yun et al., 2015***). During this period, four releasing mechanisms were revealed which accelerated the development of numerous oral and transdermal controlled release formulations (***Yun et al., 2015***). The most frequently used mechanisms were dissolution-controlled and diffusion-controlled systems. Osmosis-based formulations had short-term popularity, but a

number of products based on osmosis is much smaller than those with the other two (***Yun et al., 2015***). The ion-exchange mechanism has not been useful without combining with diffusion-controlled mechanism (***Yun et al., 2015***).

Different from 1G drug delivery formulations, the second generation (2G) technologies have been less successful, taking into account the number of clinical products produced (***Yun et al., 2015***). The drug delivery systems developed during the 2G period faced more difficult issues in comparison with the 1G technologies (***Yun et al., 2015***). The technologies developed during the 2 G period are presented in Table 1.

Table 1. Historical overview of drug delivery technology from 1950 to the present and the technology necessary for the future (***Yun et al., 2015***).

1950 1980 2010 2040

1st Generation	2nd Generation	3rd Generation
Basics of controlled release	Smart delivery systems	Modulated delivery systems
Oral delivery: -Once a day, twice a day	Zero order release -First order vs Zero order	Poorly soluble drug delivery -Non-toxic excipients
Transdermal delivery: -Once a day, once a week	Peptide and protein delivery: -Long-term depot using biodegradable polymers -Pulmonary delivery	Peptide and protein delivery: -Delivery for >6 months -Control of release kinetics -Non-invasive delivery
Drug release mechanisms: -Dissolution -Diffusion -Osmosis -Ion-exchange	Smart polymers and hydrogels: -Environment-sensitive -Self-regulated release (working only in vitro)	Smart polymers and hydrogels: -Signal specificity and sensitivity -Fast response kinetics (working in vivo)
	Nanoparticles: -Tumor-targeted delivery -Gene delivery	Targeted drug delivery -Non-toxic to non-target cells -Overcoming blood brain barrier
Successful control of physicochemical properties of delivery systems	Inability to overcome biological barriers	Need to overcome both physicochemical and biological barriers

Different oral controlled release formulations were developed in order to achieve zero-order release. However, the zero-order release achieved in various in vitro dissolution systems did not result in maintenance of the constant drug concentration in vivo, mainly due to variations in the

drug absorption properties along the gastrointestinal tract (***Yun et al., 2015***). The drug release from a formulation in vivo is not only dependent on the formulation properties, but also on the biological environment surrounding the formulation (***Yun et al., 2015***). This fact makes the prediction of the drug release kinetics in vivo and bioavailability, more complicated (***Yun et al., 2015***). In vivo-in vitro correlation (IVIVC) hasn't been found for most parenteral formulations of biotech drugs, making it difficult to predict the in vivo bioavailability from the in vitro release profiles, especially for long term depot formulations (***Cadot, 2009***). Additionally, there are not standard in vitro drug release tests methods that can reliably predict in vivo pharmacokinetic profiles (***Martinez et al., 2008***). Shortly, the difficulty faced by 2G drug delivery systems is mainly due to inability of the drug delivery systems to struggle with biological barriers (***Yun et al., 2015***). The 3G drug delivery technologies will have to be advanced much beyond 2G technologies to overcome both physicochemical and biological barriers (***Yun et al., 2015***). Some of the barriers to overcome for developing successful 3G drug delivery systems are listed in Table 2.

Table 2. Barriers to overcome by the 3G drug delivery systems

Delivery technology	Formulation barriers	Biological barriers
Poorly water soluble drug delivery	-New excipients for increasing drug solubility	-Non-toxic to the body -No drug precipitation in the blood -IVIVC -Long-term delivery up to year -Non-invasive delivery -Controlling biodistribution through altering vascular extravasation, renal clearance, metabolism, etc… -Navigating microenvironment of diseased tissues to reach target cells -Crossing endothelial barriers (e. g., blood-brain barrier) -Crossing mucosal barriers -Functional inside the body -Functional over the lifetime of drug delivery
Peptide/protein/nucleic acid delivery Targeted drug delivery using nanoparticles	-Control of drug release kinetics -Control of drug loading -Control of therapeutic period -Control of nanoparticle size, shape, surface chemistry, functionality and flexibility -Surface modification with ligands -Stimuli-sensitive delivery systems	
Self-regulated drug delivery	-Signal specificity and sensitivity -Fast responsive kinetics -Ability to stop drug release	

1.2. Delivery of poorly water-soluble drugs

Poor water-solubility of drugs represents one of the most important issues in drug development nowadays (***Yun et al., 2015***). The descriptive terms used in US Pharmacopeia and National Formulary to announce approximate drug solubilities in water are shown in the Table 3.

Table 3. Solubility definitions.

Descriptive terms	Parts of solvent required for one part of solute	Solubility range	
		mg/mL	%
Very soluble	Less than 1	>1000	>100
Freely soluble	From 1 to 10	100 - 1000	10 – 100
Soluble	From 10 to 30	33 – 100	3.3 – 10
Sparingly soluble	From 30 to 100	10 – 33	1 – 3.3
Slightly soluble	From 100 to 1000	1 – 10	0.1-1
Very slightly soluble	From 1000 to 10 000	0.1 – 1	0.01-0.1
Practically insoluble	10 000 and over	≤ 0.1	≤ 0.1

The term "poorly soluble" usually refers to the drugs that belong to "practically insoluble" group. Their aqueous solubility is 0.1 mg/mL or less. Many new drug candidates are poorly water soluble which disables them to be converted into clinically useful formulations (***Yun et al., 2015***). According to the analysis of 200 orally administered drug products, practically insoluble drugs represent almost 40% of the total drugs (***Takagi et al., 2006***). Delivering these drugs effectively through the GI tract for therapeutically effective bioavailability is still an important problem (***Yun et al., 2015***). The dissolution rate of practically insoluble drugs may be so slow that dissolution takes longer than the GI transit time resulting in very low bioavailability (***Horter et al., 2001***).

Technologies to dissolve poorly soluble drugs in water have been investigated for decades, and some of the approaches are shown in Table 4 (***Yun et al., 2015***). Poorly soluble drugs have inherently low water solubility, so appropriate excipients are added to increase the solubility. These usually include surfactants, polymer micells, hydrotropic agents, complexing agents (e. g., cyclodextrins and proteins), cosolvents, and lipid formulations (e. g., self-emulsifying systems) (***Pouton, 2006, Kawabata et al., 2011, Lu et al., 2013***). For weakly acidic or basic drugs, pH can

be controlled to increase the drug solubility (***Yun et al., 2015***). Alternatively, drug solubility and dissolution kinetics can be increased through the selection of appropriate polymorph, making solid dispersions (i. e. maintaining amorphous structure of the drug using polymers), reducing drug particle size and improving wetting with surfactants (***Yun et al., 2015***).

Table 4. Methods to improve drug dissolution.

Enhancing drug solubility	Enhancing dissolution kinetics
Using surfactant micelles	Selecting appropriate polymorph
Using polymer micelles	Making amorphous forms (solid dispersions)
Using hydrotropic agents	Reducing particle size (nanocrystals)
Using complexing agents	Adding surfactant for better wetting)
Using cosolvents	
Using self-emulsifying systems	
Controlling pH	

1.3. Fenofibrate

Fenofibrate (propan-2-yl 2-[4-(4-chlorobenzoyl)phenoxy]-2-methylpropanoate) (Figure 1) is a highly lipophilic drug used to normalize the plasma titer of low-density lipoproteins and cholesterol in patients with hypercholesterolemia and hypertriglyceridemia (***Guay, 1993; Genest et al., 2002***).

Chemically it belongs to synthetic phenoxy-isobutyric acid derivates ***(Source: PubChem: URL: https://pubchem.ncbi.nlm.nih.gov)***.

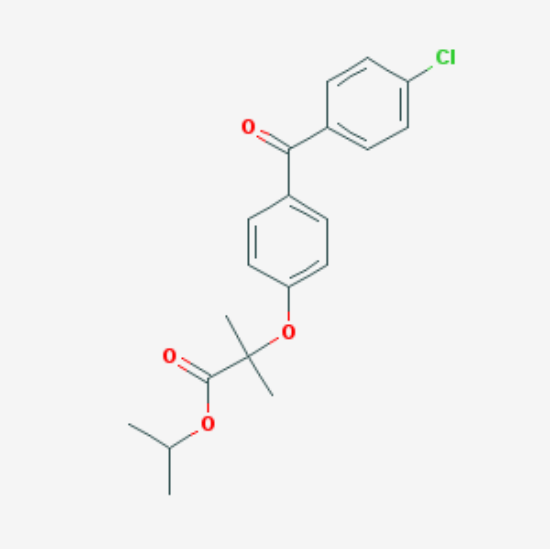

Figure 1. Chemical structure of fenofibrate (propan-2-yl 2-[4-(4-chlorobenzoyl)phenoxy]-2-methylpropanoate) (***Source: PubChem: URL: https://pubchem.ncbi.nlm.nih.gov***)

Mechanisms of action of fenofibrate include induction of lipoprotein lipolysis, induction of hepatic fatty acid uptake, reduction of hepatic triglyceride production, increased removal of LDL particles, reduction in neutral lipid (cholesteryl ester and triglyceride) exchange between LDL and HDL, increase in HDL production and stimulation of reverse cholesterol transport (***Staels et al., 1998***). Fenofibrate is indicated in primary hypertriglyceridemia, type III dysbetalipoproteinemia, primary hypercholesterolemia and non-insuline-dependent diabetes mellitus (***Staels***). As a typical Biopharmaceutical Classification System class 2 compound (log p ¼ 5.24), it is virtually insoluble in water and physiological fluids (***Ming-Thau et al., 1994***). Its insufficient absorption from the aqueous environment of the gastrointestinal tract results in very low systemic exposure after oral administration (***Guay, 1993***). Thus, oral bioavailability of fenofibrate may be improved by increasing its aqueous solubility (***Yousaf et al., 2015***). Although over the past few years, several conventional formulation techniques, such as micro- and nanonization (***Hens et al., 2015***) formation of liposomes (***Chen et al., 2009***) various polymeric nanoparticulated systems (***Yousaf et al., 2015***) and lipid-based formulations (***Fei et al., 2013***) have been employed to enhance the oral bioavailability of fenofibrate, the number of marketed applications of these technologies remains very limited.

1.4. Ordered mesoporous silica

Ordered mesoporous silica materials (Figure 2) with different arrangement of mesopores have been intensively examined for a broad spectrum of applications such as molecular separation, optics, drug delivery, catalysis and template nanotubes synthesis (***Corma, 1997; Scott et al., 2001; Vallet-Regi et al., 2007; Zheng et al., 2002; Taguchi et al., 2005***). During the last decade the focus of interest for ordered mesoporous silicates has been shifted to drug delivery systems for poorly soluble drugs (***Van Speybroeck et al., 2010***).

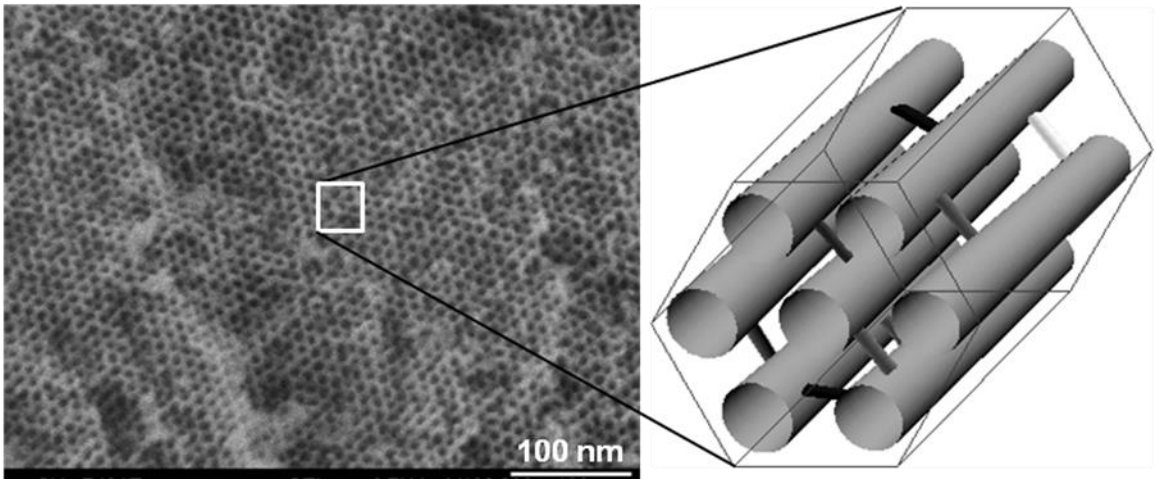

Figure 2. Ordered mesoporous silica (SBA-15 material). Left: High resolution FESEM image of the pore structure of SBA-15; Right: Representation of the pore arrangement (***Kleitz 2009***).

The synthesis of ordered mesoporous silicates is being performed in basic or acidic conditions via a sol-gel derived process where surfactants or polymers serve as a template for the polymerizing silica (***Kresge et al., 1992; Zhao***) (Figure 3). When the polymerization of the silica is complete, the template can be eliminated through either chemical or thermal treatment, which consequently induces porosity (***Van Speybroeck et al., 2010***). Owing to this template-assisted synthesis, the end product has very narrow pore size distribution (***Van Speybroeck et al., 2010***). Additionally, these materials have a very high specific surface area (up to 1500 m^2/g) and pore

volume (up to 1.5 cm^3/g). Through careful selection and optimization of the synthesis conditions, the pore diameter and particle morphology of silica material can be adjusted to the requirements of the user (***Grun et al., 1999; Zhao et al., 2000***).

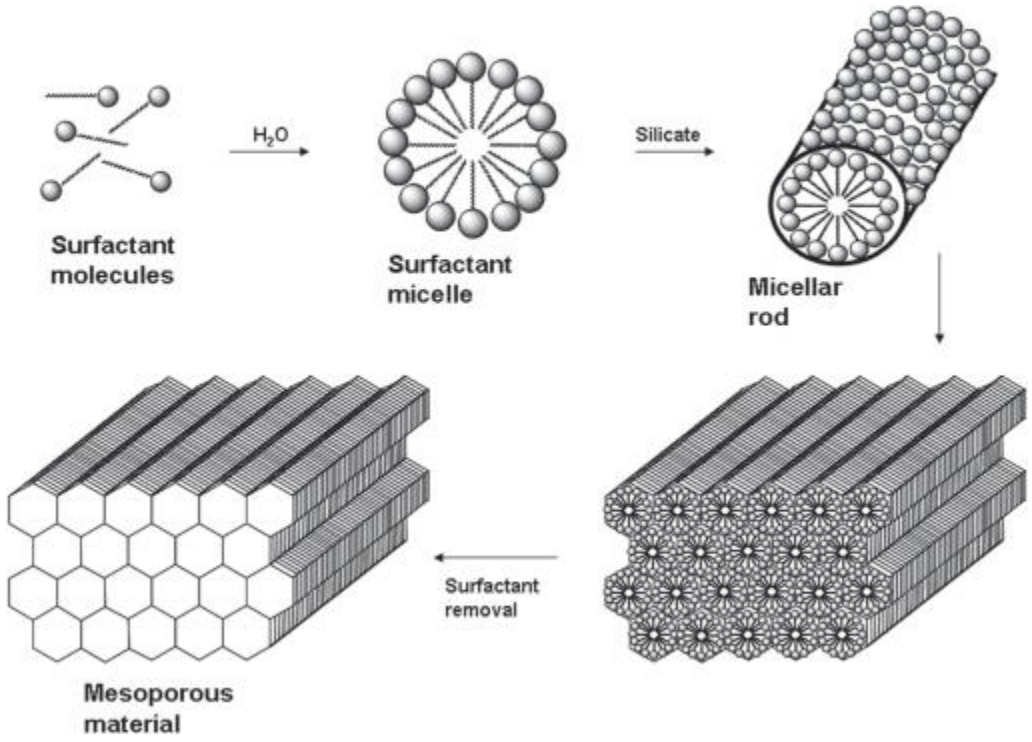

Figure 3. Schematic representation of liquid crystal mechanism used to describe the synthesis of silica-based ordered mesoporous materials (***Colilla et al., 2008***).

The pore size of mesoporous silica can be controlled by using swelling agents, surfactants with different chain length and hydrothermal restructuring (***Corma et al., 1997***). With respect to the three above mentioned synthetic strategies for pore tailoring, adding of swelling agents and changing the length of the surfactant micelle are the most widely used for the pore size control (***Xu et al., 2013***). Using these approaches, the pore diameters can be increased by 0-10 nm depending on the used procedures (***Xu et al., 2013***). On the other hand, the change in the pore diameter is only within 1 nm if hydrothermal restructuring has been applied (***Corma et al., 1997***). The most frequently used swelling agents include hydrophobic organic compounds such as trimethylbenzene and hexane (***Xu et al., 2013***). The mechanism of action for these molecules

is based on the penetration into the cores of the amphiphilic surfactant micelles to enlarge the size of template micelles (***Boissiere et al., 2003***). For instance, Kruk and Cao successfully synthesized highly ordered SBA-15 with adjustable pore diameters in the range from 9.4 to 18.2 nm with the usage of hexane (***Kruk et al., 2007***). Hydrophilic anions like organic amines or inorganic salts can also be considered as pore swelling agents (***Xu et al., 2013***). One of good examples is study performed by Sayari et al (1999) where amines were added as expanders in direct synthesis and post synthesis procedures to expand the pore size of MCM-41 materials (***Sayari et al., 1999***). The pore size adjustment in the range from 3.5 to 7.5 nm was achieved by adding appropriate amounts of N, N-dimethylhexadecylamine. Even though the easiest way to control the pore size is changing the length of the surfactant micelle, this strategy is not always feasible due to the limited availability of commercial surfactants (***Xu et al., 2013***).

Another important concern in the development of mesoporous silica materials for biomedical applications is controlling the particle morphology **(*Xu et al., 2013*)**. Studies have shown that inorganic or organic additives, hydrolysis and condensation of silicates, and the shapes of surfactant micelles are the main factors affecting the morphology of silica particles (***Du et al., 2009***). Varying of these parameters enables the synthesis of the mesoporous silica with the different morphologies such as fibers, spheres and rods (***Xu et al., 2013***). Study performed by Grun et al. (1999) investigated the effect of short chain alcohols like ethanol and isopropanol on the morphology of MCM-41 (***Grun et al., 1999***). Usage of short chain alcohol as a co-solvent gives a homogeneous system which leads to the formation of spherical MCM-41 particles. Subsequent studies (***Yu et al., 2004; Zhao et al., 2000***) explained the mechanism of morphology control. It was discovered that the morphology of SBA-15 was very dependent on surface curvature energy at the interface of inorganic silica and organic block copolymer species. The addition of polar co-solvent, co-surfactant and concentrated strong inorganic salts can lower the local curvature energy and ease the formation of highly curved particle morphologies for SBA-15 such as doughnut-, sphere-, gyroid-, and discoid-like particles (***Wan et al., 2007***).

The term mesoporous refers to the materials that have pores with a diameter in the mesopore size range from 2 to 50 nm (***Van Speybroeck et al., 2010***). The term ordered designates that these materials are characterized by long-range ordering, even though their pore walls consist of amorphous silica. Because of their unique features, ordered mesoporous silicates are very

efficient in the enhancement of drug dissolution (***Van Speybroeck et al., 2010***). Numerous studies have shown that drugs lose their crystallinity when they are deposited onto the surface of mesoporous silicate, which consequently improves their dissolution rate (***Charnay et al., 2004, Heikkila et al., 2007, Mellaerts et al., 2010***). Mesoporous silicates have an advantage in comparison with the non-porous high surface area materials. The deposited molecules are not just adsorbed onto the silica surface, but also confined to the pores that are only a few molecular diameters wide, which inhibits the recrystallization of the drug molecules (***Alba-Simionesco et al., 2006***).

Consequent to influx of water, the adsorbed drug molecules are being removed from the silica surface and diffuse out of the pores (***Mellaerts et al., 2008***). In the case of poorly soluble drugs, this gives concentrations that are not achievable by dissolution of the low-energy crystalline form (***Van Speybroeck et al., 2010***).

Table 5. Poorly soluble drugs studied on mesoporous materials.

Drug	MW (g/mol)	Solubility[a] (mg/mL)	Carrier	Particle size (µm)	Drug loading capacity (wt. %)	In vitro	In vivo	Ref.
Atazanavir	704.9	4.0-5.0	NFM-1 AMS-6 STA-11	10.16 9.44 9.85	28.2 31.5 32.8	x	x	***Xia et al. (2012)***
Carvedilol	406.5	0.583	SBA-16 MCM-41 TiO_2 Hydroxycarbonate apatite	2.0-3.0 1.0 0.15/0.30 0.20-0.30	25.0 25.0 22.8/23.9 22.5-48.7	x		***Hu et al. (2012)*** ***Hu et al. (2012)*** ***Jiang et al. (2012)*** ***Zhao et al. (2012)***
Celecoxib	381.4	0.003	Carbon	0.5-0.8/5.0-40.0	28.5-37.5	x	x	***Zhao et al. (2012)***
Ezetimibe	409.4	0.0085[b]	SBA-15	N[c]	17.9	x	x	***Kiekens et al. (2012)***
Fenofibrate	360.8	0.25	SBA-15 MCM-41	N N	20.0/40.0 20.0	x		***Van Speybroeck et al (2010)*** ***Van Speybroeck et al***

								(2010)
			SBA-15	0.2-1.0	21.5			***Van Speybroeck et al (2009)***
Flurbiprofen	244.3	0.008	FSM-16	N	30.0	x		***Tozuka et al. (2005)***
Furosemide	330.7	0.25	TCPSi	N	39.0			***Kaukonen et al. (2007)***
			TCPSi	<38.0	41.3	x		***Salonen et al. (2005)***
			TOPSi	<38.0	41.3			***Salonen et al. (2005)***
Glibenclamide	494.0	0.004	SBA-15	N	22.5	x	x	***Van Speybroeck et al. (2011)***
Griseofulvin	352.8	0.009	TCPSi	<38.0	16.5			***Salonen et al. (2005)***
			TCPSi	<38.0	16.5	x		***Salonen et al. (2005)***
			TOPSi	0.17	17.3			***Bimbo et al. (2011)***
Ibuprofen	206.3	0.049	Psi	<38.0	36.8			***Limnell et al. (2007)***
			TCPSi	<38.0	30.9			***Limnell et al. (2007)***
			TOPSi	<38.0	36.5			***Limnell et al. (2007)***
			THCPSi	<38.0	31.9			***Limnell et al. (2007)***
			Spherical mesoporous silica	0.5-0.95	21.3-24.3	x		***Xu et al. (2009)***
			TCPSi	<38.0	29.3			***Hekkila et al. (2007)***
			MCM-41	<38.0	10.5/37.2			***Hekkila et al. (2007)***
			SBA-15	~50.0	50.4			***Hekkila et al (2007)***
			APTES modified	N	16.9-37.2			***Song et al. (2005)***
			SBA-15	N	41.0			
Indomethacin	357.8	0.0009	Syloid 244	2.5-3.7	28.9			***Limnell et al. (2011)***
			MCM-41	<125	27.0			***Limnell et al. (2011)***
			3DOM	N	25.0-50.0	x		***Hu et al. (2011)***
			SBA-15	0.1-1.0	18.6		x	***Van Speybroeck et al. (2009)***
			TOPSi	13.6	5.6		x	***Wang et al. (2010)***
Itraconasole	705.6	0.0096[b]	Syloid AL-1	6.5-8.1	21.0/25.1			***Kinnari et al. (2011)***
			Syloid AL-244	2.5-3.7	21.9/32.8	x		***Kinnari et al. (2011)***
			TOPSi	25.0-75.0	11.2			***Kinnari et al. (2011)***

			TCPSi	25.0-75.0	11.3			***Kinnari et al. (2011)***
			SBA-15	13.8	19.1			***Vialpando et al. (2011)***
			COK-2	19.0	18.1			***Vialpando et al. (2011)***
			SBA-15	0.2-1.0	21.3		x	***Mellaerts et al. (2008)***
Lovastatin	404.5	0.0004	Mesoporous carbon	5.0-40.0	25.6-36.3	x		***Zhao et al. (2012)***
Telmisartan	514.6	0.0035[b]	MCM-41 SBA-15	~0.05/1.0 -2.0	27.5	x	x	***Zhang et al. (2012)***
Carbamazepine	236.3	0.018	SBA-15	0.0-1	22.5	x		***Van Speybroeck et al (2009)***
Cinnarizine	368.5	0.75			20.7			
Danazol	337.5	0.018[b]			20.9			
Griseofulvin	352.8	0.0086			19.7			
Ketoconazole	531.4	0.00009			20.4			
Nifedipine	346.3	0.018[b]			20.7			
Phenylbutazone	308.4	0.048			19.8			

[a]Solubility based on experiments in water at 25ºC unless otherwise stated.

[b]Practically insoluble in water at 25ºC. The solubility is predicted based on theory.

[c](N) The particle size was not mentioned in the study.

All the examined drugs except furosemide (BSC class IV) belong to BSC class II.

1.4.1. Methods of drug loading

Due to low concentration of the poorly soluble drugs in aqueous solution, the loading of drugs into the mesoporous carriers is performed with the method of organic solvent immersion, incipient wetness impregnation or the melt method (***Mellaerts et al., 2008***). According to the available literature, solvent immersion has been most frequently used (***Xu et al., 2013***). The drug loading process of mesoporous materials by immersion includes three steps: (1) immersing mesoporous materials into concentrated drug solution and filling of the pores through capillary action, (2) diffusion of drug molecules into the mesopores and their adsorption on the pore walls, (3) collecting of the drug loaded mesoporous materials from the solution (***Xu et al., 2013***).

Incipient wetness impregnation is a technique where very concentrated drug solution is used to achieve a high loading degree (***Xu et al., 2013***). The volume of the drug solution equals to the pore volume of mesoporous carriers, which is one of the main differences in comparison with the immersion method (***Xu et al., 2013***). In both cases capillary action is responsible for the withdrawal of the solution and dissolved drug molecules into the pores (***Xu et al., 2013***). The impregnation method is chosen when small amounts of drug are available (***Xu et al., 2013***). It is simple to determine the amount of the loaded drug in advance, however it is complicated to control the uniformity of the drug distribution (***Xu et al., 2013***). Another disadvantage is that the residual drug can re-crystallize on the external surface of mesoporous materials after solvent evaporation (***Xu et al., 2013***).

The melt method assumes the heating of physical mixture of the drug and mesoporous carrier above the melting point of the drug (***Xu et al., 2013***). This method could be considered as a special case of the impregnation method (***Xu et al., 2013***). Unfortunately, for many drugs melting is usually followed with the degradation (***Xu et al., 2013***). Also in some cases, high viscosity of the melted drug can be limiting factor for successful drug loading (***Xu et al., 2013***).

There are several factors that can influence the loading degree of the drug when the molecules are loaded in the confined space of the mesopores (***Xu et al., 2013***). The maximum loading degree which can be defined as the ratio of the drug mass to the total mass of the drug when the pores are completely filled, sometimes can be predicted on the basis of the pore volume of mesoporous carrier and the packing density of the payload drug (***Xu et al., 2013***). High loading degrees such as 60 wt. % can be obtained for the carriers with very high porosity (***Xu et al., 2013***). The loading method have an influence on the achieved loading degree, the packing of the molecules in the pores and their distribution in the carrier (***Xu et al., 2013***).

In terms of the loading of the drugs in mesoporous carriers, one of the most critical decisions is to choose appropriate loading conditions so that the drug molecules do not degrade due to the treatment (***Xu et al., 2013***). Concerning this, the right choice of the solvent and the chemical surface properties of the carrier are essential (***Xu et al., 2013***). If the fast release of the drug molecule is required there must not be any strong interaction between the payload molecules (***Xu et al., 2013***). The pore size should also be adjusted to ease the diffusion of the molecules out from the pores (***Xu et al., 2013***). The most important point in an improving the dissolution behavior is a reduction of the lattice energy of well-ordered crystalline structures by creating

amorphous or disordered structures by confining the drug molecules in a restricted space (***Xu et al., 2013***). The factors that can affect drug loading degree are described in the following sections.

1.4.1.1. Effect of pore size

The pore size is essential for the drug loading because the mesopores basically represent molecule sieves and in this manner they can determine how large molecules can be loaded into the carrier materials (***Xu et al., 2013***). The ratio of pore diameter/drug molecule size must be >1 so that the pores are accessible for drug molecules (***Xu et al., 2013***). Additionaly, if the full usage of surface area and high drug loading is required, the ratio should be higher than 3 (***Xu et al., 2013***). Mesoporous MCM-41 with different pore sizes was produced by varying surfactant molecules with different lengths of alkyl chain and then the effect of pore size on the drug loading was investigated (***Horcajada et al., 2004***). The results showed that after immersing mesoporous MCM-41 in a hexane solution with ibuprofen (molecule size 1 nm x 0.5 nm), higher loading efficiency was achieved with the pore size of 3.6 nm (loading degree of 19 wt. %) in comparison with a pore size of 2.5 nm (11 wt.%). Another poorly soluble drug, telmisartan, examined on the spherical mesoporous silica, showed an increase in the loading degree from 49 % to 60 % as the pore size changed from 3.6 to 12.9 nm (***Zhang et al., 2010***).

1.4.1.2. Effect of surface area and pore volume

When the drug molecules adsorb on the surfaces of mesoporous materials, they can form a monolayer or multilayers on the surfaces (***Xu et al., 2013***). If the drug forms monolayer, the loading capacity is directly proportional to the surface area (***Xu et al., 2013***). In that case, the pore volume of the materials doesn't have any influence on the drug loading (***Xu et al., 2013***). The forming of the drug monolayer can be described with a Langmuir isotherm (***Andersson et al., 2004***). However, if there is a significant interaction between the drug molecules, or if a highly concentrated drug solution is used, the drug molecules form multimers or multilayers on the surface of the pores (***Xu et al., 2013***). So in this case, both the surface area and the pore volume can influence the drug loading capacity (***Zhang et al., 2010***)

1.4.1.3. Effect of surface chemistry

The interfacial interactions between the surface of mesoporous materials and the drug molecules represent the driving force for the drug loading (***Xu et al., 2013***). Physical and chemical adsorption are the two common mechanisms which are mostly determined by surface chemistry of mesoporous carriers (***Xu et al., 2013***). In the case of poorly soluble drugs, physical adsorption is preferred if improved drug dissolution is required since this is a reversible process (***Xu et al., 2013***). Usual forms of the physical adsorption between drugs and mesoporous carriers are hydrogen bonding, electrostatic and hydrophobic interactions (***Xu et al., 2013***). Unmodified mesoporous carriers have the surface covered with –OH groups, so hydrogen bond is expected form of the interaction (***Salonen et al., 2008***). Surface functionalization can induce electrostatic or hydrophobic interactions, which either increases or decreases the drug loading efficiency of the carriers (***Xu et al., 2013***). For example, on mesoporous Al_2O_3 (***Kapoor et al., 2009***), functionalization with hydrophobic Si-CH_3 groups resulted in a lower loading degree of ibuprofen (approximately 20%) whereas hydrophilic groups gave significantly higher drug loading efficiency. The same study showed that highest drug loading (about 45%) was achieved after (3-aminopropyl)-triethoxysilane (APTES) modification. Improved drug loading capacity was explained with the electrostatic interaction between –NH on modified carriers and the –COOH of ibuprofen. So, it may be concluded that the surface modification method can significantly contribute to the drug loading capacity (***Song et al., 2005***).

1.4.1.4. Effect of solvent

The polarity of solvent also can influence the drug loading (***Xu et al., 2013***). As it was previously mentioned, a dominant interaction between drug molecules and the surface of carriers for unmodified mesoporous silica materials is hydrogen bonding (***Xu et al., 2013***). Very polar solvents such as dimethyl sulfoxide (DMSO), can be in the competition with the drug molecules, which can adversely affect the drug loading (***Xu et al., 2013***). The effect of solvent on the loading of poorly soluble drug has been studied with numerous solvents including dimethylformamide (DMF), dimethylacetamide (DMA), DMSO, ethanol and hexane (***Charnay et al., 2004***). Ibuprofen was not adsorbed onto MCM-41 surface in DMA due to its extreme

polarity. On the other hand, in hexane, the loading capacity was up to 37% wt. The solvent effect has a similar influence on silicon, Al_2O_3 and TiO_2 based mesoporous materials because of their polar surface properties (***Xu et al., 2013***). For carbon based mesoporous materials with the nonpolar surface, the adsorption of drug molecules is enhanced from the solvent with high polarities (***Xu et al., 2013***).

1.4.2. Characterization of drug loaded carriers

The characterization of drug-loaded carriers includes: drug-carrier interactions, the amount of the loaded drug (loading degree/efficiency) and physical characteristics of the loaded drug (***Xu et al., 2013***). Drug-carrier interactions are usually examined by Fourier transform infrared spectroscopy (FTIR) or by defining the absorption isotherms of the drug, which can reveal significant information about the possible chemisorption or physisorption on the carrier surface (***Jarvis et al., 2011***).

Drug loading degree of the carrier is commonly determined by the extraction and thermogravimetry (TG) (***Xu et al., 2013***). After the extraction that is performed to release the drug from the carrier, the drug concentration in the medium is measured which gives the information about the total loading degree (***Xu et al., 2013***). The most frequently used technique for drug concentration assay is high performance liquid chromatography (HPLC) since it can additionally give information about the possible degradation of the payload molecules (***Xu et al., 2013***). UV/VIS spectroscopy is an alternative method for the determination of the drug concentration for the drug molecules with absorption in the range of ultraviolet or visible light (***Xu et al., 2013***). If the mentioned techniques are applied, care should be taken that payload material has been extracted completely from the carriers. Very often the release can be incomplete (***Xu et al., 2013***). Thermogravimetric analysis assumes the measurement of the weight of the sample in the function of temperature (***Xu et al., 2013***). It is easy to observe the mass of the loaded drug since the thermal decomposition of the organic drug occurs at lower temperatures than decomposition of the carrier (***Xu et al., 2013***).

During the characterization process it is very important to become familiar with the state of the drug in the mesoporous carriers (***Xu et al., 2013***). Poorly soluble drug that is adsorbed on the external surface of the carrier particle can stop the release of the drug and have a negative

influence on the release rate of the drug (***Xu et al., 2013***). This drug material that is located outside the pores can be easily distinguished from the drug inside the pores by the size of the crystallites (***Xu et al., 2013***). In the pores, the crystalline size is limited by the pore walls whereas outside the pores such restraints do not exist and crystallites tend to grow significantly larger (***Xu et al., 2013***). The physical state of the drug is usually characterized by XRD and differential scanning calorimeter (DSC) (***Heikkila et al., 2007***). Both methods can be applied to detect crystalline phases as well as size of the crystallites in the loaded materials (***Xu et al., 2013***). Additionally, some other techniques such as pycnometry, nitrogen sorption and NMR can be used to gain an information about the loaded drug (***Babonneau et al., 2004***).

Drug inside the pores can be in an amorphous or in different crystalline phases (***Xu et al., 2013***). It has been confirmed that the drug confined in small, few nm wide pores drugs is in an amorphous state (***Van Speybroeck et al., 2009***). The amorphous state can be dispersed on the pore walls of the material leaving the center of the pore free or it can fill the center of the pore (***Mellaerts et al., 2008***). The amorphous compounds, ibuprofen and indomethacin, are highly mobile in the pores at least when they form a thin layer on the surface without strong drug-carrier interactions (***Azais et al., 2006***).

It is important to note that the crystallization of the loaded drugs is not possible as long as the critical nucleus is bigger than the pore (***Xu et al., 2013***). In this case, it would be energetically unfavourable for a nucleus to grow, i. e. the drug to crystallize in the pores (***Xu et al., 2013***). If the pore and the drug cluster in the pore are larger than the critical nucleus, crystallization is possible (***Xu et al., 2013***). Crystals of the drug inside the pores have significantly different properties compared with bulk crystals (***Xu et al., 2013***). It is well known that the crystal size affects the solubility or a melting temperature of the material (***Xu et al., 2013***). Additionally, loaded drug does not crystalize completely, but a thin non crystallizing layer, the known as δ-layer, appears always between the pore wall and crystalline core (***Riikonen et al., 2009***). Confinement in the mesopores can also affect the crystal structure of the drug (***Xu et al., 2013***). It has been observed that crystal structures that are unstable in bulk can become stable in the mesoporous because the relative stability of the polymorphs can be dependent on the size of the crystals (***Rengarajan et al., 2011***). One of the studies even reported that previously unknown polymorphs have been detected to be formed under confinement (***Ha et al., 2009***). Furthermore, the crystal orientation in the pores may not be random (***Xu et al., 2013***).

1.4.3. Drug release and mechanism studies

Poorly water soluble drugs are known to have numerous of negative clinical effects, such as rate-limiting dissolution, slow absorption and low bioavailability (***Xu et al., 2013***). One of the most important issues is that these drugs tend to be eliminated from the gastrointestinal tract before they have the opportunity to fully dissolve and be absorbed into the systemic blood circulation (***Xu et al., 2013***). Consequently, the dosage of poorly soluble drugs should be very high to reach a required therapeutic drug concentration in blood, which can induce local toxicity and discomfort on patients (***Xu et al., 2013***).

1.4.3.1. In vitro studies

The first goal for the delivery of poorly soluble drugs is to increase their dissolution rate in biological fluids (***Xu et al., 2013***). Several factors have an influence on the drug release from mesoporous carrier (***Xu et al., 2013***). Since the release of the drug molecules is mainly controlled by the diffusion mechanism, the effect of pore size plays an important role (***Xu et al., 2013***). For example, in the system of ibuprofen loaded MCM-41, the drug release rate decreased clearly as the pore size changed from 3.6 to 2.5 nm (***Horcajada et al., 2004***). The pore size effect was further verified on the model drug indomethacin, which was loaded in the mesoporous SBA-16. The amount of the drug released from the pore sizes of 4.3 nm, 6.8 nm and 9.0 nm were 75%, 81% and 90 % within 60 minutes, respectively (***Hu et al., 2011***).

Another important factor that have an influence on the release rate is the surface chemistry (***Xu et al., 2013***). The release rate of celecoxib from mesoporous carbon was found to be higher than from SBA-15 (***Zhao et al., 2012***). Post-grafting of alkyl groups increased the surface hydrophobicity, so the diffusion of H2O molecules from the biological fluids into the pores was slower. Consequently, the release of drug from mesoporous carriers decreased (***Xu et al., 2009***).

Finally, the pore architectures of mesoporous carriers also affected drug release rate (***Xu et al., 2009***). Due to the 3D connected pore structure of SBA-16 and TUD-1, these samples exhibited faster drug release than the mesoporous carriers such as MCM-41with 2D pore channels (***Hu et al., 2012***). The 3D mesoporous structure obviously provided more favourable mass transfer which simplified drug release without pore blocking (***Xu et al., 2009***).

1.4.3.2. In vivo studies

Improving the bioavailability of poorly soluble drugs in biological fluids is one of the greatest challenges for pharmaceutical scientist today (***Xu et al., 2009***). Animal tests play an important role in the formulation development due to the poor correlation frequently observed between the *in vitro* and *in vivo* results (***Xu et al., 2009***). Unfortunately, many of the studies are limited only to in vitro evaluations or in the best case on the experiments conducted with cells (***Xu et al., 2009***).

Poorly soluble drugs loaded into mesoporous materials are in an amorphous form and in vitro tests usually show the enhanced drug dissolution (***Xu et al., 2009***). Therefore, an improved bioavailability could also be expected in *in vivo* tests (***Kiekens et al., 2012***). For example, an enhanced in vivo pharmacokinetics was successfully confirmed with indomethacin loaded TOPSi. The study revealed that the value of T_{max} was reduced to a one fourth, C_{max} increased 200 % and bioavailability was significantly enhanced when the mesoporous carrier was used in comparison with either pure indomethacin or commercially available product Indocid (***Wang et al., 2010***). Another study performed by Mellaerts et al., (2008) investigated the in vivo performance of ordered mesoporous silica for itracinasole in two animal species - rabbits and dogs. After oral administration of crystalline itraconasole to dogs (20 mg), no systemic itraconasole could be detected; on the other hand, the area under the curve 0-8 h (AUC_{0-8}) was 681 ± 566 nM h when the drug was formulated with the mesoporous carrier. In rabbits, the AUC_{0-24} increased to 1069 ± 278 nM h and T_{max} decreased from 9.8 ± 1.8 to 4.2 ± 1.8 h , when the SBA-15 was employed. Mesoporous carbon also showed an enhanced bioavailability of poorly soluble drug celecoxib when it was used as the carrier (***Zhao et al., 2012***). Results showed that the AUC_{0-24} of celecoxib loaded in mesoporous carbon was about 1.68-fold of that for commercial celecoxib capsules (Pfizer Pharmaceuticals LLC). These are just some of the examples where the subsequent in vivo studies confirmed the in vitro results.

1.5. Sodium diclofenac

Sodium diclofenac (sodium; 2-[2-(2,6-dichloroanilino)phenyl]acetate) (Figure 4) belongs to a group of nonsteroidal anti-inflammatory drugs (NSAID) of the phenylacetic acid class with combined anti-inflammatory, analgesic and antipyretic properties (***Altman et al., 2015***). Chemically diclofenac sodium is the sodium salt form of diclofenac, a benzene acetic acid derivate (***Source: PubChem: URL: https://pubchem.ncbi.nlm.nih.gov***)

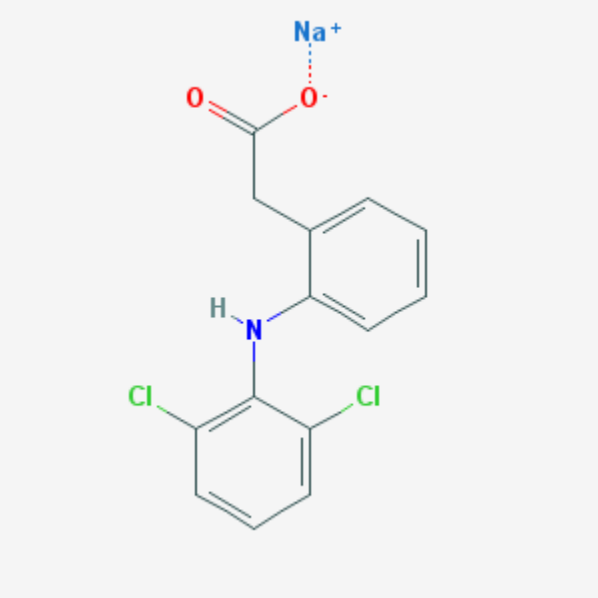

Figure 4. Chemical structure of sodium diclofenac (sodium; 2-[2-(2,6-dichloroanilino)phenyl]acetate). (***Source: PubChem: URL: https://pubchem.ncbi.nlm.nih.gov***)

Opposed to the action of many traditional NSAIDs, diclofenac inhibits cyclooxygenase (COX)-2 enzyme stronger than it does COX-1 (***Altman et al., 2015***). The mechanism of action is based on the binding of diclofenac to COX isozymes and inhibition of the synthesis of prostanoids (i. e., prostaglandin (PG)-E_2, PGD_2, PGF_2, prostacyclin (PGI_2) and thromboxane (TX) A_2 (***Vane, 1971***). PGE_2 is the dominant prostanoid produced in inflammation, and the inhibition of its

synthesis by NSAIDs is assumed to be the main reason for the potent analgesic and anti-inflammatory features of these drugs (***Patrono et al., 2001***).

After oral administration, systemic absorption of diclofenac is generally very fast and directly proportional to the dose (***Davies et al., 1997***). Approximately 60% of the intact diclofenac enters the systemic circulation due to first-pass metabolism (***Todd et al., 1988***). It has been confirmed that the main metabolite, 4'-hydroxydiclofenac has weak anti-inflammatory and analgesic activities (***Fowler et al., 1983***). Finally, after the biotransformation to glucoroconjugated and sulphate metabolites, diclofenac is excreted in the urine (***Todd et al., 1988***).

Diclofenac, as the other NSAIDs, can cause serious dose-related gastrointestinal, cardiovascular and renal side effects (***Brater et al., 2002, Lewis et al., 2002, Salvo et al., 2011***). The main cause of the gastrointestinal adverse effects is decreased synthesis of prostanoids and consequent limited secretion of mucus and bicarbonate that normally protect the gastric mucosa from damage (***Sinha et al., 2013***). PGI_2 which is known to be a major product of COX-2-mediated metabolism of arachidonic acid in vascular endothelial cells, act as a potent vasodilator and platelet inhibitor (***Patrono et al., 2014***). Extensive clinical and preclinical studies indicate that suppression of PGI_2 synthesis significantly increases the risk for hypertension and thrombosis (***Yu et al., 2012***).

1.6. Erythrocyte ghosts as controlled drug delivery systems

Erythrocytes represent the most abundant cells in the human body (~5.4 million cells/mm^3 blood in a healthy male and ~4.8 million cells/mm^3 blood in a healthy female (***Gothoskar, 2004***). These cells were described in human blood samples by Dutch scientist Lee Van Hock in 1674 (***Gothoskar, 2004***). Erythrocytes have the shape of the biconcave disc with an average diameter of 7.8 μm, a thickness of 2.5 μm in periphery, 1μm in the center, and a volume 85-91 μm^3 (***Guyton, 1996***). The flexible, biconcave shape enables erythrocytes to squeeze through narrow capillaries, which may be only 3 μm wide (***Gothoskar, 2004***). Mature erythrocytes have very simple structure, they do not contain a nucleus and other organelles (***Gothoskar, 2004***). Their plasma membrane encloses hemoglobin, a heme-containing protein that is responsible for O_2-CO_2 binding inside the erythrocytes (***Gothoskar, 2004***). Erythrocytes have the role in the transport of O_2 from the lungs to tissues and the CO_2 produced in the tissues back to lungs

(***Gothoskar, 2004***). Thus, erythrocytes represent highly specialized O_2 carrier system in the body (***Gothoskar, 2004***).

The life span of erythrocytes is approximately 120 days (***Gothoskar, 2004***). Old erythrocytes are being eliminated from circulation and destroyed in the spleen and liver (RES) (***Gothoskar, 2004***). Within the body, erythrocytes are produced in red bone marrow under the regulation of hemopoietic hormone erythropoietin in the process called erythropoiesis (***Torotra et al., 1993***).

1.6.1. Source and isolation of erythrocytes

Different types of mammalian erythrocytes have been used as drug delivery systems, including erythrocytes of mice, cattle, pigs, dogs, sheep, goat, monkeys, chicken, rats and rabbits (***Gothoskar, 2004***). The first step in isolation of erythrocytes is collection of the blood in heparinized tubes by venipuncture (***Gothoskar, 2004***). Fresh whole blood is preferably used for loading purposes because it has been shown that the encapsulation efficiency of the erythrocytes isolated from fresh blood is higher than that of the aged blood (***Gothoskar, 2004***). Fresh whole blood is defined as the blood that is collected and immediately chilled to 4 ºC and stored for less than two days (***Gothoskar, 2004***). The erythrocytes are then separated and washed by centrifugation (***Gothoskar, 2004***). The washed cells are suspended in buffer solution at various hematocrit values as required and are usually stored in acid-citrate-dextrose buffer at 4 ºC for as long as 48 h before use (***Gothoskar, 2004***). The detail protocol for the isolation of erythrocytes has been established by Jain and Vyas (***Vayas et al, 2002***).

1.6.2. Advantages of erythrocytes as drug carriers

The most important feature of erythrocytes as drug carriers is their biocompatibility, particularly when autologous cells are used, eliminating possibility of triggered immune response (***Lewis, 1984***). Erythrocyte membranes are biodegradable and do not generate toxic products (***Lewis, 1984***). These carriers have considerably uniform size and shape (***Telen, 1993***) and relatively inert intracellular environment (***Adriaenssens, 1976***). The wide variety of chemicals can be

entrapped (***Jaietely et al., 1996, Sprandel, 1987***) with possibility to modify pharmacokinetic and pharmacodynamic parameters of drug (***Jain, 1997***). Large quantity of drug can be encapsulated within a small volume of cells ensuring dose sufficiency (***Vyas et al., 2002***). These carriers allow attainment of steady-state plasma concentration of drug, decrease fluctuations in concentration (***Lewis, 1984***) and consequently eliminate side effects (***Lewis et al., 1984***). They have ability to target organs of RES (***Lewis, 1984***) and offer the possibility of ideal zero-order drug-release kinetics (***Eichler, 1986***). Techniques and facilities for isolation, separation, handling, transfusion and working with erythrocytes are very well developed and available (***Lewis, 1984***).

1.6.3. Methods of drug loading

There are several methods that can be used to load drugs or other bioactive entities in erythrocytes and they can be roughly divided on physical osmosis-based systems and chemical methods (***Gothoskar, 2004***). Independently of the method used, successful entrapment of the compound requires the drug to have high water solubility, resistance against degradation within erythrocytes, lack of physical and chemical interaction with erythrocyte membrane, as well as defined pharmacokinetic and pharmacodynamic properties (***Hamidi et al., 2003***).

Hypotonic hemolysis is a process based on the intrinsic ability of erythrocytes to reversibly swell in a hypotonic solution (***Gothoskar, 2004***). Erythrocytes can reversibly change their shape with or without accompanying volume change and can undergo reversible deformation under stress (***Gothoskar, 2004***). An increase in volume induce a change in the shape from biconcave to spherical (***Gothoskar, 2004***). The cells obtain a spherical shape to accommodate additional volume while keeping the surface area constant (***Gothoskar, 2004***). An increase in volume is approximately ~25-50% **(*Gothoskar, 2004*).** The upper limit of tonicity for cells to maintain their integrity is ~150 mosm/kg, above which the membrane ruptures, releasing hemoglobin and other cellular content (***Gothoskar, 2004***). At this point (just before cell lysis), some transient pores of 200-500 Å appear on the membrane (***Gothoskar, 2004***). After cell lysis, cellular contents are released and residual material represent an erythrocyte ghost (***Jain, 1997***). These ruptured erythrocytes can be used as drug vechicles because ruptured membranes can be easily resealed

by bringing back the cells into the isotonic conditions (***Gothoskar, 2004***). After the incubation, the cells recover their original biconcave shape and original impermeability (***Ihler et al., 1987***).
Alternative approaches for the drug loading include use of red cell loader (***Magnani et al., 1998***), hypotonic dilution (***Iher et al., 1973***), hypotonic preswelling (***Rechsteiner, 1975***), hypotonic dyalisis (***Klibansky, 1959***), isotonic osmotic lysis (***Bird et al, 1983***), chemical perturbation of the membrane (***Deuticke et al, 1973***), electro-insertion or electroencapsulation (***Zimmermann, 1975***), entrapment by endocytosis (***Schrier, 1976***), loading by electric cell fusion (***Tsong et al., 1985***) and loading by lipid fusion (***Nicolau et al., 1979***).

1.6.4. Applications of resealed erythrocytes

Erythrocytes and erythrocyte ghosts have broad spectrum of applications in various fields of human and veterinary medicine (***Gothoskar, 2004***).

1.6.4.1. Slow drug release

Numerous studies reported the usage of erythrocytes for the sustained delivery of antineoplastics (***Updike et al, 1983***), antiparasitics (***Summers, 1983***), veterinary antiamoebics (***Jaitely, 1996***), vitamins (***Eichler, 1985***), steroids (***Jenner et al., 1981***), antibiotics (***Jain et al., 1995***), and cardiovascular drugs (***Tajerzadeh et al., 2000***).
Several mechanisms were described for the drug release and they include passive diffusion, specialized membrane associated carrier transport, phagocytosis of resealed cells by macrophages of RES, accumulation of erythrocytes in lymph nodes after subcutaneous administration followed by hemolysis to release the drug (***Gothoskar, 2004).*** Possible routes of administration for erythrocyte based formulations are intravenous (which is the most common), subcutaneous, intraperitoneal, intranasal and oral (***Jain et al., 1997***). Improved efficacy of different drugs administered in this form in animal models have been extensively described and published (***Gothoskar, 2004).*** Some of the examples are an improvement of anti-inflammatory effect of corticosteroids in experimentally inflamed rats (***Jenner, 1981***), increase of half-life of

isoniaside (***Jain et al., 1995***), levothyroxine (***Field et al., 1989***), cytosine arabinoside (***Deloach et al., 1982***), and interleukin 2 (***Deloach et al., 1987***); prolongation of plasma half-life of erythropoietin from 30 minutes to 35 hours in mice (***Garin, 1996***).

1.6.4.2. Drug targeting

Ideal controlled drug delivery system should be site-specific and target-oriented to show maximal possible therapeutic effect with minimum adverse effects (***Gothoskar, 2004)***. Erythrocytes and erythrocyte ghosts have a potential to be used as drug carriers and targeting tools as well (***Gothoskar, 2004)***. One approach to target organs of mononuclear phagocytic system/reticuloendothelial system is surface modification because the changes in the membrane are normally recognized by macrophages (***Alvarez, 1998***) Furthermore, erythrocytes also can be used to target organs other than those of RES (***Gothoskar, 2004).***

1.6.4.3. Targeting RES organs

Phagocytic Kupffer cells in liver and spleen are responsible for the elimination of the damaged and altered erythrocytes from circulation (***Gothoskar, 2004).*** Therefore erythrocytes and their ghosts can be used to target the liver and spleen after the modification of their membrane (***Gothoskar, 2004)***. Different techniques can be employed to modify the surface characteristics of erythrocytes: surface modification with antibodies, gluteraldehyde, carbohydrates such as sialic acid (***Alvarez et al., 1998***), sulphhydryl etc. (***Gothoskar, 2004)***. One of the possible options is also ex vivo artificial pre-ageing of the cells to increase their uptake by phagocytic cells (***Bourgeaux et al., 2016***). Pre-aging process can be performed by enzymatic, thermal or chemical methods (***Bourgeaux et al., 2016***). The efficiency of neuraminidase enzyme to eliminate sialic acid from the surface of the erythrocyte membrane in order to induce cell deterioration has been thoroughly examined in one preclinical study (***Zocchi et al., 1987***). Heat treatment (ie, 42 ºC for 90 minutes or 48 ºC for 30 minutes) has also been investigated for the pre-aging of cells by energy depletion (***Zocchi et al., 1987***). Glutaraldexyde as a crosslinker reacts extensively with proteins in the erythrocyte membrane and also can be used to target the spleen and the liver (***Bourgeaux et al., 2016***). After the treatment, resulting erythrocytes become

extremely rigid which can compromise their use for in vivo applications (***Bourgeaux et al., 2016***). Much better option is the usage of bis(sulfosuccinimydil)suberate because the treatment is less aggressive and leads to the crosslinking of specific proteins such as Bend 3. It has been confirmed that bis(sulfosuccinimydil)suberate treated erythrocytes are less rigid then glutharaldexyde treated cells so they are more suitable for clinical use (***Bourgeaux et al., 2016***).
The two main applications of the RES targeting strategy by erythrocytes are:

1. The delivery of small chemical entities such as antiretroviral nucleoside analogs (***Magnani et al., 1992***),
2. The encapsulation of antigens for vaccination or tolerance induction (***Banz et al., 2010***).

1.6.4.4. Targeting the liver

The deficiency of enzymes in the body and consequent metabolic disorders can be treated by administering these enzymes in the replacement therapy (***Gothoskar, 2004***). However, the exogenous enzyme therapy is faced with many obstacles such as shorter circulation half-life of enzymes, allergic reactions, toxic manifestations etc. (***Gothoskar, 2004)***. These issues could be successfully solved by using erythrocytes and their gosts (***Gothoskar, 2004***). Some examples already exist in the literature and they include β-glucosidase, β-glucoronidase, β-galactosidase (***Jaitely et al., 1996; Eichler, 1986; Deloach et al., 1977***).
Nowadays hepatic tumors represent one of the most prevalent types of cancer (***Gothoskar, 2004***). Antineoplastic drugs such as methotrexate (***Jaitely et al., 1996***), bleomycin (***Zimmerman, 1973***), asparginase (***Updike et al., 1983***) and adriamycin (***Al-Achi et al., 1990***) have been successfully delivered by erythrocytes.
Resealed erythrocytes selectively accumulate within RES organs which also makes them appropriate for the delivery of antiparasitic agents (***Gothoskar, 2004***). Parasites are known to be highly concentrated in the RES organs which opens the possibility to successfully control parasitic diseases by this method (***Gothoskar, 2004***). Proven efficiency is already described in animal models for erythrocytes loaded with antimalarial (***Summers, 1983***), antileishmanial (***Summers, 1983***) and antiamoebic drugs (***Jaitely, 1996***).

1.6.4.5. Targeting organs other than RES

Organs outside the RES can also be targeted by erythrocytes (***Gothoskar, 2004***). Some of the examples include encapsulation of paramagnetic particles or photosensitive material in erythrocytes together with the drug, the use of ultrasound waves and antibody attachment to the surface of erythrocyte membranes to get specificity of action (***Gothoskar, 2004***). Study performed by Zimmerman et al., described encapsulation of small paramagnetic particles that can be localized to a particular location in the body when they are controlled by an external magnetic field (***Zimmerman et al., 1975***). The entrapment of ferrofluids (colloidal suspension of magnetite) has been described by Sprandel et al (***Sprandel et al., 1980***). Antiinflammatory drugs diclofenac sodium and ibuprofen were successfully encapsulated in magnetoresponsive erythrocytes (***Jain et al., 1994***). There is also an example of the photosensitized erythrocytes that have been developed as phototriggered carrier and delivery system for methotrexate (***Flynn et al., 1994***). Possibility to target cytotoxic T-cells in vitro after the attachment of Thy-1.2 monoclonal antibody to the surface of erythrocytes has been reported by Chiarantini et al. (***Chiarantani, 1995***).

1.6.4.6. Delivery of antiviral agents

Antiviral agents can also be successfully encapsulated in resealed erythrocytes for the delivery and targeting (***Ihler, 1983***). In most cases, antiviral drugs chemically belong to a group of nucleotides or nucleoside analogs, so their transport through the membrane (entrapment and exit during the releasing) requires careful consideration (***Gothoskar, 2004***). Nucleosides can pass rapidly through the membrane whereas nucleotides cannot, so they are suitable for the carriers with prolonged release profiles (***Gothoskar, 2004***). Before the release, nucleotides need to be converted to purine and pyrimidine bases (***Gothoskar, 2004***). Examples of the usage of erythrocytes as controlled drug delivery systems for antiviral agents are numerous and include the delivery of deoxycytidine derivatives (***Ihler, 1983***), recombinant herpes simplex virus type 1 (HSV-1) glycoprotein B (***Chiarantini et al., 1995***), azidothymidine derivatives (***Benatti, 1989***), azathioprene, acyclovir (***Magnani, 1998***), and fludarabine phosphate (***Fraternale et al., 1996***).

1.6.4.7. Delivery of anti-inflammatory agents

Encapsulation of anti-inflammatory drugs such as glucocorticoids including dexamethasone into erythrocytes, is a promising approach for the enhancement of the bioavailability of these poorly-soluble drugs and selectivity of their delivery to active phagocytes in the RES and other components of immune system (***Muzykantov, 2010***). This concept was extensively studied and developed by Magnani et al. and was tested in the human patiens with disease conditions associated with inflammation (***Magnani et al., 1998, Magnani et al., 2002***). In one of the studies RBC-loaded with dexamethasone were re-infused in ten patients suffering from chronic obstructive pulmonary disease, COPD. The treatment was well tolerated and resulted in a sustained elevation of blood DEX level after a single injection (***Rossi et al., 2001***). In other lung disease with a major inflammatory component, cystic fibrosis, re-infusions in the patients of autologous RBC-loaded DEX at monthly intervals provided sustained low level of DEX for 28 days in the blood stream. This treatment was also well tolerated and provided significant reduction of inflammatory reactions (***Rossi et al., 2004***). Furthermore, the similar concept was tested in patients with inflammatory bowel disease where three repetitive re-infusions of autologous RBC loaded with DEX (every for weeks) were administered. Prolonged increase in DEX blood level was achieved and patients were not forced to take previously prescribed poorly tolerated steroids anymore. Additionally, achieved remission has been maintained for several months (***Annese et al., 2005***). Encouraging results in previously described studies suggest that RBC-mediated delivery of anti-inflammatory agents may be very useful in treatment of acute and chronic inflammation (***Muzykantov, 2010***).

1.6.4.8. Enzyme therapy

In clinical practice enzymes have numerous applications such as replacement therapies to treat diseases caused by their deficiency (e. g., Gaucher's disease, galactosuria), degradation of toxic compounds secondary to some kind of poisoning (cyanide, organophosphorus), and as drugs (***Bird et al., 1983***). After administration, enzyme-loaded erythrocytes can release enzymes into circulation upon hemolysis (***Zimmerman, 1983***); act as 'circulating bioreactors' in which

substrates enter into the cell, interact with enzymes and generate products (***Magnani, 1989***); or accumulate enzymes in RES upon hemolysis for future catalysis (***Lewis et al., 1984***).

The first successful clinical trial of the erythrocytes loaded with enzymes was performed in 1997. with β-glucoserebrosidase for the treatment of Gaucher's disease (***Beutler, 1977***).

Asparaginase, the enzyme that degrades asparagine, an amino acid vital for cell, was entrapped into erythrocytes for the treatment of neoplasms in children (***Gothoskar, 2004***). This treatment is proven to prevent remission of pediatric acute lymphocytic leukemia (***Tan, 1972***) which is followed with many reports of improved intensity and duration of action in animals (***Updike et al., 1983; Alpar et al., 1985***) and humans (***Jain et al., 1997***). RBC-loaded enzyme replacement therapy using thymidine phosphorilase has been thoroughly examined in patients with a genetic mitochondrial deficiency of this enzyme: treatment improved biochemical readouts but the patients' clinical condition did not improve (***Moran et al., 2008***).

Other examples and attempts include urease (***Zimmerman et al., 1976***), galactose-1-phosphate uridyl transferase (***Harris, 1977***), uricase (***Ihler et al., 1975***) and acetaldehyde dehydrogenase (***Tan, 1972***).

1.6.4.9. Anti-cancer agents

The main benefits of the loading anti-cancer drugs into carriers are reduction of their toxicity and improvement of their delivery to tumors (***Muzykantov, 2010***). During the last decade different technologies such as liposomes, linear polymers and polymer micelles were developed as carriers for anti-cancer drugs (***Muzykantov, 2010***). However, in comparison to these conventional concepts, RBC carriers offer an advantage in tumor treatment, for example, by providing formulation with prolonged circulation (***Muzykantov, 2010***). For instance, hydrophobic anti-tumor agent dequalinium was encapsulated into mouse RBC which resulted in much longer half-life in circulation than PEG-liposomal formulation (5-6 days vs 4 hours) (***Lizano et al., 2003***).

Anticancer drugs such as antibiotic doxorubicin have been encapsulated into carrier RBC using different loading strategies including glutaraldehyde cross-linking of RBC membrane (***Attaulakhanov et al., 1996***). As it was previously mentioned, this procedure improves RBC uptake by macrophages and other cells exerting active phagocytosis (***Alvarez et al., 1998***). As it

was expected, doxorubicin- loaded RBC successfully delivered the drug into macrophages in culture and concentrated in the liver after intravenous injection in animals including dog (***Tonetti et al., 1991***). This intervention showed good efficiency in treatment of lymphoid tumor in dogs without cardiac toxicity which is known to be a common adverse effect of doxorubicin (***Matherne et al., 1994***). Human autologous erythrocytes encapsulated with antracycline antibiotic daunorubicin were tested in patients with acute leukemia and showed prolonged drug level in plasma and decrease in side effects in comparison to the free drug (***Skorokhod et al., 2004***).

Among other carriers, erythrocytes represent a unique, promising and still underdeveloped platform for drug delivery (***Muzykantov, 2010***). After initial burst of interest and research efforts for three decades, drug delivery by RBC was overshadowed by artificial carriers offering wider range of applications, as well as better control over formulation, storage and utilization of drug delivery system than original RBC-based concepts (***Muzykantov, 2010***). Studies on RBC drug delivery systems started with in vitro experiments using isolated RBC and within two decades, progressed to extensive animal studies and clinical trials (***Muzykantov, 2010***).

1.6.5. Novel approaches in product formulation

Some novel approaches and techniques applied in the production of controlled drug delivery systems based on erythrocytes and erythrocyte ghosts include layer-by-layer microcapsules template on erythrocyte ghost carriers (***Shaillender et al., 2011***), surface modification (***Sternberg et al., 2011***) and nanoerythrosomes. Schaillender et al. described successful coating of encapsulated erythrocyte ghosts with the biocompatible polyelectrolytes, poly-l-arginine hydrochloride and dextran sulfate (Figure 5). This study has shown that the release profiles of the encapsulated molecules can be controlled over a wide range by changing the number of polyelectrolyte layers. Alternative polymeric systems that could be used for the coating include: chitosan/alginate, protamine sulfate/dextran sulfate, poly-L lysine/poly-L glutamic acid sodium salt, poly-L lysine/dextran sulfate (***Shaillender et al., 2011***). Aggregation of loaded ghosts can be easily followed by using optical microscopy (***Shaillender et al., 2011***). Since erythrocyte ghosts are very soft and fragile, in order to avoid their breakage due to deposition of

polyelectrolytes it is important to stabilize them with glutaraldehyde prior to coating (***Shaillender et al., 2011***). Polyelectrolyte layering process can be monitored by measuring ζ-potential after each coating step (***Shaillender et al., 2011***). It is well known that the surface of erythrocyte ghosts is negatively charged and it converts to a positive value after the deposition of the first cationic polyelectrolyte layer (***Shaillender et al., 2011***). This change in the surface charge enables the subsequent deposition of the anionic polyelectrolyte layer (***Shaillender et al., 2011***).

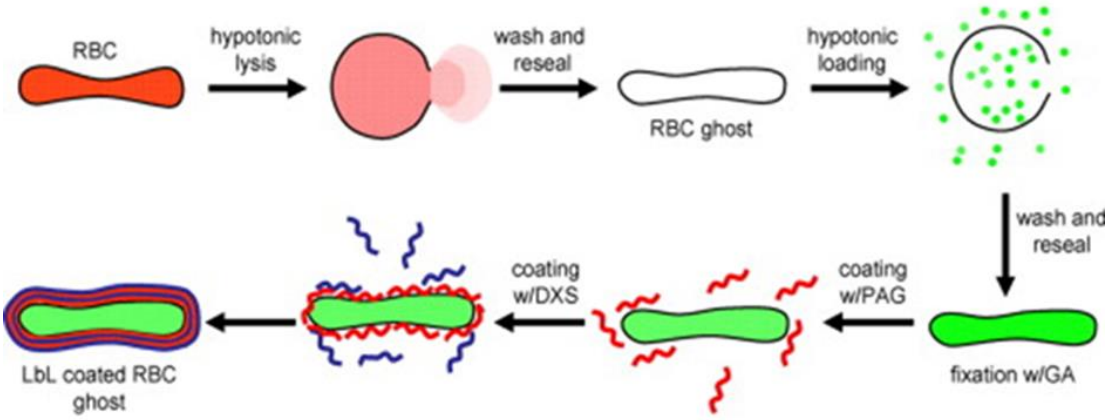

Figure 5. Schematic illustration of the production of layer by layer microsapsules using erythrocyte ghosts as template (***Shaillender et al., 2011***).

Interesting approach in the development of controlled drug delivery systems based on erythrocytes is attachment of various molecules such as proteins or peptides to the functional groups on the cell surface (***Chambers et al., 2004***). Even though there are various reversible and reversible conjugation approaches, the non-covalent attachment using biotin-avidin bridge is considered to be the most biocompatible and successful way of surface modification of erythrocytes (***Muzykantov, 2010***). This technology is especially useful when the drug targeting to non-RES sites of the body is desired (***Sternberg et al., 2011***). One such example is described in 2011 by Sternberg et al. In this study albumin-loaded erythrocytes were subsequently surface conjugated with insulin and IgG via biotin–streptavidin. Insulin-conjugated erythrocytes were observed to attach and to be internalized by cultured endothelial cells. On the other hand, uptake was not observed for carrier-RBCs non-specifically modified with IgG (***Sternberg et al., 2011***).

Nanoerythrosomes, engineered derivative or erythrocytes with an average diameter of 100 nm, are being prepared by hypotonic lysis of erythrocytes followed by extrusion usually through polycarbonate membranes (***Gupta et al., 2014***). Their physicochemical properties (***Deák et al., 2015; Kuo et al, 2016***) as well as their potential application (Gupta et al., 2014) are extensively described in the literature.

One of the first successful encapsulations of the drug in nanoerythrosomes was performed in 1994. by Lejeune et al. using daunorubicin as a model compound (***Lejeune et al., 1994***). Gupta et al. gave detail insight in preparation and characterization of nano-engineered erythrocyte ghosts as inhalational carriers for delivery of fasudil (***Gupta et al., 2014***) (Figure 6). Fasudil, a potent Rho kinase inhibitor and vasodilator, is used in the inhalation therapy for pulmonary arterial hypertension (***Gupta et al., 2014***). However, fasudil has very short half-life which can be extended by encapsulating in liposomes (***Gupta et al., 2014***). Alternative option could be nanoerythrosomes - insufficiently examined cell based capsules with semipermeable membrane (***Gupta et al., 2014***).

Nanoerythrosomes were prepared by reducing the size of erythrocyte ghosts containing fasudil (***Gupta et al., 2014***). In this study, three different size reduction techniques were used to produce nanosized erythrosomes: 1. bath sonication, 2. probe sonication, 3. extrusion (***Gupta et al., 2014***). Sizing with sonication gave polydispersed particles and significantly decreased entrapment efficiency (***Gupta et al., 2014***). However extrusion performed with polycarbonate membranes of different sizes had minimal effect on entrapment efficiency indicating little or no disruption of cells (***Gupta et al., 2014***). This study has shown that produced nanoerythrosomes can be easily taken up by rat pulmonary arterial smooth muscle (PASM) cells, can extend the half-life of fasudil and appear to be safe for intratracheal delivery (***Gupta et al., 2014***). Additionally, the final formulation had satisfying entrapment efficiency, in vitro release and stability profiles (***Gupta et al., 2014***).

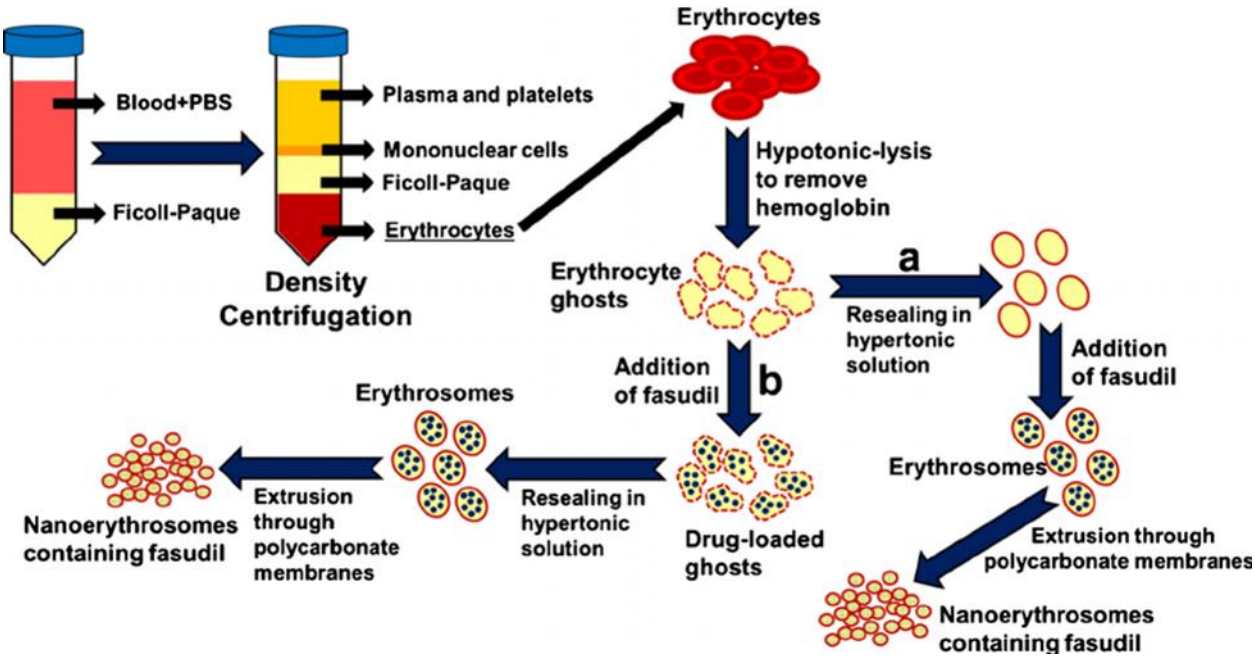

Figure 6. Schematic representation for preparation of nanoerythrosomes from rat whole blood using hypotonic lysis followed by extrusion method. (***Gupta et al., 2004***).

Recently Agnihotri et al. developed artesunate-loaded nanoerythrosomes that offered improved pharmacokinetic profile with assurance of increased therapeutic efficacy (***Agnihotri et al., 2015***). According to the current opinion, nanoerythrosomes represent "golden eggs in novel drug delivery systems" taking into account their tremendous potential (***Nangare et al., 2016***).

EXPERIMENTAL PART

1. Controlled drug delivery system based on mesoporous silica

1.1. Ordered Mesoporous Silica

Ordered mesoporous silica (OMS) material was synthesized according to the synthesis procedure described by Jammaer et al. (***Jammaer et al., 2009***). Briefly, a citric acid buffered solution Pluronic® P123 (BASF, Ludwigshaven, Germany) was prepared overnight. To this surfactant solution, a sodium silicate (NaSi) solution was added and the mixture was stirred. The final synthesis mixture was kept nonstirred 24 h at room temperature followed by 48 h at 75 ºC. The material is then filtered, washed with deionized water, and dried. Finally the OMS material was calcined under ambient conditions at 550 ºC.

1.2. Fenofibrate Loading Procedure

Loading of fenofibrate into the OMS material was carried out with an automated granulator (Mipro 900, ProCepT, Zelzate, Belgium). Pure API (8.19 g) was dissolved in 80 mL of dichlormethane. The API solution was filtered through a 0.45 µm PTFE filter and added to the OMS in the granulator bowl in two steps using an atomization nozzle. Each dosing step was followed by a drying step (30°C) of 45 minutes. The loading of the OMS was 29% (w/w) of API. The loaded material was further dried for 3 days in circulating air oven at 25°C to remove residual dichloromethane.

1.3. Drug Load Quantification

In order to determine the amount of fenofibrate loaded into the OMS, approximately 7.5 mg of the loaded silica was weighed in a volumetric flask of 25.0 mL. Dimethyl sulfoxide (5.0 mL) was added and then filled up with acetonitrile. The suspension was sonicated for 30 minutes in a

Branson 8200 ultra-sonic bath, filtered afterwards using a 0.45 µm PTFE membrane filter (VWR International, USA) and analyzed with high performance liquid chromatography (HPLC) with UV detection.

1.4. Dosage Form

The fenofibrate loaded OMS was blended with silicified microcrystalline cellulose (Prosolv® HD 90, JRS Pharma) and croscarmellose sodium (AcDiSol®, FMC Biopolymer, USA), see Table 6. Blending was performed in the MiPro Granulator. Two capsule formulations (eq. 33.5 mg fenofibrate and eq. 16.75 mg fenofibrate) were compared to the commercially available forms Lipanthyl® and Tricor®. All formulations were evaluated *in vitro* prior to the *in vivo* dog and human study.

Table 6. Compositions of Fenofibrate-Loaded OMS Capsules.

Dosage Form	Formac OMS Capsules	
	Eq. 33.5 mg (%)	Eq. 16.75 mg (%)
Fenofibrate loaded OMS	57.76	50.20
Acetone*		
Sodium crosscaramelose	10.00	10.00
Silicified microcrystalline cellulose	32.34	39.80

*Not present in the final formulation.

1.5. In Vitro Dissolution Study

To study the release of fenofibrate out of the OMS carrier, the loaded formulations were suspended in 900mL 0.1N HCl (VWR Prolabo, Belgium) + 0.1% Tween 80 (Acros Organics, Belgium). Dissolutions were performed using a Hanson Vision® Elite 8 dissolution apparatus (USP II – Padlle). The paddle speed was set at 50 rpm. The experiment was performed at 37 °C. Samples of 1.0 mL were taken at 5, 10, 15, 30, 60 and 120 minutes and filtered over a 0.45µm PTFE membrane filter (VWR International, USA). The volume withdrawn is replaced by the

same amount of fresh medium. The samples were diluted and analyzed using HPLC with UV detection (see below).

1.6. High Performance Liquid Chromatography (HPLC)

Measurements of the assay and *in vitro* dissolution samples were performed using an isocratic HPLC method. The HPLC system was a VWR Hitachi Elite LaChrom with a L-2200 UV detector set at 287 nm. The analytical column used is a Lichrospher 60 (125mm – 4,6mm; 5µm). A mobile phase made up of 25mM ammonium acetate buffer pH 3.5 / acetonitrile (30:70; v:v) with a flow rate of 1mL/min was used. The column temperature was set at 30°C and the injection volume was 20µL.

1.7. Preclinical trial in beagle dogs

1.7.1. Analysis of plasma samples

A bioanalytical method was used for the quantification of fenofibrate and fenofibric acid in the dog oxalate plasma in the range of 0.02 – 4.00 ng/mL and of 10.00 - 2000.00 ng/mL, respectively. The dog plasma samples were thawed at room temperature, homogenized and centrifuged. 50 µL of supernatant was mixed with 450 µL of a solution of the internal standard (fenofibrate-d6 (0.05 ng/mL) and fenofibric acid-d6 (1250 ng/mL)) in acetonitrile and subsequently centrifuged at high speed. For the analysis of fenofibric acid, 50 µL of the elution was then transferred to a 96-well plate, mixed with acetonitrile/water (90:10 v/v), shaken for 5 minutes and then 6.0 µL was injected into UPLC-MSMS system. For the analysis of fenofibrate, the rest of the elution was evaporated at 50 ºC, dissolved in 50 µL acetonitrile/water (90:10 v/v), shaken for 5 minutes and then 10.0 µL was injected into UPLC-MSMS system. The targeted compounds were analyzed on Acquity UPLC BEH C18 column (50*2.1mm, dp = 1.7µm), applying acetonitrile:water:ammonium acetate (10:85:5, v/v/v) and (90:5:5, v/v/v) in the linear gradient mode as mobile phase. Quantitation method was based on peak area ratio and the response versus concentration data were fitted using quadratic regression with $1/x^2$ weighting.

1.7.2. Pharmacokinetic analysis

Pharmacokinetic (PK) parameters were evaluated after single oral administration in 4 male Beagle dogs (31 – 36 months old, body weight range 10.8 – 11.8 kg; Marshall BioResources, Italy).

From all animals approximately 4 mL blood samples were taken from the jugular vein using vacutainers and potassium oxalate/sodium fluoride (Greiner Bio-One, Bad Haller, Austria) as anticoagulant. Blood was sampled at predose and 0.5, 1, 1.5, 2, 4, 6, 8, 12 and 24 h after dosing. Within 30 minutes after sampling, blood was centrifuged at 5 ºC. Immediately after centrifugation, plasma was stored in labeled polypropylene tubes at – 75 ºC prior to analysis.

This study protocol was reviewed and agreed by the Animal Welfare Officer and the ethical Committee of NOTOX (00 – 34) as required by the Dutch Act on Animal Experimentation (February 1997). The animals were treated in accordance with the Directive 2010/63/EU.

The study procedures were based on the following guidelines, recommendations and requirements:

- Workshop/Conference Report – Quantitative Bioanalytical Methods Validation and Implementation: Best practices for Chromatographic and Ligand Binding Assays. C. T. Viswanathan, et al. The AAPS Journal, 9, 2007, E30 – E42.
- Guidance for industry: Bioanalytical Method Validation. US Department of Health and Human Services, Food and Drug Administration, Center for Drug Evaluation and Research (CDER) and Center for Veterinary Medicine (CVM). May 2001.

All PK parameters were calculated from the curves constructed from individual animals, using the WinnonLin 5.2 program. Noncompartmental analysis was applied using the extravascular model. The lower limit of quantification (LLOQ) of fenofibrate was 0.020 ng/mL and for fenofibrate acid the LLOQ was 10.00 ng/mL. All values below the LLOQ after C_{max} were excluded from the pharmacokinetic evaluation. If a value was below the LLOQ prior to C_{max}, than this value was set to 0 ng/mL. In case several intermediate not quantifiable concentrations were present, all not quantifiable concentrations and all following time points were excluded from the kinetic evaluation. In case one intermediate not quantifiable concentration was present,

this time point was excluded was excluded from the kinetic evaluation. Nominal sampling times were used (deviations were less than 20 %).

The following pharmacokinetic parameters were calculated:

- C_{max} – maximum observed plasma concentration.
- C_{last} – last measurable plasma concentration.
- t_{max} – time point at which maximum plasma concentration was reached, assessed directly from the data.
- t_{last} – time point of last measurable plasma concentration.
- AUC_{last} – area under the plasma concentration-time curve from time of administration until the last measurable plasma concentration (t_{last}), calculated using the linear trapezoidal rule (for both parent and metabolite).
- AUC_{∞} - area under the curve after a single dose from time of administration until infinity, calculated as $AUC_{last} + C_{last}/\lambda_z$ where C_{last} is the last measurable concentration. If the data set did not allow extrapolation to infinity, then the AUC up to the last measurable time point was calculated. Extrapolations of more than 15% of the total AUC were reported as approximation.
- λ_z – elimination rate constant, determined by linear regression of the terminal points of the In-linear concentration-time curve.
- $t_{1/2}$ – elimination half-life, calculated as $\ln(2)/\lambda_z$. The following requirements had to be met for an acceptable calculation of $t_{1/2}$:
    1. at least three time points had to be available to be used in the calculation
    2. correlation coefficient (r^2) was at least 0.9
    3. span of time points used in $t_{1/2}$ was at least twice the calculated value of $t_{1/2}$

Values that did not meet these criteria were reported as approximations. C_{max} and AUC values were also normalized to a dose of 1 mg/kg.

A descriptive statistical analysis was performed (mean values and standard deviations). A one-way ANOVA was performed for the dose-normalized values of C_{max} and area under the curve (AUC_{last}) for each compound to determine a possible statistical difference between the various compounds.

1.8. Stability program

OMS capsules containing fenofibrate (33.5 mg) were stored at 25 ºC/60% relative humidity (RH) and 40 ºC/75% RH in both open and closed conditions. After 1, 2 and 6 months of storage, the formulation was evaluated for *in vitro* release (Hanson Vision® Elite 8) and the absence of crystallinity (DSC, Mettler-Toledo DSC 822e; Mettler-Toledo, Zaventem, Belgium). For the purpose of the thermal analysis, about 3 - 4 mg of the sample was placed in DSC aluminum pans and heated from -30 to 150 ºC with constant heating rate of 10 ºC/min.

1.9. Clinical trial

1.9.1. Subjects

The clinical trial was conducted at SGS Life Science Services (Clinical Pharmacology Unit Antwerp, Belgium). Details of the subject population are provided in Table 7.

Table 7. Demographic data by treatment sequence (safety population).

Parameter	Sequence AB N=6	Sequence BA N=6	All subjects N=12
Age, years			
Median (range)	49 (40-55)	43 (21-49)	46.5 (21-55)
Height, cm			
Median (range)	178 (168-192)	180 (175-192)	178 (168-192)
Weight, kg			
Median (range)	80.5 (73-101)	80 (66-90)	80 (66-101)
BMI, kg/m^2			
Median (range)	25.9 (24.4-27.4)	24.5 (20.8-27.8)	25.2 (20.8-27.8)
Sex, n (%)			
Male	6 (100)	6 (100)	12 (100)
Race, n (%)			
Caucasian	6 (100)	6 (100)	12 (100)

N = number of subjects; n = number of subjects with that observation; Treatment A: single oral dose of 33.5 mg Fenofibrate-OMS; Treatment B: single oral dose of 67 mg Lipanthyl®.

The subjects were in a good health as assessed by detailed medical history, physical examination, 12-lead electrocardiogram (ECG), clinical laboratory tests and urinary drug screen. All subjects were non-smokers. The time span between the screening visit and the last follow-up visit was at most 6 weeks. Subjects were to discontinue all medications, except occasional paracetamol (maximum dose of 2 g/day and maximum of 10 g/2 weeks), at least 2 weeks prior to the first study drug administration. In addition, subjects were to agree not to use any medications during the course of the study. Subjects were not to take any alcohol and grapefruit-containing foods from 48 hours before to 96 hours after each study drug administration or xanthine-containing beverages and food from 12 hours before to 96 hours after each study drug administration. Subjects with a history of hypersensitivity to fenofibrate or a significant allergic reaction to any drug, an immunosuppressive condition, malignancy within the past 5 years, significant blood

loss within 8 weeks prior to study start, diseases of the gastrointestinal tract, liver, kidneys or any other conditions known to interfere with the absorption, distribution, metabolism or elimination of drugs were excluded from the study. Individuals with active drug or alcohol abuse within 2 years prior to the initial study drug administration or consumption of large quantities of coffee or tea were also excluded.

All subjects were Caucasian males. The subjects' median (range) age was 46.5 (21-55) years. Their median (range) BMI was 25.20 (20.8-27.8) kg/m². There were no relevant differences in demographic data between the treatment sequences. Serology screening tests for hepatitis B and C and HIV, urine drug screening, and alcohol breath tests at screening were negative for all subjects. A wide range of medical history was reported across the subjects; none of these were thought to have influenced the course of the study. Concomitant diseases were reported in 1 subject (16.7%) in each treatment sequence. Both were Gilbert's Disease. Previous medication was reported in none of the subjects and 1 subject (8.3%) was administered Ditemer (tetanus, diphtheria vaccine) in Dosing Period 2 due to a head injury reported as an AE in Dosing Period 1.

In each of the two dosing periods, the subjects were admitted to the clinical centre on Day -1 and remained hospitalized until approximately 24 hours after dosing (Day 2). Thereafter, subjects were to return to the clinical centre on Days 2 (evening), 3, 4, and 5 for post-dose bioanalysis blood sampling. A follow-up visit was planned between 5 to 7 days after the last intake of study drug. The two dosing periods were separated by a 7-day wash-out period. All study drug intakes occurred under the supervision of the investigator or his designee. The study drugs were administered between 8 and 10 a.m. In each dosing period, the subjects received an evening meal on Day -1, at least 9 hours before intake of study drug, and a lunch, snack, and evening meal on Day 1. During confinement at the clinical centre, no food intake other than the standard meals was authorized. On the days of blood sampling for bioanalysis water intake was prohibited from 2 hours pre-dose until 2 hours post-dose, with the exception of the water intake of 200 mL with dosing. Water was available ad libitum from 2 hours post-dose onwards. Subjects who discontinued the study prior to completion of the scheduled study procedures for reasons such as adverse events (AE) or withdrawal of consent were invited for a follow-up visit 5 to 7 days after the last study drug intake. In case of an AE, the appropriate follow-up procedure was applied.

1.9.2. Safety monitoring

In each dosing period, subjects underwent a physical examination, an assessment of vital signs and a 12-lead ECG recording on Day 1 pre-dose. Blood and urine sampling for clinical laboratory tests (haematology, serum biochemistry and urinalysis) were performed in fasting conditions. All assessments were performed within 2 hours pre-dose. Subjects were discharged from the clinical centre upon agreement of the investigator on Day 2, after safety assessment (blood and urine samples for clinical laboratory tests, ECG, vital signs) and the last blood sampling for bioanalysis. The subjects returned to the clinical centre 5 to 7 days after the last dose administration for the follow-up visit for a physical examination and vital signs (HR, SBP, DBP, oral body temperature) assessment. Blood and urine samples for clinical laboratory tests were taken in fasting conditions. Any adverse or unusual event occurring from the study inclusion date to the last subject's visit, whether it is observed by the investigator, his staff or the subject, was recorded.

1.9.3. Blood sampling

Blood samples for the determination of fenofibric acid in plasma were taken at pre-dose and at 30 minutes and 1, 2, 2.5, 3, 3.5, 4, 5, 6, 7, 8, 12, 16, 24 hours (Day 2 morning), 36 hours (Day 2 evening), 48 hours (Day 3), 72 hours (Day 4) and 96 hours (Day 5) post-dose in each dosing period. Samples on Days 1 and 2 (morning) were taken during the subject's stay in the clinic and the subjects needed to return to the clinic for blood sampling on Days 2 (evening), 3, 4, and 5.

Each sample (4 mL) was taken by venipuncture (or indwelling cannula) in the arm and collected in vacuum tubes containing lithium heparin (Venoject green top or equivalent). Samples were chilled immediately in an ice bath and centrifuged (at 4-8°C for 10 minutes at ca. 1500 g) within 30 minutes after blood collection. The plasma obtained was transferred into two polypropylene tubes (around 500 µL of plasma per tube) and stored at -20°C after appropriate labelling.

One aliquot was shipped on dry ice to the analytical laboratory where the plasma was stored at -20°C pending analysis. The remaining sample was shipped separately and was stored for back-up analysis.

1.9.4. Analysis of plasma samples

An analytical method for the determination of fenofibric acid in lithium heparinized human plasma was developed and validated by SGS Life Science Services, Wavre, Belgium. The frozen plasma samples were thawed at room temperature, homogenized and centrifuged. 20 µL of the supernatant was mixed with 20 µL of a solution of the internal standard (fenofibric acid d_6) and 70 µL of acetonitrile and subsequently centrifuged at high speed. 20 µL of the supernatant was then transferred to a 96-well plate, mixed with 80 µL of a 0.05% v/v formic acid solution and centrifuged. 10 µL of the supernatant layer was then analyzed by LC/MS-MS. The LC/MS-MS system consisted of an Agilent 1100 series HPLC system (Agilent, Brussels, Belgium) equipped with a CTC HTS PAL autosampler (Cohesive Technologies, Milton Keynes, U.K.) and connected with a API 4000 mass spectrometer in the negative ion mode (AB Sciex, Nieuwerkerk a/d Ijssel, The Netherlands). The analytical column used was a Chromolith Fastgradient, RP-C18, 50 x 2.0 mm I.D. (VWR, Leuven, Belgium). A gradient program was followed with two mixtures of acetonitrile and a 0.05 % v/v aqueous solution of formic acid: 10/90 v/v and 90/10 v/v.

The analytical method was validated with a lower limit of quantification (LLOQ) of 10 ng/mL and an upper limit of quantification (ULOQ) of 5000 ng/mL. The response versus concentration data were fitted with a first order polynomial with $1/C^2$ weighting. The within and between-series precision, expressed as the coefficient of variation (CV) and accuracy expressed as the relative error of measurement (RE), were both below 20 % at the LLOQ and below 15% at the higher concentrations which is in accordance with the preset criteria. The average carry-over was less than 20% for the analyte and less than 5% for the internal standard and the normalized matrix factor was within the acceptance criteria. The average extraction recovery was consistent over the investigated range and the 10-fold dilution of the samples did not affect precision or

accuracy of the analytical results. The stability of fenofibric acid was assessed for various conditions of use and storage of the plasma samples and extracts.

1.9.5. Pharmacokinetic analysis

The pharmacokinetic analysis of the bioanalytical data was performed by SGS Life Science Services, Wavre, Belgium using the SAS version 9.1.3. WinNonlin version 5.2. The following pharmacokinetic parameters were determined from the individual plasma concentration vs time profiles:

C_{max}	Maximum observed plasma concentration
C_{max}/dose	C_{max} normalized to unit dose (1 mg)
t_{max}	Time of occurrence of C_{max}
AUC	Area under the plasma concentration versus time curve from time zero to the last sampling time at which concentrations were at or above the limit of quantification [AUC_{0-t}], up to 24 hours post-dose [AUC_{0-24h}], or up to 48 hours post-dose [AUC_{0-48h}] calculated by the linear trapezoidal rule
AUC_{0-t}/dose	AUC_{0-t} normalized to unit dose (1 mg)
AUC_{0-24h}/dose	AUC_{0-24h} normalized to unit dose (1 mg)
AUC_{0-48h}/dose	AUC_{0-48h} normalized to unit dose (1 mg)
$AUC_{0-\infty}$	Area under the plasma concentration versus time curve from time zero to infinity, calculated from $AUC_{0-t} + (C_t/\lambda_z)$, where C_t is the last observed quantifiable concentration
$AUC_{0-\infty}$/dose	$AUC_{0-\infty}$ normalized to unit dose (1 mg)
λ_z	Apparent terminal elimination rate constant

$t_{1/2,\lambda z}$	Apparent terminal elimination half-life, calculated from $(\ln 2)/\lambda_z$

Calculation of pharmacokinetic parameters was performed using the actual sample collection times. If the actual sampling time of an individual sample was greater than 20% different from the scheduled sampling time, the individual concentration was excluded from the descriptive statistics for the concentration-time table and mean concentration-time graphs. If the percentage of the AUC extrapolated exceeded 20% of the total $AUC_{0-\infty}$, the $AUC_{0-\infty}$ was excluded from any statistical evaluation. λ_z was to be calculated using at least 3 data-points not including the peak plasma concentration (C_{max}). The acceptable adjusted R^2 value was ≥ 0.85. If this condition was not fulfilled, then the related parameters were not tabulated.

1.9.6. Statistical methods

Descriptive statistics applied in this study included the number of data (N), arithmetic mean, standard deviation (SD), coefficient of variation (CV), standard error (SE), % confidence interval (CI) of the mean, median, minimum and maximum. For continuous parameters, descriptive statistics were presented when the number of non-missing data points was greater or equal to 2. All statistical inferential tests were interpreted at the 5% two-sided significance level.

Strict statistical criteria were not used to determine the sample size for this study. The number of subjects included in this study should give reasonable precision around the estimates derived for the pharmacokinetic analysis. Allocation of each subject to one of the 2 treatment sequences (AB and BA) was described in a randomization list prepared by the Biostatistics Department of SGS Life Science Services using SAS software (SAS Inc., Cary, NC, USA).

The two-period, two-sequence cross-over design with phases of treatment separated by an adequate wash-out period was chosen in such a manner that any formulation effect could be distinguished from other effects. The cross-over design provided a within-subject comparison for the treatments.

Comparison between treatments was assessed on ln-transformed parameters (C_{max}/dose, AUC_{0-t}/dose, AUC_{0-24h}/dose, AUC_{0-48h}/dose, $AUC_{0-\infty}$/dose, $t_{1/2,\lambda z}$) by means of a mixed-effect analysis of variance (ANOVA) with treatment, sequence, and period as fixed effects, and subject (nested within sequence) as random effect. Point estimates were calculated as the geometric mean of the individual ratios of each parameter for the test treatment (33.5 mg Fenofibrate-OMS) relative to the reference treatment (67 mg Lipanthyl®) and expressed as a percentage. The 90% CIs of the point estimates (PE) were calculated using the mean square error of the ANOVA. As t_{max} is a discrete variable dependent on selected blood sampling times, the same comparison (33.5 mg Fenofibrate-OMS versus 67 mg Lipanthyl®) was assessed using a non-parametric test (Koch procedure). The 90% CI was calculated by the Hodges-Lehmann method.

1.9.7. Regulatory compliance

This study was conducted in accordance with the ethical principles that have their origin in the Declaration of Helsinki and the International Conference on Harmonization (ICH) Note for Guidance on Good Clinical Practice (GCP) (CPMP/ICH/135/95) and with applicable local requirements. Prior to the performance of any study-specific procedure, written informed consent was obtained from each subject. The final clinical trial protocol (CTP) as well as the informed consent and other information that required pre-approval were reviewed and approved by an Independent Ethics Committee (IEC; *Commissie voor Medische Ethiek – Ziekenhuisnetwerk Antwerpen* – ZNA/OCMW, Antwerp, Belgium) according to specifications outlined in the applicable regulations.

2. Controlled drug delivery system based on erythrocyte ghosts

2.1. Erythrocyte samples

Porcine slaughterhouse blood and human outdated blood were used as a starting biological material for erythrocytes isolation. Porcine blood was from the slaughterhouse "PKB Imes" in Belgrade, Serbia. Transport and treatment of the Swedish Landrace swine in the slaughterhouse was in obedience to the National Regulation on Animal Welfare, and performed in compliance with institutional animal care and use policies. The porcine blood collection and transport was done according to the protocol described in Kostic et al. (Kostic et al., 2015). The human erythrocytes concentrates were from Institute for Transfusiology and Hemobiology, Military Medical Academy, Belgrade, Serbia. The blood was from healthy blood donors. The erythrocytes were enriched by the standard procedure and preserved in SAGM solution (each 100 mL contains 0.900 g dextrose monohydrate, 0.877 g sodium chloride, 0.0169 g adenine, and 0.525 g mannitol) for 42 days at 4 °C. The outdated cell packs were anonymized prior to distribution, and the link to the donor was broken. If were not used for the research, these cell packs would be discarded after the expiration date. Preparation of packed porcine and human erythrocytes suspensions were performed as described in Kostić et al. (***Kostic et al., 2015***).

2.2. Erythrocyte ghosts' preparation and encapsulation (loading) with SD

In order to prepare erythrocyte ghosts, porcine and human erythrocytes were undertaken to the osmosis based process-gradual hypotonic hemolysis (***Kostic et al., 2015***).

According to known literature data regarding the different osmotic properties of porcine and human erythrocytes (***Kostic et al., 2015.; Doucet et al., 2004***) hypotonic 35 mM sodium phosphate/NaCl buffer for porcine and 5 mM sodium phosphate buffer for human erythrocytes

were introduced gradually for 30 min with flow rate 150 mL/h in 50 mL of packed erythrocytes in PBS (with hematocrit value of 0.5) and continuously mixed. After the hemolysis the erythrocyte ghosts were isolated, washed three times in hypotonic solution used in gradual hemolysis process and finally in isotonic PBS solution.

For the purposes of encapsulation, gradual hypotonic hemolysis process was performed as previously described but in the presence of SD in concentration of 120 mg/L. After the hemolysis, the erythrocyte ghosts were precipitated (40 min centrifugation at 3220xg, at 4°C), supernatant containing hemoglobin was discarded and erythrocyte ghosts were washed four times in the buffer solution used for the gradual hypotonic hemolysis process. Densely packed erythrocyte ghosts in the volume of 2 mL were incubated with 8 mL of PBS containing 120 mg/L SD, 90 minutes at 37 °C. After the incubation, samples were stored at 4 °C over the night. The next day, erythrocyte ghosts were precipitated by 40 min centrifugation at 3220xg. The erythrocyte ghosts in the volume of 220 µL were dispersed in test tubes containing 1780 µL of hypertonic 2xPBS solution with SD (120 mg/L) and 0.01% glutaraldehyde and then incubated for 30 minutes at 37 °C in test tubes. The encapsulated ghosts were precipitated by 5 min centrifugation at 10000xg and washed out twice in PBS solution without SD, to remove non-encapsulated SD.

2.3. Sample preparation for qualitative and quantitative analysis of encapsulated (loaded) SD

From the final suspension of encapsulated erythrocyte ghosts, 100 µL was taken and dispersed in 2 mL of distilled water and mixed with 2 mL of methanol. Test tubes were stored at the room temperature for 30 minutes and then centrifuged 15 minutes at 14000xg. Obtained supernatants were filtered through the filters with pore size 0.2 µm into the vials and used for the below described HPLC analysis.

2.4. Qualitative and quantitative analysis of encapsulated SD

SD is quantified in samples of loaded ghosts using an UHPLC/DAD/-HESI-MS/MS method. Separation, identification, and quantification of diclofenac was performed using Dionex Ultimate 3000 UHPLC system (ThermoFisher Scientific, Bremen, Germany) coupled to diode array detector (DAD), and connected to TSQ Quantum Access Max triple-quadrupole mass spectrometer (ThermoFisher Scientific, Basel, Switzerland). Elution was performed at 30 ºC on Hypersil gold C18 column (50 × 2.1 mm) with 1.9 μm particle size (ThermoFisher Scientific, USA). The mobile phase consisted of (A) water + 0.1% formic acid, and (B) acetonitrile (MS grade, Fisher Scientific UK, Leics, UK), which were applied in the gradient elution previously described in Kostić et al. (***Kostic et al., 2015***) The flow rate was set to 0.4 mL min^{-1} and the detection wavelengths to 230 and 280 nm. The injection volume was 10 μL. All the analyses were performed in triplicate.

Mass spectrometer was equipped with an heated electrospray ionization (HESI) source, and was used with vaporizer temperature kept at 350 °C, and ion source settings as follows: spray voltage 3500 V, sheet gas (N2) pressure 28 AU, ion sweep gas pressure 0 AU and auxiliary gas (N2) pressure at 4 AU, capillary temperature at 270 °C, skimmer offset 0 V. Mass spectrometry data were acquired in negative mode, in m/z range from 100 to 1000. Collision-induced fragmentation experiments, including product ion scanning (PIS) and selected reaction monitoring (SRM), were performed using argon as the collision gas, and collision energy (cE) was set to 20 eV. SRM experiment for quantitative analysis was performed by using two MS2 fragments, which were previously defined as dominant in PIS experiments. Quantification of SD was based on the calibration curve of pure compound. Total amount of SD in each sample was evaluated by the calculation of peak areas, and is expressed as ng ml^{-1}. Chromeleon Xpress softver (Thermo Fisher Scientific, Bremen, Germany) was used for used for the data acquisition and method/run control.

2.5. Loading parameters

Two parameters were determined and were used for evaluation of loading efficiency of the method (***Hamidi et al., 2011***):

1. Loaded amount: The amount of SD encapsulated in 0.1 mL of the final packed erythrocyte ghosts.
2. Encapsulation efficiency: The percent ratio of loaded amount of SD to amount added per 0.1 mL during the encapsulation process.

2.6. SD effect on gradual hypotonic hemolysis

In order to investigate the effect of SD on gradual hypotonic hemolysis process, the 1 mL aliquots of the erythrocyte suspension were sampled at the beginning of the process, and in 1 minute time interval for the first 5 minutes of hemolysis, in 3 minutes time intervals for the next 15 minutes, and in the time intervals of 5 minutes by the end of the experiment.

As a control, the same test was performed in gradual hypotonic hemolysis processes without SD. The samples were centrifuged at 15 000 g for 20 minutes, and hemoglobin and potassium content in the supernatants were determined by cyanmethemoglobin method (***Van Asendelft et al., 1984***) and ion selective electrode, respectively. The percent of hemoglobin and potassium release were determined in reference to the total amount released at the end of gradual hypotonic hemolysis (100% hemolysis).

2.7. Particle size analysis

Particle size and size distribution analysis of starting erythrocytes and resulting empty and SD loaded ghosts was performed by using laser-based particle size analyser Mastersizer Hydro 2000S (Malvern Instruments Ltd, U.K.). For this purpose, the samples were analysed while suspended in isotonic PBS in a suitable concentration, according to instrument operation conditions.

2.8. FT-IR analysis

The FT-IR spectra of SD, lyophilized empty and SD loaded erythrocyte membranes were obtained by means of Fourier transform infrared spectroscopy (FTIR spectrometer Bomem MB, series Hartmann & Braun) with a resolution of 2 cm^{-1}, by the KBr method. The spectra were taken in the wavelength region 4000–400 cm^{-1} at room temperature.

2.9. Zeta potential determination

Zeta potential determination of starting erythrocytes, empty and encapsulated human and porcine erythrocyte ghosts were performed using a Zetasizer Nano ZS (Malvern Instruments, U.K.) apparatus operating at λ= 633 nm produced by an He–Ne laser at scattering angle 173° at 25± 0.1 °C. The calculation of zeta potential values of diluted samples (according to the manufacturer instructions) were done by computer software from electrophoretic mobility using the Smoluchowski equation: $\xi = \mu\eta/\varepsilon$, where ξ is the zeta potential, μ is the mobility, η is the viscosity of the solution, and ε is the dielectric constant of the solvent. The results represent the average value of three consecutive measurements for each sample.

2.10. Atomic force microscopy

In order to perform morphological examination by AFM, the samples were fixed onto the surface of a coverslip by incubation with 2.5% glutaraldehyde in PBS for 1 hour. The samples were further fixed with osmium tetroxide (0.1 %) in PBS for 1 hour. Osmium tetroxide was removed by washing twice in PBS. The drying of samples was performed with an increasing concentrations of ethanol (10%, 30%, 50%, 70%, 95% and 100%) and finally in acetone. Topographic AFM measurements were performed in the semi-contact mode under ambient conditions using the NTEGRA Prima system from NT-MDT (NT-MDT Co. Moscow, Russia). NSG01 probes from NT-MDT with a typical tip curvature radius of about 6 nm and a typical force constant of 5 N/m were used. Topographic images were processed using the instrument-

equipped software by the plane subtraction or by the fitting with the first order lines. For the calculation of the root-mean-square (RMS) of the surface roughness, only cell surfaces were selected from AFM images and then RMS was directly generated by the instrument software, using a total of 10 cell measurements for each ghost preparations.

2.11. Drug release

To examine the release behaviour of SD from porcine and outdated human erythrocyte ghosts, 100 µL of densely packed suspension in each test tube was diluted to 1 mL by adding 900 µL of PBS solution. The tubes (n=5) were mixed on the orbital shaker at 240 rpm and incubated at 37 ºC. After 1, 2, 24, 48 and 96 h one of the samples was harvested and after centrifuging at 10 000 g for 10 min, 100 µL of the supernatant was used for the HPLC analysis. These experiments were carried out in triplicate and the percent of SD release was determined in reference to a completely lysed sample (100% release). Due to possible microbial contamination drug releasing test was not performed longer than 4 days.

2.12. Statistical analysis

Experimental results were mean ± SD of at least three measurements. Statistical analysis of the data regarding antihemolytic effect of SD, number based diameter distribution and ζ-potential was performed by Student t test with the Origin 9.0 Statistical Analysis Software. The values $p < 0.05$ were regarded as significant.

2.13. Two photon excitation fluorescence microscopy of erythrocytes and erythrocyte ghosts

Imaging of erythrocytes and empty erythrocyte ghosts was performed at 730 nm excitation wavelength using the home-made two-photon experimental set up developed by Rabasovic et al. (***Rabasovic et al., 2015***).

The excitation wavelength is of the great importance in this study and it has to be carefully selected according to its availability and the properties of the samples. Selection of the wavelength can significantly affect the chemical selectivity of the imaging, providing excitation of the specific and desired objects, and quality of the images by means of excitation efficiency 1 and fluorescence strength. The excitation wavelength in this study is selected to be 730 nm by the following criteria:

- Different excitation wavelengths within Ti:Sapphire laser tuning range (700-1000nm) were tested. Obtained excitation spectrum is consistent with spectrum shown in study of Zheng et al., i.e. the excitation is the most efficient for the shortest wavelengths (***Zheng et al., 2010***).
- The two photon excitation signal from hemoglobin at 650 nm excitation wavelength is reported to be more efficient but we were not able to utilize shorter wavelengths than 700 nm due to laser tuning range (700-1000nm). Also, there is a significant leakage of the laser light to the PMT for wavelengths shorter than 730 nm. The cut-off wavelength of the dichroic mirror (hot mirror M254H45, Throlabs, Inc) is (700±10) nm with transmission >97% for wavelengths longer than 710 nm, whereas full width at half maximum of the laser line is approximately 12 nm.
- The two photon excitation signal from glass (coverslips and microscope slides) is pronounced for wavelengths shorter than 730 nm. Thus, 730 nm is the shortest possible choice for the excitation wavelength to produce still high quality images.

Erythrocytes (hematocrit 5% i.e. 15 5% suspension) and ghosts in amount of 20 μL were allowed to settle onto a microscopic slide and covered by coverslips.

RESULTS AND DISCUSSION

1. Controlled drug delivery system based on mesoporous silica

1.1. Preclinical trial in beagle dogs

In this study, two OMS formulations - Formac capsules, with different content of fenofibrate (33.5 and 16.75 mg) were compared with two referent systems Lypanthil® and Tricor® in terms of *in vitro* release and systemic exposure of fenofibrate and its metabolite when administered orally to dogs. The release profiles of the examined concepts are presented in Figure 7. The amount released of fenofibrate from the nanosized product Tricor® was 7.50 mg after 5 min. After 15 min, a steady-state was reached and lasted to the end of the experiment. The microsized product Lipanthyl® showed initial burst release with only 0.40 mg released after 5 minutes, reflecting very low solubility of the drug. It reached its maximum release after 120 min. On the other hand, OMS capsule containing the same amount of fenofibrate (33.5 mg), had higher initial burst release (0.72 mg after 5 min). The progress of the OMS capsule (eq. 16.75 mg) followed OMS capsule (eq. 33.5 mg) but with approximately twofold lower concentrations at each time point. At the end of the experiment the amount of fenofibrate released from Lipanthyl® and Tricor® was approximately 30 % from the initial dose. Both OMS capsules containing 33.5 and 16.75 mg of fenofibrate attained a relatively high release of 66 and 60 % of their dose, respectively. These data clearly illustrate that the slow dissolution kinetics and low water solubility of fenofibrate from the marketed products could be overcome by loading it into OMS.

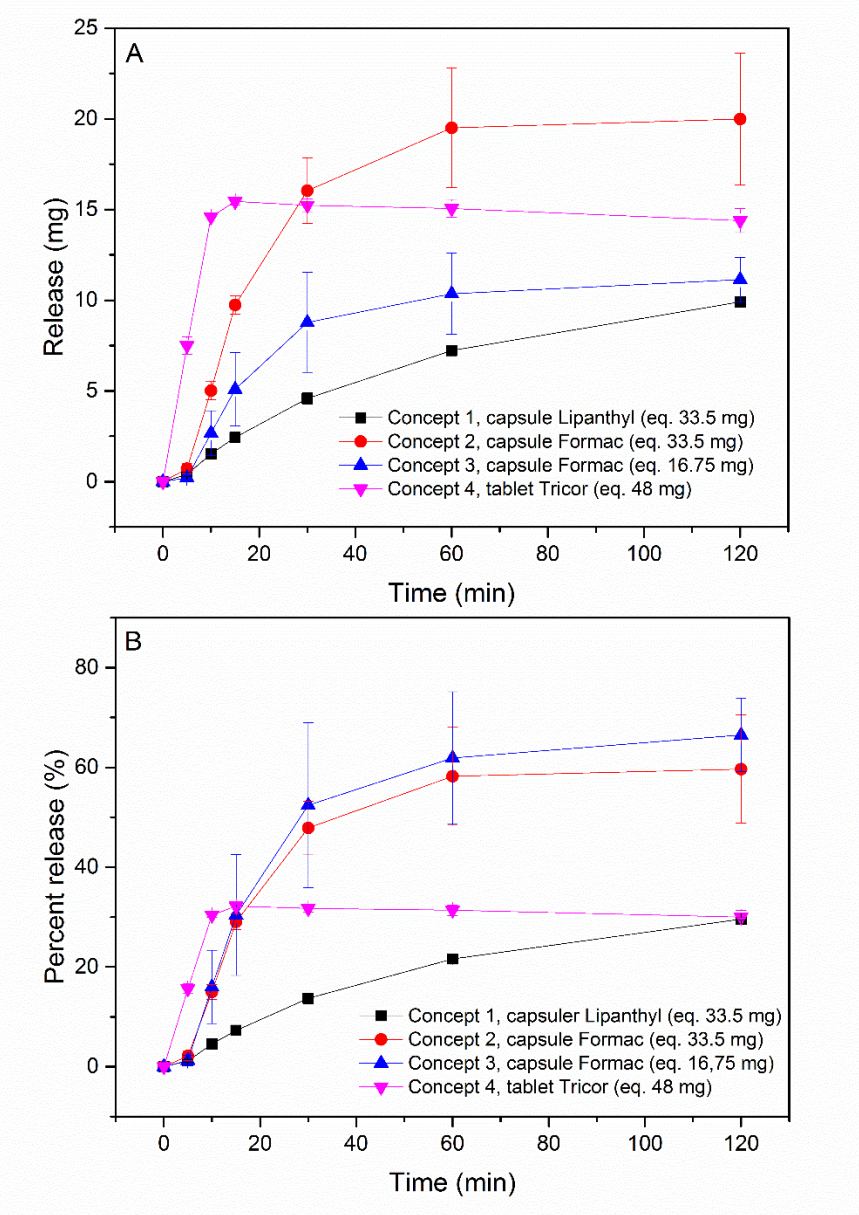

Figure 7. Dissolution/release experiments of Lipanthyl®, Tricor® and two OMS capsules in 900 mL 0.1 N HCl + 0.1 % Tween 80: (A) released amounts in milligrams and (B) percent of the original form released. Results are mean ± SD of three experiments.

Beagle dogs were selected to examine whether the fast *in vitro* release kinetics can be translated into an increased bioavailability of the drug. The animals were dosed orally with fenofibrate at a dose level of 33.5 (Lipanthyl®), 16.75 (OMS based formulation), 33.5 (OMS based formulation) and 48 (Tricor®) mg/animal in respectively period 1, 2, 3 and 4 (Table 2). During the study period no mortality occurred. Body weight of the beagle dogs was not significantly changed.

There were no clinical signs noted during the observation period. Single doses of Fenofibrate-OMS were safe and well tolerated. No relevant differences in safety and tolerability profile were observed when comparing a single dose of Fenofibrate-OMS with Lipanthyl® and Tricor®.

Figure 8 shows the average plasma concentrations versus time curves of fenofibrate and the active metabolite fenofibric acid after dosing. Low concentrations of fenofibrate were measured in plasma, with several peaks. Statistical analysis on the rate and extent of absorption were performed on the dose-normalised data. This dose-normalisation was justifiable due to the demonstrated dose proportionality in the present study between a 16.5 mg and 33.5 mg fenofibrate following oral administration. The mean systemic exposure for fenofibrate expressed as dose normalized AUC_{last} was 0.04, 0.39, 1.03 and 0.88 h*ng/mL for the consecutive periods after oral dosing of fenofibrate. Mean dose normalized C_{max} was respectively 0.056, 0.399, 0.249 and 0.477 ng/mL for period 1 to 4. The mean systematic exposure for fenofibric acid expressed as dose normalized AUC_{last} was 736, 2440, 2780 and 2750 h*ng/mL for the consecutive periods after oral dosing of fenofibrate. After oral dosing t_{max} was fast, varying between 0.5 and 2.0 hours after dosing. Mean dose normalized C_{max} was respectively 145, 623, 524 and 562 ng/mL for period 1 to 4. After oral dosing of fenofibrate the interindividual variation in the PK parameters, as evaluated by % CV, was low to moderate: 38-67%, 25-31%, 31-62% and 10-43% for respectively period 1 to 4.

Table 8. Plasma concentrations of fenofibrate and fenofibric acid of the different concepts.

		Lipanthyl®	OMS capsule 16.75 mg	OMS capsule 33.5 mg	Tricor®
Fenofibrate pharmacokinetic data					
Dose level	mg/kg	2.96 ± 0.119	1.48 ± 0.064	2.97 ± 0.105	4.28 ± 0.131
t_{last}	h	1.5 - 2.0[a]	1.5 - 6.0[a]	4.0 - 12.0[a]	4.0 – 12.0[a]
t_{max}	h	1.0 – 2.0[a]	1.0 – 1.5[a]	1.0 – 8.0[a]	0.5 – 4.0[a]
C_{max}	ng/mL	0.163 ± 0.092	0.591 ± 0.393	0.733 ± 0.476	1.99 ± 2.69
C_{max}[b]	(kg ng)/(mL mg)	0.056 ± 0.033	0.399 ± 0.242	0.249 ±0.162	0.477 ± 0.65
C_{last}	ng/mL	0.098 ± 0.099	0.048 ± 0.024	0.111 ± 0.104	0.048 ± 0.019
AUC_{last}	h ng/mL	0.117 ± 0.065	0.58 ± 0.38	3.0 ± 2.52	3.70 ± 3.66
AUC_{last}[b]	h kg ng/mL/mg	0.04 ± 0.023	0.39±0.26	1.03 ± 0.873	0.88 ± 0.883
Fenofibric acid pharmacokinetic data					

Dose level	mg/kg	2.96 ± 0.119	1.48 ± 0.064	2.97 ± 0.105	4.28 ± 0.131
t_{last}	h	12 – 24[a]	24.0	24.0	24.0
t_{max}	h	1.0 – 1.5[a]	0.5 – 1.5[a]	1.0 – 1.5[a]	0.5 – 2.0[a]
C_{max}	ng/mL	433 ± 169	922 ± 283	1560 ± 892	2410 ± 1030
C_{max}[b]	(kg ng)/(mL mg)	145 ± 54.6	623 ± 190	524 ± 294	562 ± 233
C_{last}	ng/mL	86.7 ± 107	64 ± 25	154 ± 74.3	233 ± 152
AUC_{last}	h ng/mL	2200 ± 1460	3600 ± 905	8210 ± 2490	11 800 ± 1170
AUC_{last}[b]	h kg ng/mL/mg	736 ± 482	2440±629	2780 ± 854	2750 ± 278
AUC_{∞}	h ng/mL	1550*	5190*	13000*	13400
AUC_{∞}[b]	h kg ng/mL/kg	512*	3450*	4440*	3110*
$t_{1/2}$	h	10.9*	14.1*	18.2*	8.71*

[a] Range

[b] Dose normalized to 1 mg/kg

*Approximation

As it may be observed from the presented data, the total exposure to fenofibrate and fenofibric acid, expressed as AUC_{last} values, between the four different compounds was comparable between fenofibrate loaded OMS capsules (16.75 and 33.5 mg) and Tricor® (period 2, 3 and 4) and was approximately a factor 3.5 higher in comparison with Lipanthyl® (period 1). The extent of absorption expressed as the dose normalized AUC_{last} was higher for fenofibrate-OMS (eq 33.5 mg) than for the marketed formulations Lipanthyl® and Tricor®. Though some variability of the *in vivo* data, fenofibrate-OMS formulations show potential to improve bioavailability of fenofibrate. Consequently, the fenofibrate-OMS formulation (eq. 33.5 mg) whose pharmacokinetic profile of fenofibrate and its active metabolite fenofibric acid is confirmed (Figure 8A and 8B), with proven safety and satisfying tolerability, is a promising candidate to be further investigated in a clinical trial setting.

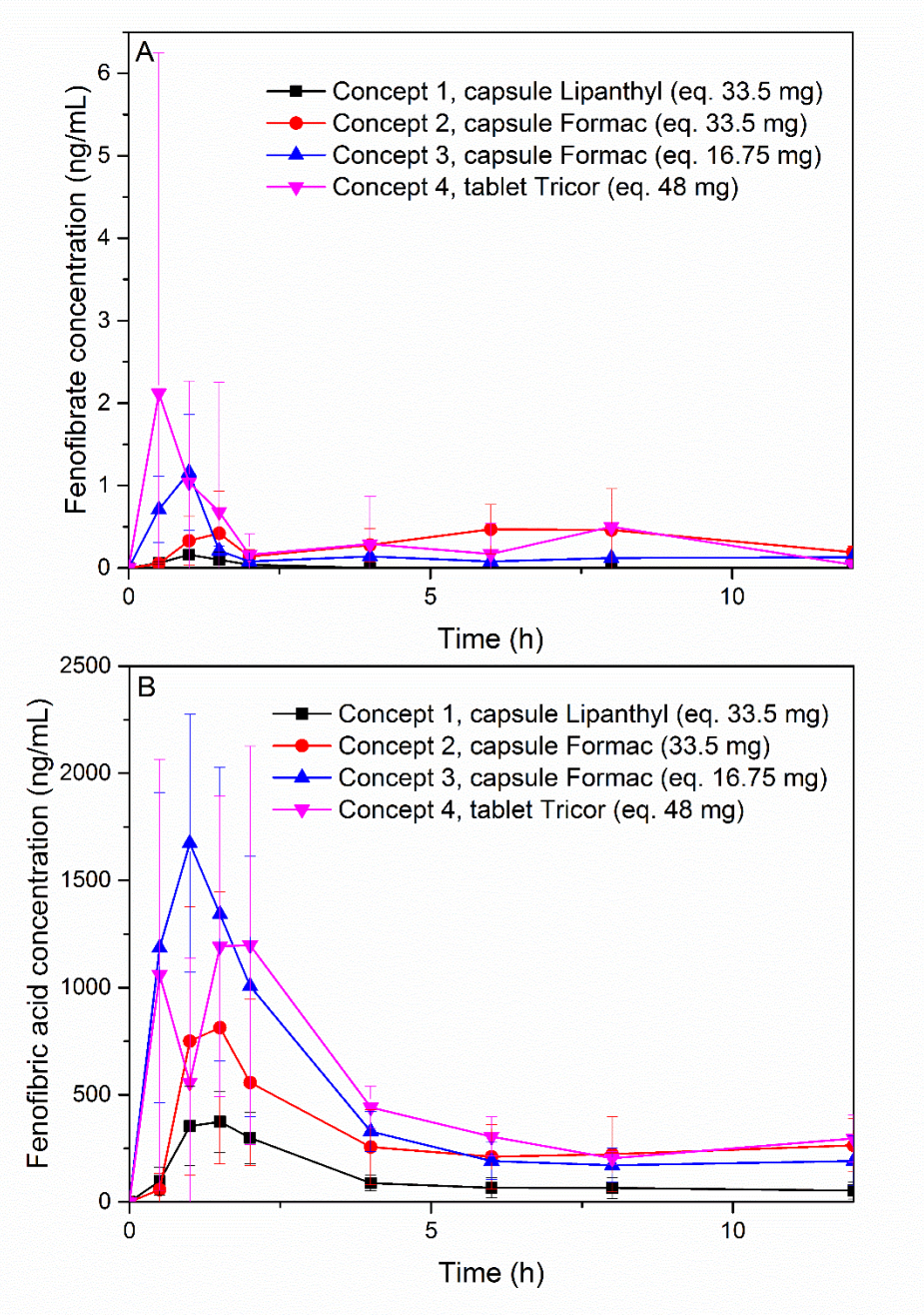

Figure 8. (A) Average plasma concentration versus time curves of fenofibrate after single dosing in male Beagle dog. **(B)** Average plasma concentration versus time curves of fenofibric acid after metabolization of fenofibrate. (The concentrations are normalized to 33.5 mg). Results are mean ± SD obtained from four animals.

Figure 9, which represents the release rate during stability testing (all conditions, 1, 2 and 6 month time points), shows that the release profiles of OMS based formulation remained

unchanged in all the examined conditions within 6 months. Results from the DSC measurements showed absence of any crystallinity during the whole stability period. These results, that support the unique stability properties of the silica technology, are in accordance with the previously reported findings regarding ezetimibe-loaded OMS (***Kiekens et al., 2011***).

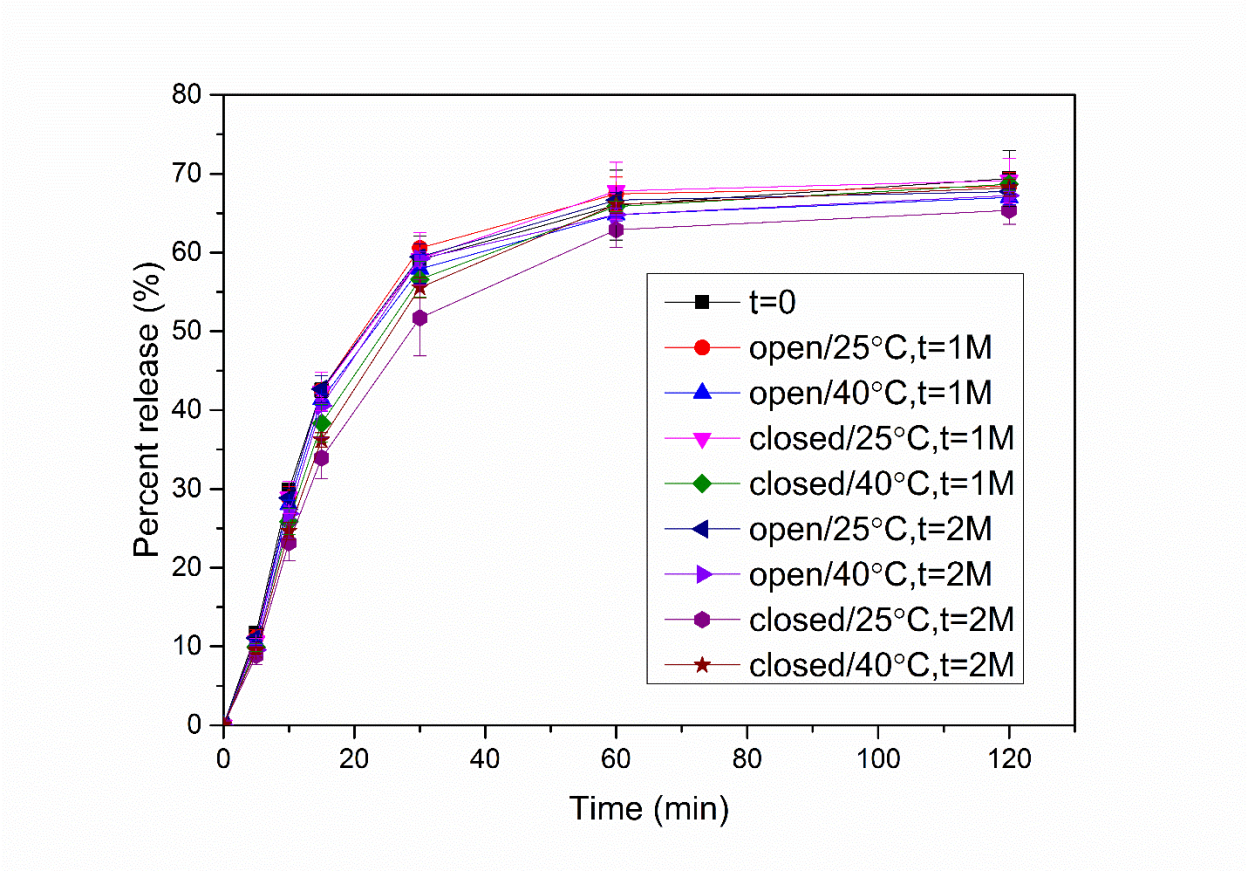

Figure 9. Dissolution/release experiments of stability samples of ordered mesoporous silica (OMS) powder (n = 3; eq. 33.5 mg fenofibrate) in 900 mL simulated gastric fluid + Tween 80. Results are mean ± SD of three experiments.

1.2. Clinical trial

In this study, the pharmaceutical performance of fenofibrate formulated with an ordered mesoporous silica material (Fenofibrate-OMS) was compared against the marketed product Lipanthyl®. Twelve healthy volunteers received a 33.5 mg dose of Fenofibrate-OMS and 67 mg of Lipanthyl® in two sequential dosing periods. Plasma concentrations of fenofibric acid, the pharmacologically active metabolite of fenofibrate, were monitored up to 96 hours post-dose. All subjects received the study drug as planned and all subjects completed the study as planned. Statistical analyses on the measures of the rate and extent of absorption were performed on the dose-normalised data. This dose-normalisation is justifiable based on the results of prior study that demonstrated dose proportionality between a 16.5 mg and a 33 mg fenofibrate dose following oral administration of Fenofibrate-OMS to fasted beagle dogs (***Bukara et al., 2016***).

In the second administration period of the study, a quantifiable pre-dose plasma concentration was found in 4 subjects. In each case, the pre-dose plasma concentration was lower than 5% of the corresponding C_{max}. In accordance with the regulatory guidelines, these data were used as such in the pharmacokinetic analysis. Since the lower limit of quantification (LLOQ) for plasma pharmacokinetic analysis was set at 10.0 ng/mL, all analytical values below this value were entered in the database '<10 ng/mL'. For each plasma sample, the difference between the actual sampling time and the scheduled sampling time was lower than 20%.

The plasma concentration vs time profiles of fenofibric acid after administration of Fenofibrate-OMS and Lipanthyl® are presented in Figure 10.

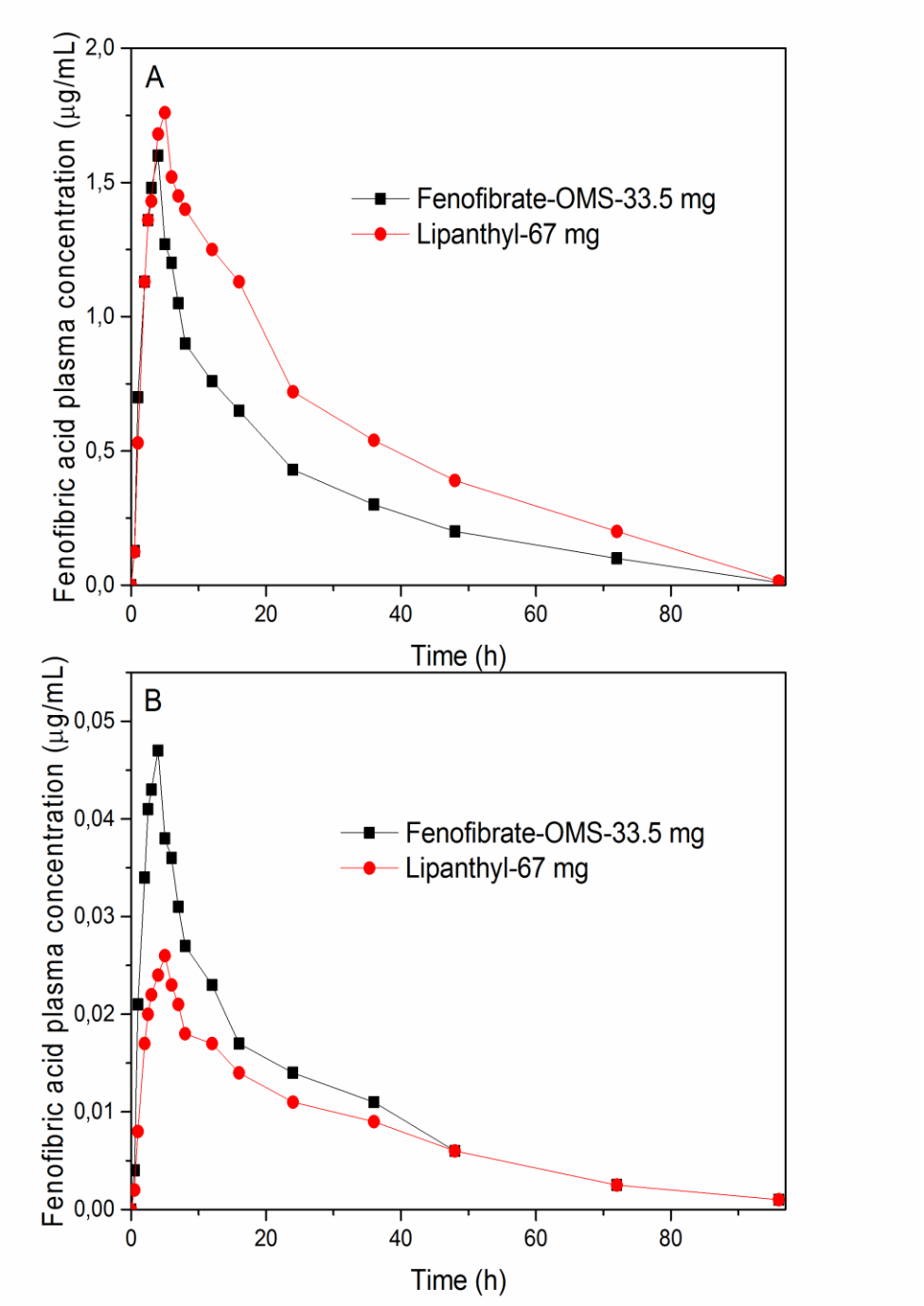

Figure 10. (A) Mean (n = 12) plasma concentration vs time profiles after single administration of one capsule containing 33.5 mg of fenofibrate formulated with OMS (Fenofibrate-OMS) or one capsule containing 67 mg of micronized fenofibrate (Lipanthyl®); **(B)** The same data after normalization to 1 mg dose.

An overview of all pharmacokinetic parameters is provided in Table 9 and a statistical comparison of the pharmacokinetic parameters is presented in Table 10.

Table 9. Fenofibric Acid Pharmacokinetic Parameters. All data (except t_{max} data) are presented as mean ± standard deviation calculated from the 12 subjects having completed the two treatment periods. For t_{max}, median values are provided with the range presented in brackets.

Pharmacokinetic Parameter	Fenofibrate-OMS	Lipanthyl®
C_{max} (µg/mL)	1.67 ± 0.29	1.96 ± 0.65
t_{max} (h)	3.50 (2.00-5.00)	4.00 (2.00-6.00)
AUC_{0-t} (µg.h/mL)	30.8 ± 13.4	47.9 ± 22.0
AUC_{0-24h} (µg.h/mL)	18.7 ± 4.7	24.9 ± 8.6
AUC_{0-48h} (µg.h/mL)	26.3 ± 9.1	37.8 ± 14.7
$AUC_{0-\infty}$ (µg.h/mL)	32.3 ± 14.7	51.9 ± 26.0
$t_{1/2,\lambda z}$ (h)	17.0 ± 6.2	22.1 ± 8.8
C_{max}/dose (µg/mL/mg)	0.0498 ± 0.0087	0.0293 ± 0.0097
AUC_{0-t}/dose (µg.h/mL/mg)	0.921 ± 0.401	0.715 ± 0.329
AUC_{0-24h}/dose (µg.h/mL/mg)	0.559 ± 0.140	0.372 ± 0.128
AUC_{0-48h}/dose (µg.h/mL/mg)	0.784 ± 0.272	0.565 ± 0.220

Fenofibrate-OMS treatment: single oral dose of 33.5 mg fenofibrate formulated with ordered mesoporous silica; Lipanthyl® treatment: single oral dose of 67 mg micronized fenofibrate.

C_{max} = maximum observed plasma concentration;

C_{max}/dose = C_{max} normalized to unit dose (1 mg);

t_{max} = time of occurrence of C_{max};

AUC = area under the plasma concentration versus time curve from time zero to the last sampling time at which concentrations were at or above the limit of quantification [AUC_{0-t}], up to 24 hours post-dose [AUC_{0-24h}], or up to 48 hours post-dose [AUC_{0-48h}] calculated by the linear trapezoidal rule;

AUC_{0-t}/dose = AUC_{0-t} normalized to unit dose (1 mg); AUC_{0-24h}/dose = AUC_{0-24h} normalized to unit dose (1 mg); AUC_{0-48h}/dose = AUC_{0-48h} normalized to unit dose (1 mg); $AUC_{0-\infty}$ = Area under the plasma concentration versus time curve from time zero to infinity, calculated from $AUC_{0-t} + (C_t/\lambda_z)$, where C_t is the last observed quantifiable concentration; $AUC_{0-\infty}$/dose = $AUC_{0-\infty}$ normalized to unit dose (1 mg);

λ_z = apparent terminal elimination rate constant; $t_{1/2,\lambda z}$ = apparent terminal elimination half-life, calculated from (ln 2)/λ_z

Table 10. Statistical Comparison of Fenofibric Acid Pharmacokinetic Parameters Between: Fenofibrate-OMS vs Lipanthyl®.

Pharmacokinetic Parameter	Fenofibrate-OMS vs Lipanthyl®	
	Point estimate (90% CI)[a]	p-value[b]
C_{max}/dose	177.1 (152.5 – 205.8)	< 0.0001
t_{max}	-0.75 (-1.25 – -0.25)	0.0344
AUC_{0-t}/dose	129.9 (120.5 –140.0)	< 0.0001
AUC_{0-24h}/dose	154.1 (136.8 – 173.5)	< 0.0001
AUC_{0-48h}/dose	140.5 (128.3 – 153.8)	< 0.0001
$AUC_{0-\infty}$/dose	127.0 (118.0 – 136.6)	0.0002
$t_{1/2,\lambda z}$	77.6 (70.0 – 86.0)	0.0012

Fenofibrate-OMS treatment: single oral dose of 33.5 mg fenofibrate formulated with ordered mesoporous silica; Lipanthyl® treatment: single oral dose of 67 mg micronized fenofibrate.

[a]Point estimate and 90% CI of the least-squares geometric percentage ratio (ANOVA).

For t_{max}, comparison was assessed between Fenofibrate-OMS and Lipanthyl® using the Koch procedure; the Hodges-Lehmann non-parametric estimate of location shift between Fenofibrate-OMS and Lipanthyl® based on untransformed data is provided with its 90% two sided CI.

[b]Probability of no difference between treatments (ANOVA; non-parametric test for t_{max}).

Statistical comparison of the dose-normalised measures of extent of exposure (Table 10) reveals significantly higher values for Fenofibrate-OMS, with point estimates of 129.9%, 154.1%, 140.5% and 126.7% for AUC_{0-t}/dose, AUC_{0-24h}/dose, AUC_{0-48h}/dose and $AUC_{0-\infty}$/dose, respectively. The data in Table 10 also show a significant increase in C_{max}/dose (point estimate

of 177%), a reduction in t_{max} (-0.75 hours) and a modest yet significant decrease in apparent terminal half-life ($t_{1/2,\lambda z}$) following administration of Fenofibrate-OMS.

No serious adverse events occurred during this study and none of the subjects prematurely discontinued the study due to an adverse event. In total, 6 treatment-emergent adverse events were reported in 3 subjects (25.0%): 2 subjects (16.7%) in the period following administration of Fenofibrate-OMS and in 1 (8.3%) in the period following administration of Lipanthyl®. All treatment-emergent adverse events were mild in severity and were seen in at most one subject (nausea and back pain in one subject each and contusion, head injury, nail injury, and spinal cord injury cervical in one subject). One event was considered by the investigator to have a reasonable possibility of causal relationship with the study drug (nausea in the period following administration of Fenofibrate-OMS). No relevant differences in clinical laboratory test data were observed between Fenofibrate-OMS and Lipanthyl® and no clinically relevant changes from baseline in median values of any ECG parameter or vital signs were observed following administration of the study drug. No abnormalities were noted in any of the subjects during physical examination.

Overall, the pharmacokinetic data revealed a significant increase in the extent of absorption following administration of Fenofibrate-OMS. The extent of absorption expressed as the dose-normalised AUC from time zero to the 24 hour (AUC_{0-24h}/dose) of 48 hour (AUC_{0-48h}/dose) was significantly higher for Fenofibrate-OMS, with point estimates of ca 154% and 140%, respectively (Table 3), indicating an increase in systemic exposure of around 54% and 40%, respectively. These differences are significant within the 90% CI, which is above the minimum acceptance interval currently required by the European Medicines Agency (EMA) to conclude to bioequivalence (80-125%). Fenofibric acid exposure assessed until the last measurable concentration (AUC_{0-t}/dose) or extrapolated to infinity ($AUC_{0-\infty}$/dose) was statistically significantly increased but to a lesser extent (30% and 27%, respectively) and with 90% CIs overlapping with the upper limit of the acceptance interval (80-125%) required to conclude to bioequivalence.

The data also indicated an increased rate of absorption for Fenofibrate-OMS: the dose-normalised maximum fenofibric acid plasma concentration (C_{max}/dose) was increased by 77% ($p < 0.0001$) and the time to reach the maximum plasma concentration (t_{max}) was reduced by 0.75

hours ($p < 0.05$). The increased rate and extent of absorption following administration of Fenofibrate-OMS can be related to the release rate of fenofibrate from OMS which is faster than the dissolution rate of micronized fenofibrate (Lipanthyl®), thus providing for a higher driving force for drug absorption during gastrointestinal transit. These results, indicative of a higher pharmaceutical performance of Fenofibrate-OMS, are in line with those obtained previously in beagle dogs (***Bukara et al., 2016***).

Single doses of Fenofibrate-OMS were safe and well tolerated. No relevant differences in safety and tolerability profile were observed when comparing a single dose of Fenofibrate-OMS and Lipanthyl®.

2. Controlled drug delivery system based on erythrocyte membranes

In this study, encapsulation of SD into porcine and outdated human erythrocyte ghosts was performed by osmosis based process, gradual hypotonic hemolysis. As previously shown (***Kostic et al., 2014; Stojanovic et al., 2012***) during the process of gradual decrease of osmotic strength of a solution surrounding erythrocytes, erythrocytes swell and hemoglobin molecules leak out. The transiently appeared membrane holes of 20–50 nm in the remaining erythrocyte membranes permit different extracellular substances to be encapsulated through these resealable pores (***Fun et al., 2012***). Beside already known phenomenon that different osmotic properties of the examined erythrocytes require the usage of different hypotonic conditions during encapsulation process, in this study the effect of the active substance - SD itself was examined on the encapsulation process, as well as on final properties of the encapsulated ghosts.

In order to identify and quantify encapsulated SD in a complex systems such as erythrocyte ghost, we developed simple, fast and reliable UHPLC/DAD/–HESI-MS/MS method. The analysis included comparison of the retention times, UV and MS/MS spectra with the available standard. Initially, full-scan UHPLC/−HESI-MS spectrum of pure SD was acquired in negative

ion mode (Figure 1SB) simultaneously with UHPLC/DAD spectrum at λ=230 and 280 nm (Figure 11).

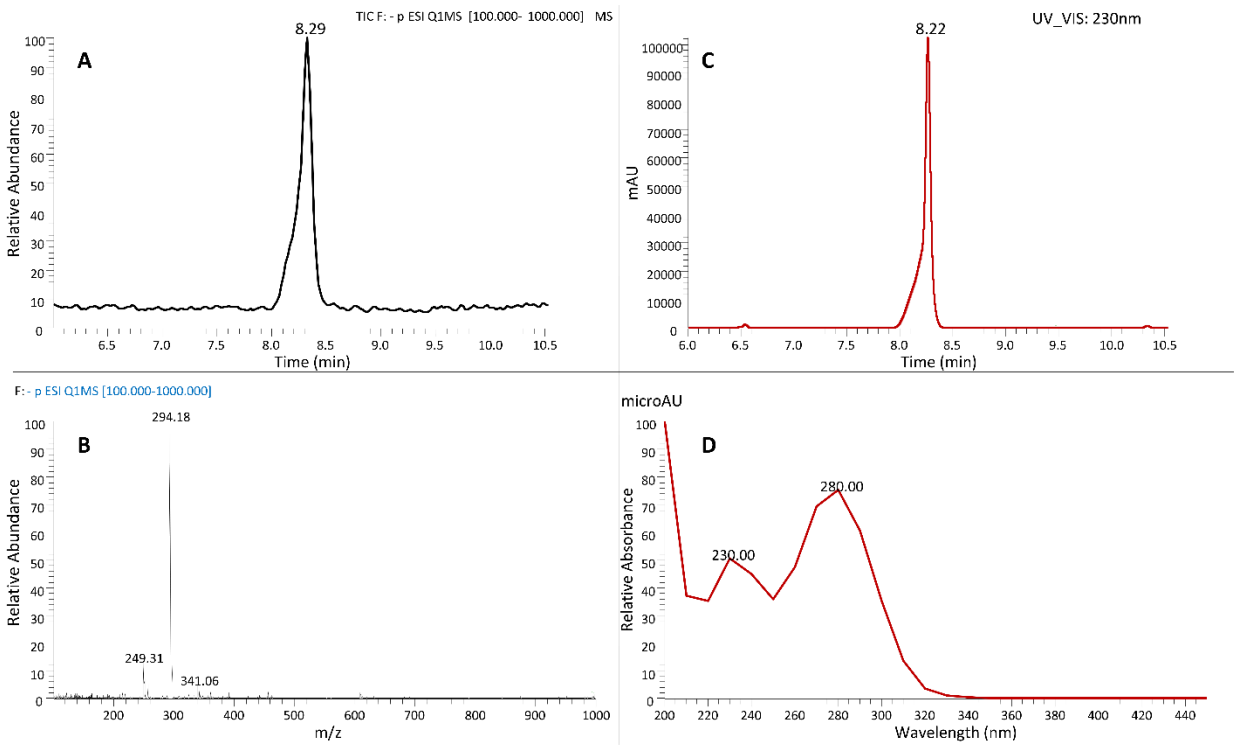

Figure 11. UHPLC/−HESI-MS total ion chromatogram (TIC) of SD (A) and corresponding MS spectrum (B). UHPLC/DAD chromatogram of SD at λ=230 (C), and corresponding UV spectrum (D).

Peak at Rt = 8.30 min corresponding to SD, showed characteristic deprotonated molecule *m/z* $[M-H]^-$ at 294, and λ_{max} at 230 and 280 nm. The UHPLC/–HESI-MS/MS analysis, with cE set to 20 eV, revealed the major $-MS^2$ product ions of SD: *m/z* $[M-H-CO_2]^-$ at 250, *m/z* $[M-H-CO_2-Cl]^-$ at 214 and *m/z* $[M-H-CO_2-2Cl]^-$ at 178. UHPLC/–HESI-MS/MS PIS chromatogram and corresponding $-MS^2$ spectrum is shown in Figure 12A1 and 12A2.

A

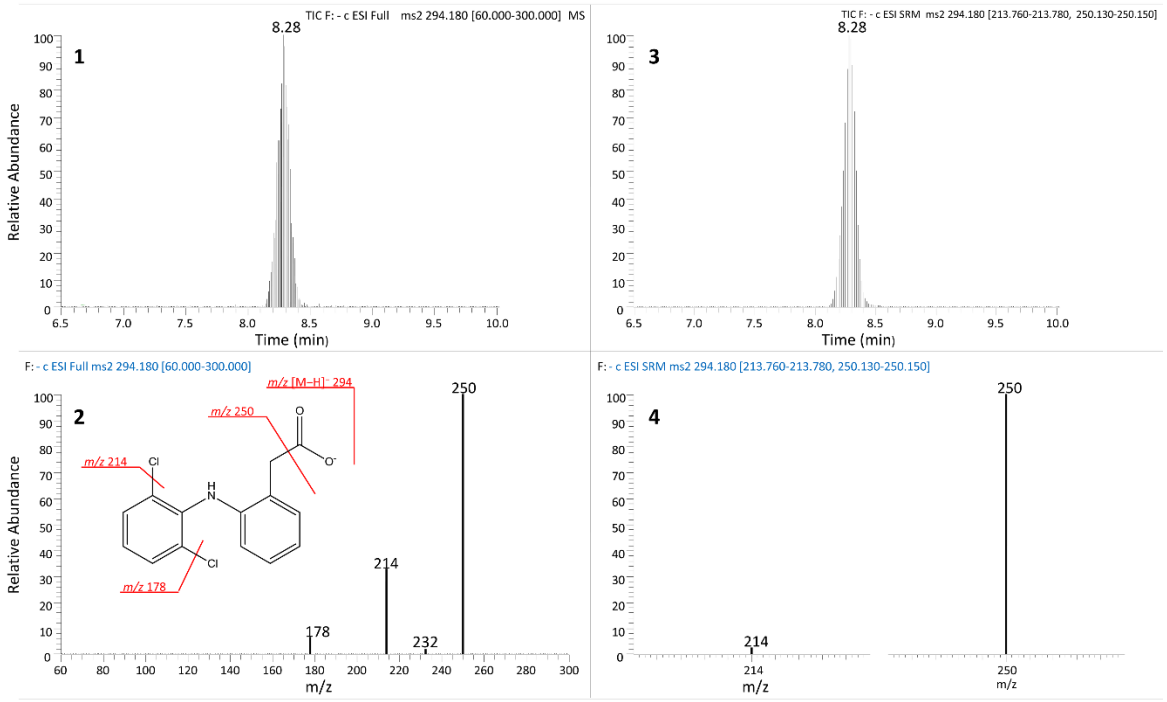
TIC F: - c ESI Full ms2 294.180 [60.000-300.000] MS
8.28
1
Relative Abundance
Time (min)
TIC F: - c ESI SRM ms2 294.180 [213.760-213.780, 250.130-250.150]
8.28
3
Time (min)
F: - c ESI Full ms2 294.180 [60.000-300.000]
2
m/z [M-H]⁻ 294
m/z 250
m/z 214
m/z 178
250
214
178
232
m/z
F: - c ESI SRM ms2 294.180 [213.760-213.780, 250.130-250.150]
4
250
214
m/z

B

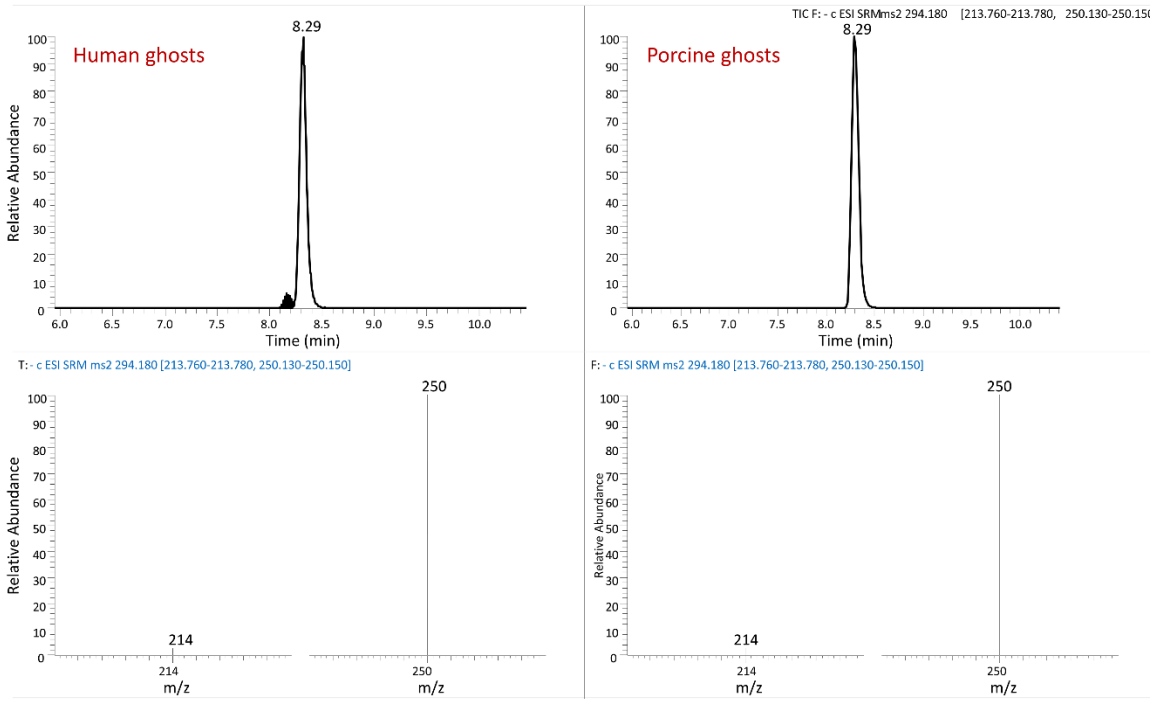
Human ghosts
8.29
Relative Abundance
Time (min)
Porcine ghosts
8.29
Time (min)
T: - c ESI SRM ms2 294.180 [213.760-213.780, 250.130-250.150]
250
214
m/z
F: - c ESI SRM ms2 294.180 [213.760-213.780, 250.130-250.150]
250
214
m/z

Figure 12. UHPLC/–HESI-MS/MS product ion scanning (PIS) chromatogram (A1) and corresponding spectrum of SD deprotonated molecule (m/z [M−H]− at 294) (A2). The proposed origin of mass fragments of SD is attached to the corresponding mass spectrum; UHPLC/–HESI-MS/MS single reaction monitoring (SRM) chromatogram (A3) and corresponding mass spectrum (A4) presenting two characteristic –MS2 fragments used in experiments for the accurate identification and quantification of SD; (B) UHPLC/–HESI-MS/MS single reaction monitoring (SRM) chromatograms of human and porcine ghosts, and corresponding mass spectrums of diclofenac identified in samples.

Proposed fragmentation pattern in negative ion mode is also presented. Two characteristic $-MS^2$ fragments, *m/z* at 250 and *m/z* at 214, were used in SRM experiment for the accurate identification and quantification of SD (Figure 12A3 and 12A4) in human and porcine ghosts (Figure 12B). Developed UHPLC/DAD/–HESI-MS/MS method allowing simple, precise and accurate determination and quantification of the SD encapsulated in erythrocyte ghost demonstrated its ability to be used as analytical method in potential biomedical/clinical use of these SD carriers.

The amount of the encapsulated SD in 100 µL of erythrocyte ghosts was 21.5 µg and 4.85 µg for porcine and outdated human samples, respectively. It corresponds to the encapsulation efficiency of 37% for porcine and 8.5% for outdated human erythrocyte ghosts. After the second washing out step during the encapsulation procedure (performed to remove all un-encapsulated drug), the detected amount of SD in the supernatant was 1.15 % and 75.5 % of the encapsulated amount for porcine and outdated human erythrocyte ghosts, respectively. The encapsulation efficiency for porcine erythrocyte ghosts under the applied conditions was consistent with the range reported in other studies where erythrocyte ghosts were used to encapsulate various agents such as drugs, enzymes, peptides, proteins, pollysacharides and DNA (***Hamidi et al., 2001; Millan et al., 2004***). Co-encapsulation methods or enriched medium which could be a source of nutrients for erythrocyte (such as Hank's balanced salt solution) were not used in this study, so encapsulation efficiency was only the result of intrinsic ability of erythrocytes' membranes to entrap the substance. On the other hand, the encapsulation efficiency for outdated human erythrocyte ghosts was much lower than the reported range for fresh human erythrocytes (***Hamidi et al., 2001; Millan et al., 2004***). This finding might be explained by the aging process and consequent

deterioration of erythrocytes during the storage. During aging/storage erythrocytes lose water, ATP, hemoglobin, proteins, surface N-acetylneuraminic acid and undergo age-related changes in band 3 (***Huang et al., 2011***). All these changes together and especially changes in band 3 which participate in hypotonic hemolysis process (***Orhan et al., 2001***) were probably responsible for the decreased ability of outdated human erythrocytes to entrap the drug.

It was noted that with the applied encapsulation process, SD loaded porcine erythrocyte ghosts retained more hemoglobin in comparison with the empty erythrocyte ghosts. UV/VIS spectrophotometric measurements confirmed this observation revealing that the concentration of the residual hemoglobin in some of SD loaded porcine erythrocyte ghosts was even 3-4 folds higher than in the suspension of corresponding empty erythrocyte ghosts. On the other hand, the level of residual hemoglobin in outdated human SD loaded and empty erythrocyte ghosts was almost equal (0.50% and 0.46% respectively). This was an incentive to investigate the effect of SD on the gradual hypotonic hemolysis process.

As it is shown in Figure 13, during the gradual hypotonic hemolysis SD had only weak antihemolytic effect on porcine erythrocytes. H50 values (the point when 50% of total hemoglobin is released from erythrocytes) were 5.3±0.73 and 5.84±0.5 minutes for erythrocytes suspension lysed in the hypotonic buffer without and with SD, respectively, and they didn't show statistically significant difference ($p > 0.05$). However during the washing out procedure as a part of encapsulation process, this effect became more pronounced and SD loaded porcine erythrocyte ghosts were losing hemoglobin slower than the corresponding empty ghosts. The difference in the hemoglobin content between SD loaded and empty erythrocyte ghosts became statistically significant after the fourth washing out step and amounted about 20% on average (Fig. 13C).

It is known that SD exerts biphasic effect on hemolysis: it stabilizes membrane at lower concentrations while causing hemolysis at higher concentrations (***Orhan et al., 2001***). In this study SD was used in steady state therapeutic concentration (***Orhan et al., 2001***) which had very mild and delayed antihemolytic effect for porcine erythrocytes. Antihemolytic effect of amphyphiles is well known and extensively described in literature (***Sato et al., 1993; Seeman, 1972; Helenius et al., 1975; Sanchez et al., 2002***). Currently, there are several hypothesis explaining this phenomenon but it requires further detailed studies (***Sato et al., 1993; Seeman,***

1972; Helenius et al., 1975; Sanchez et al., 2002). Regardless the mechanism involved, observed mild and delayed antihemolytic effect of SD did not affect encapsulation process adversely.

It is interesting to note that in the present study SD didn't show antihemolytic effect on the outdated human erythrocytes. These erythrocytes are known to have impaired signalling pathways (***Bosman et al., 2008***) which together with our finding supports the assumptions that some active mechanism is involved in antihemolytic effect of amphiphiles.

Furthermore, the potassium concentration during the gradual hypotonic hemolysis of porcine erythrocytes was measured with and without presence of SD. As it may be observed from the Figure 1B slight increase in potassium efflux was detected in the presence of SD between 11^{th} and 17^{th} minute. However, the difference between the samples was not statistically significant ($p > 0.05$). Increased potassium efflux is the common effect shared by the most amphiphiles (***Isoma et al., 1986***). According to Isomaa et al. (***Isoma et al., 1986***) amphiphiles increase the permeability of the membrane lipid bilayer to the small ions, such as potassium, by decreasing order of packing of the hydrocarbon chains of the lipids in the bilayer.

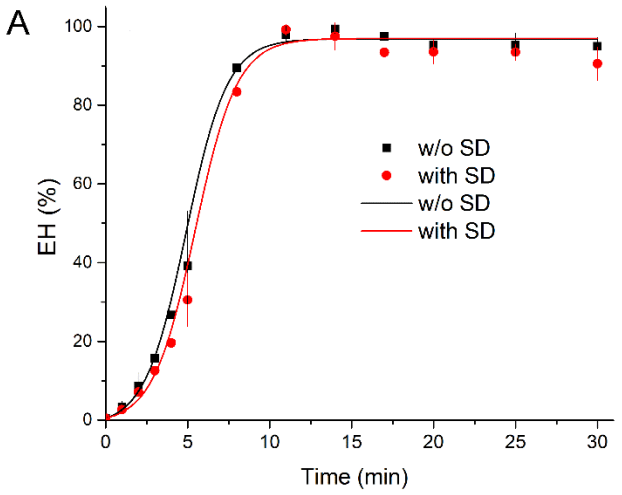
A
EH (%)
Time (min)
w/o SD
with SD
w/o SD
with SD

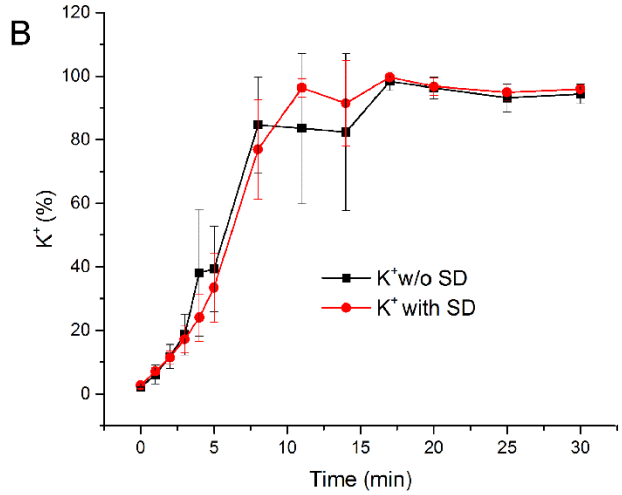
B
K+ (%)
Time (min)
K+w/o SD
K+ with SD

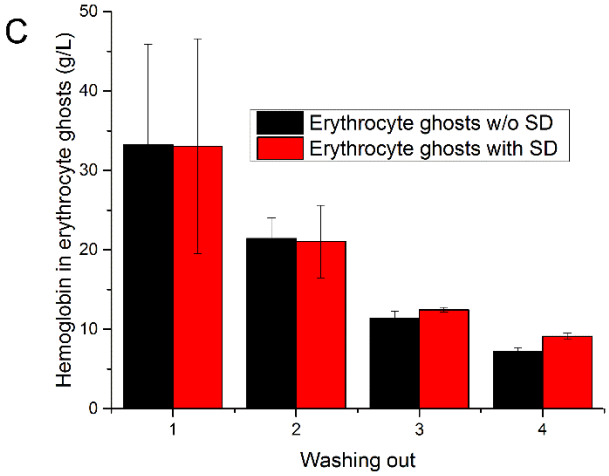
C
Hemoglobin in erythrocyte ghosts (g/L)
Washing out
Erythrocyte ghosts w/o SD
Erythrocyte ghosts with SD

Figure 13. Effect of SD on: (A) the gradual hypotonic hemolysis, (B) potassium efflux during the gradual hypotonic hemolysis (C) washing out procedure of porcine erythrocyte ghosts. Results are mean ± SD of three experiments.

Number-based particle hydrodynamic diameter distribution curves and statistical measures of the porcine and outdated human erythrocytes, erythrocyte ghosts and erythrocyte ghosts loaded with SD are shown in Figure 14. The results confirmed that porcine erythrocytes were smaller than human erythrocytes. Porcine ghosts with and without SD were also smaller than the corresponding outdated human samples. It is obvious from the statistical data that the empty ghosts and ghosts loaded with SD were unidispersed introducing important property for their potential application as drug carriers. After the gradual hypotonic hemolysis process and washing out procedure, porcine empty erythrocyte ghosts were on average about 13% smaller that the intact erythrocytes. On the contrary, outdated human empty erythrocyte ghosts showed an increase in size for about 10% in comparison with erythrocytes. Subsequently applied encapsulation process caused an increase in ghosts' size of both examined species. Porcine erythrocyte ghosts loaded with SD were about 9% larger than the empty ghosts but still smaller than starting erythrocytes. Outdated human erythrocyte ghosts loaded with SD were approximately 14 % larger than empty ghosts and larger than starting erythrocytes.

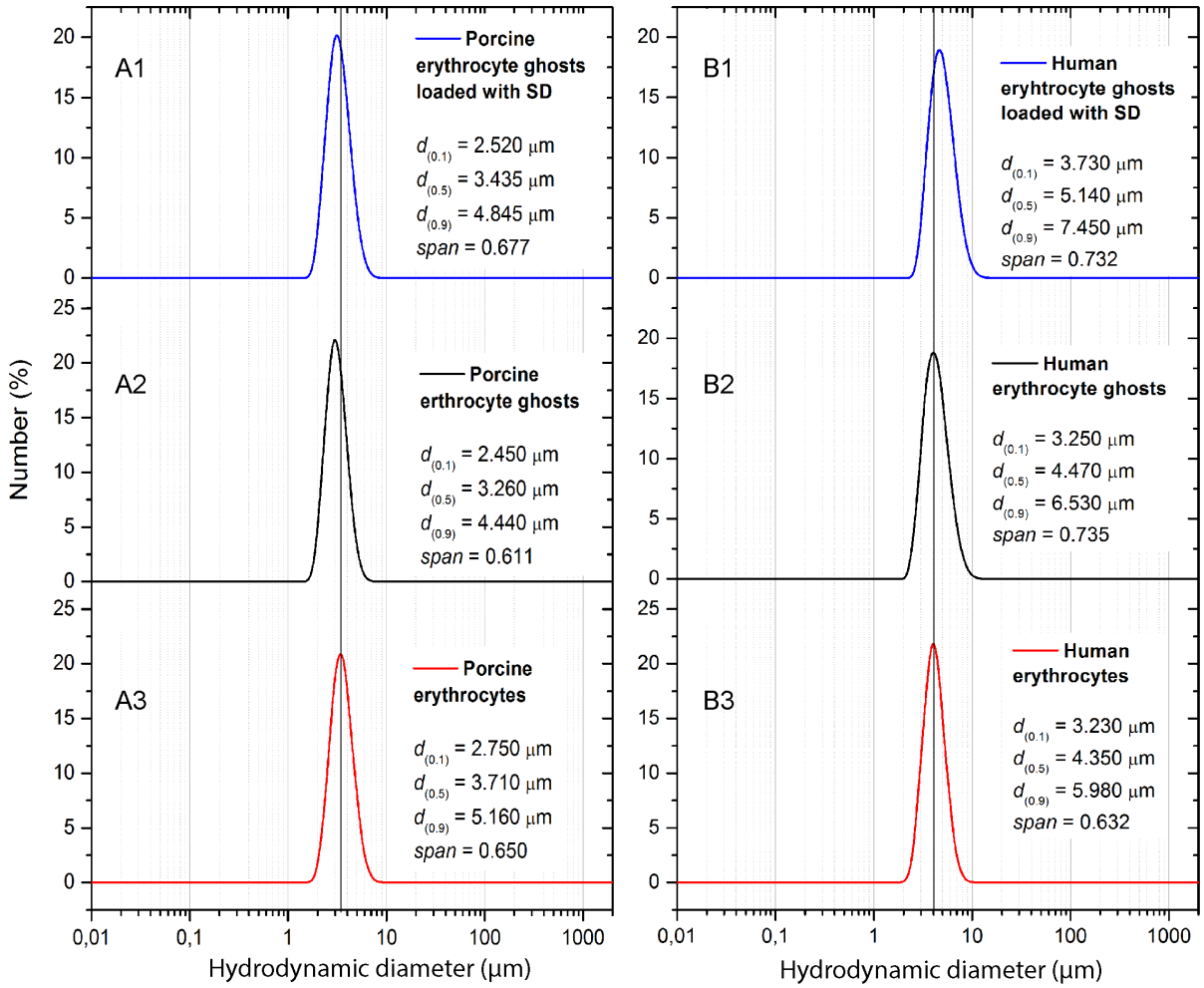

Figure 14. Number based hydrodynamic diameter distribution and relevant statistical parameters of **(A1)** porcine erythrocytes, **(A2)** porcine erythrocyte ghosts, **(A3)** porcine erythrocyte ghosts loaded with SD, **(B1)** outdated human erythrocytes, **(B2)** outdated human erythrocyte ghosts **(B3)** outdated human erythrocyte ghosts loaded with SD. ($p > 0.05$ when intact erythrocytes and empty erythrocyte ghosts were compared and when empty erythrocyte ghosts and SD loaded erythrocyte ghosts were compared).

The decrease in erythrocytes' size in gradual hypotonic hemolysis process has been previously reported for porcine erythrocytes (***Kostic et al., 2014***). Montes et al. (***Montes et al., 2008***) showed threefold smaller human erythrocyte ghosts than the original cells using isolation by classical hemolysis, i.e. osmotic shock. In the present study where an increase in the size of the ghosts was detected, outdated human erythrocytes obviously lost ability to shrink. On the other

hand, porcine erythrocyte ghosts retained size smaller than the original cells. Surface active drugs as well as non-steroidal anti-inflammatory compounds are reported to self-associate and bind to membranes causing the disruption and solubilisation as in detergent-like way (***Lopes et al., 2004***). Lopes and co-workers showed that SD associates with the lipid bilayer of liposome causing its destruction and the decrease in size (***Lopes et al., 2004***). This phenomenon was not observed in our study. Erythrocyte ghosts which contain spectrin - actin network (membrane skeleton) in addition to the lipid bilayer (***Bennett et al., 1979***), seem to be resistant to SD's surface active property offering the advantage in comparison with liposomes.

Possible interactions between SD and erythrocyte ghosts as well as changes induced by the applied encapsulation process were investigated by FT-IR (Figure 15).

The spectra of SD had been described by Bouchal et al. (***Bouchal et al., 2016***). In the high frequencies range signals due to N-H stretching were found at 3382 and 3258 cm^{-1} (Fig. 15). Signals due to C-H stretching in the aliphatic and aromatic part of molecule were found in 3100-2850 cm^{-1} range (***Bouchal et al., 2016***). Peaks at 1572 and 1401 cm^{-1} belong to asymmetric and symmetric stretching modes of carboxylate group, respectively (***Bouchal et al., 2016***). Signals in 1603–1586 cm^{-1} range are the consequence of NH deformation modes and ring stretching modes (***Bouchal et al., 2016***). Lower frequency range consists of C–N stretching modes (1300–1200 cm^{-1}), in plane (1200–1000 cm^{-1}) and out of plane (900–690 cm^{-1}) CH deformations (***Bouchal et al., 2016***).

The analysis of IR spectra of porcine and human erythrocyte ghosts not loaded with SD (Fig. 15) revealed the presence of amide I region predominantly containing α-helix structure at 1656 cm^{-1} and amide II region at 1543 cm^{-1} (***Dong et al., 1994***). The relative intensity decrease of amide II band compared to amide I in the case of outdated human erythrocyte ghosts loaded with SD indicates change in the tertiary structure evoked by the presence of SD.

According to Casal and Mantsch phospholipid infrared bands in the spectrum can be divided into three different regions corresponding to the hydrophobic, interfacial and polar moieties of the lipid (***Casal et al., 1984***). C-H stretching vibrations give rise to bands in the hydrophobic 3100–2800 cm^{-1} region (***Mantsch et al., 1991***). As it may be observed from the Figure 15, asymmetric and symmetric CH_2 bands at 2926 and 2852 cm^{-1}, respectively, which are the strongest ones in a phospholipid spectrum (***Mantsch et al., 1991***) are clearly observable in porcine and human

erythrocyte ghosts, as well as in their SD loaded forms. Shifting of the symmetric CH_2 band toward higher frequencies that is according to Szalontai et al. (***Szalontai et al., 2002***) attributed to the 'structural' disorder imposed on the lipids was not detected after the applied encapsulation process. The most prominent band arising from the interfacial region is due to stretching vibrations of the carbonyl group involved in ester bonds and it is found at 1730 cm^{-1} and 1737 cm^{-1} for porcine and human ghosts, respectively (***Mantsch et al., 1991***). This band that is very responsive to changes in its environment (***Mantsch et al., 1991***), is found at the same positions in the corresponding SD loaded porcine and human ghosts.

The antisymmetric PO_2^- stretching mode (***Mantsch et al., 1991***) appeared at 1245 cm^{-1} in both porcine and human empty and SD loaded ghosts. The symmetric PO_2^- stretching mode (***Mantsch et al., 1991***) appeared at 1085 cm^{-1} in human ghosts and was slightly shifted to 1093 cm^{-1} after the applied encapsulation process (signed with asterisk). Also, this mode was observed at 1121 cm^{-1} in porcine ghosts but was shifted to 1092 cm^{-1} in SD loaded ghosts (signed with asterisk). The band shift observed for the symmetric PO_2^- stretching bands suggest that the SD might be located close to the phosphate moiety of lipid molecules. This finding is in agreement with the study which has previously shown that SD has a potential to interact with phosphate of phosphatidylcholine head groups in liposomes (***Lopez et al., 2004***). Comparing the spectra of porcine and human empty erythrocyte ghosts with ghosts loaded with SD, no new absorption peaks appeared.

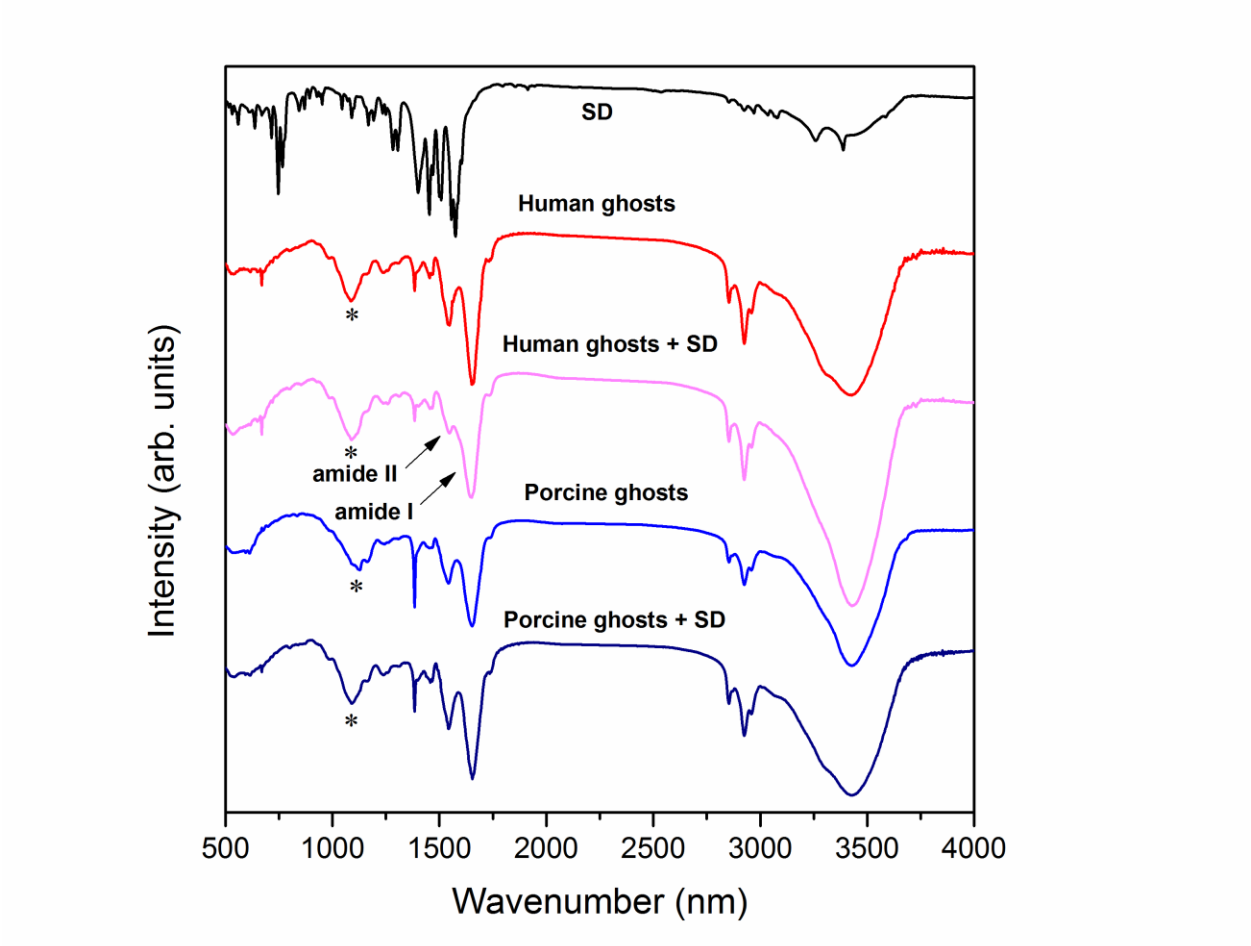

Figure 15. FTIR spectra of sodium diclofenac (SD), human erythrocyte ghosts, human erythrocyte ghosts loaded with SD, porcine erythrocyte ghosts, porcine erythrocyte ghosts loaded with SD. (Asterisk - a band corresponding to the symmetric PO_2^- stretching mode).

Table 11 shows the values of zeta (ζ)-potential and conductivity (σ) of the examined porcine and human erythrocyte samples. As it may be observed, gradual hypotonic hemolysis and encapsulation process didn't affect significantly surface charge and conductivity of the starting porcine erythrocyte suspension. The maintenance of this feature is important for two reasons: (1) when the expression of sialic acid in the erythrocyte surface is reduced, the electrostatic repulsive force decreases and erythrocyte aggregation is accelerated (***Shiga et al., 1990***), (2) negatively charged cells represent a good template core for layer by layer coating (***Shaillender et al., 2011***). Statistically significant difference in ζ-potential between human erythrocytes and erythrocyte ghosts ($p < 0.05$) indicates increased loss of N-acetylneuraminic acid probably

caused with an aging process potentiated in the seven week storage conditions (***Huang et al., 2011***). A slight decrease in the surface charge of both porcine and outdated human SD loaded erythrocyte ghosts in comparison with the corresponding empty ghosts and intact erythrocytes might be a contribution of the negatively charged SD attached to the membrane surface.

Table 11. Values of zeta (ζ)-potential and conductivity (σ) for porcine and human erythrocyte samples.

Sample	ζ-potential (mV)	σ (mS/cm)
Porcine erythrocytes	-9.4±0.61	15.9±0.66
Porcine erythrocyte ghosts	-9.6±0.70	15.6±0.66
Porcine erythrocyte ghosts loaded with SD	-10.1±0.12	15.7±0.50
Human erythrocytes	-12.5±0.89	15.7±0.58
Human erythrocyte ghosts	-11.7±0.59[a]	15.6±0.47
Human erythrocyte ghosts loaded with SD	-13.0±0.43	15.8±0.47

[a]Significant difference in ζ-potential value of the human erythrocytes.

Zhbanov et al. (***Zhbanov et al., 2015***) showed the increase of blood conductivity due to aggregation of erythrocytes both theoretically and experimentally. Since changes regarding conductivity were not detected, this result might be a confirmation for the low aggregation ability of the SD loaded ghosts in the final formulation.

Atomic force microscopy revealed significant difference between isolated porcine and outdated human erythrocytes' morphology (Figure 16A1, 16B1). As it may be observed, starting porcine erythrocytes had echynocytic morphology (Fig. 16A1), contrary to the biconcave morphology of outdated human erythrocytes (Fig. 16B1). Gradual hypotonic hemolysis induced significant distortion in erythrocyte shape and altered surface texture in both species. Additionally, nanoscale alterations and damages were noted in empty erythrocyte ghosts originating from outdated human erythrocytes. Surface roughness values for empty porcine and outdated human erythrocyte ghosts amounted 37±3 nm and 7±2nm, respectively. After the applied encapsulation process R_{rms} surface roughness value did not change significantly for porcine sample and it amounted 33±9 nm. On the other hand, R_{rms} surface roughness value of SD loaded outdated human erythrocyte ghosts increased to 23±4 nm. Since erythrocytes are not flat surfaces and

curvature effect might affect surface roughness values, they were not compared with empty and SD loaded ghosts.

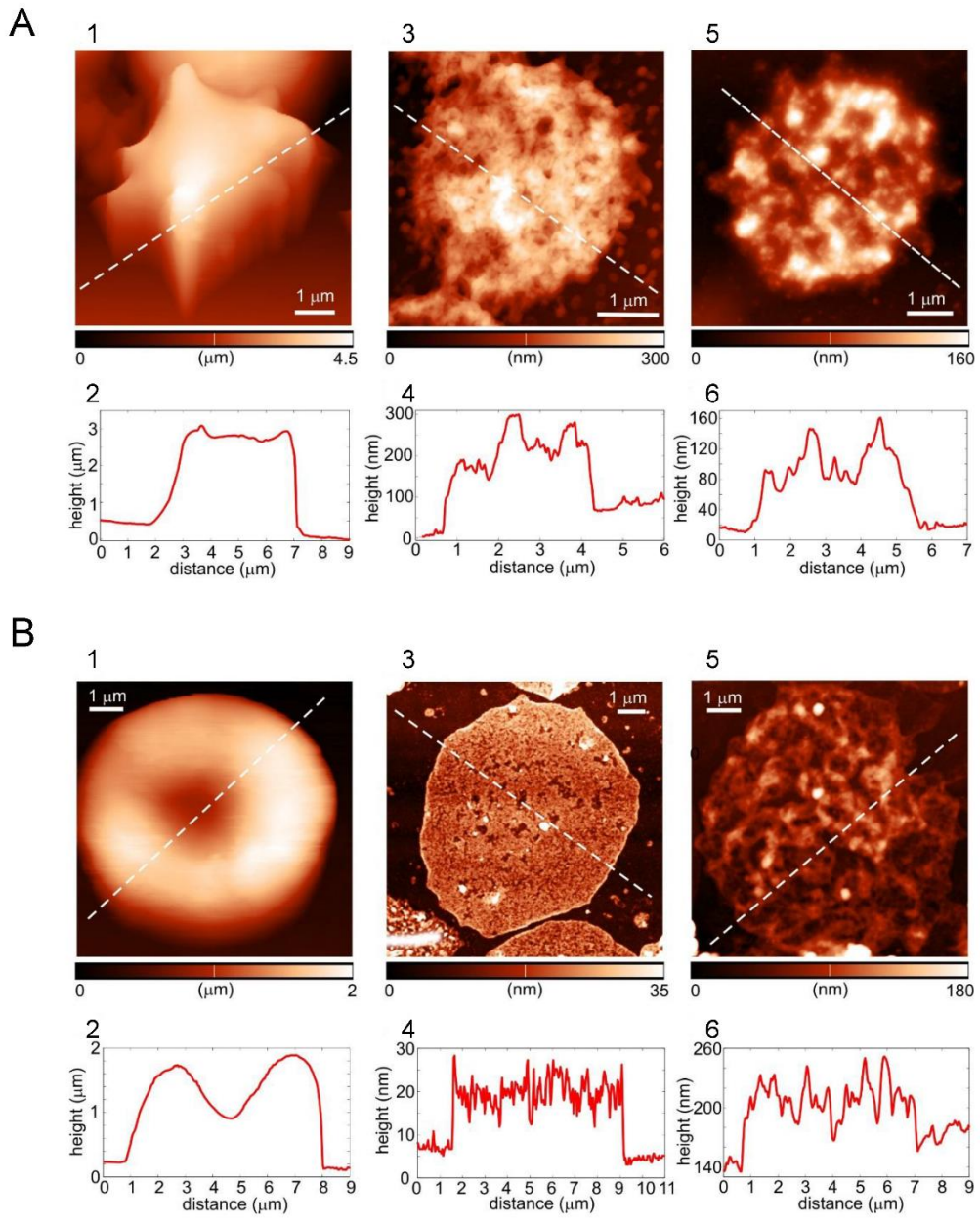

Figure 16. Representative AFM images and corresponding width/height plots for (A) porcine samples: (1, 2) erythrocytes, (3, 4) erythrocyte ghosts, (5, 6) erythrocyte ghosts loaded with SD and (B) human samples: (1, 2) erythrocytes, (3, 4) erythrocyte ghosts, (5, 6) erythrocyte ghosts loaded with SD.

The echynocyte morphology of porcine erythrocytes represents a common artefact in handling of porcine blood (***Barger, 2010***). Even though it was expected that outdated human erythrocytes would also have echinocyte morphology due to in vitro aging during the storage (***Girasole et al., 2010***), they had "normal" shape of flattened biconcave disc. The observed nanoscale damages on the outdated human erythrocyte ghosts indicated their impaired membrane-skeleton integrity and higher sensitivity in comparison with the fresh porcine erythrocytes. The damages of the outdated human erythrocytes might be one of the reasons for relatively high level of SD leakage during the washing out procedure and low level of SD encapsulation. Erythrocyte membrane roughness is a morphological parameter that links together the development of nanoscale alterations on the cell membrane with an occurrence of membrane-skeleton defects (***Girasole et al., 2010***). In the case of porcine erythrocyte ghosts, crosslinking of spectrin with glutaraldehyde during the encapsulation process (***Shiga et al., 1990***) seems to 'improve' surface properties making the membrane smoother. On the other hand SD loaded outdated human erythrocyte ghosts had higher R_{rms} values in comparison with the corresponding empty membranes which indicates further rearrangement and perturbations of the surface induced by the encapsulation process. During storage the most central biochemical change is a decrease in ATP which is important in the maintenance of membrane structure and integrity (***Bosman et al., 2008***). Due to its loss, erythrocytes become effete (***Bosman et al., 2008***), so higher susceptibility of the outdated human samples to the surface roughness changes was not surprising.

Data given in Figure 17 show that SD loaded porcine and outdated human erythrocyte ghosts had different drug releasing profiles. Porcine erythrocyte ghosts showed very slow initial release with only 8% of the drug released within the 2 hours, followed by 35% of the encapsulated SD released after 96 hours. On the other hand, outdated human erythrocyte ghosts initially released about two fold higher amount (~16%) of the encapsulated SD within 2 hours in comparison with porcine ghosts. The established steady-state of SD between human erythrocyte ghosts and the buffer solution used for the release test within 1 hour, has not changed significantly during the next 96 hours.

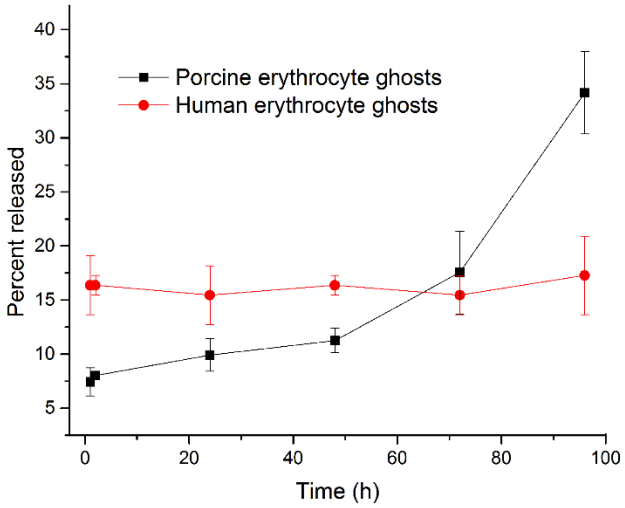

Figure 17. Release profile of SD from porcine and outdated human erythrocyte ghosts as a function of time.

Porcine erythrocyte ghosts didn't show undesirably high burst release which may lead to toxicity and wastage of an encapsulated agent (***Shaillender et al., 2011***). The amount of released drug within 2 hours from porcine ghosts was much lower in comparison with the other reported SD controlled drug delivery systems such as solid lipid nanoparticles (***Liu et al., 2014***), chitosan spheres (***Liu et al., 2014***), PLGA-nanoparticles (***Liu et al., 2014***) and rat erythrocyte ghosts (***Kozakevych et al., 2013***). In addition to the lower burst release, porcine ghosts had slower release rate in comparison with the previously mentioned systems. These findings indicate that the porcine erythrocyte membranes derived from the slaughterhouse blood are minimally porous and responded very well on the exposure to the resealing hypertonic solution which is intended to cause shrinkage during the encapsulation process. This is in accordance with the retained ability of porcine ghosts to shrink reflected through the smaller size of SD loaded ghosts in comparison with the starting erythrocytes. Membrane holes successfully closed along with cross-linked membrane proteins with 0.01 % glutaraldehyde were suitable for achievement of slow and extended (prolonged) SD release profile where release rate was based on equilibrium of released and drug retained within ghosts.

On the other hand, SD loaded human erythrocyte ghosts prepared from the outdated erythrocytes with impaired structure and function due to aging during the storage (***Huang et al., 2011***) showed entirely different SD release pattern from porcine ghosts. As it was shown in Figure 17, during the *in vitro* drug release testing, an increase in SD concentration was not detected with

time indicating zero-order drug release. SD which probably interacted with the membrane (but was not entrapped inside the membranes due to proven loss of ability to shrink) was released in the medium to the moment when the concentration equilibrium was established. This was in agreement with assumed mechanism of SD retaining in outdated human ghosts by FTIR analysis. According to Briones et al. who obtained similar drug releasing profile for zidovudine in rat erythrocytes, this type of behavior allows the system to work as a drug reservoir, providing sustained release into the body (***Briones et al., 2010***).

After comparing encapsulation efficiency of fresh porcine erythrocytes obtained in this study with data on those of fresh human erythrocytes found in the scientific literature, we assumed that preserved structure and function of the membranes seem to be a prerequisite for their usage in encapsulation process.

As it was previously mentioned, during the process of gradual decrease of ionic strength of the solution surrounding erythrocytes, they swell and hemoglobin molecules leak out, remaining intact erythrocyte membranes (***Kostic et al., 2014; Danon, 1961***). Preparation of ghosts is being followed by an extensive washing out procedure (to remove extracellular hemoglobin released from lysed erythrocytes). However, a small amount of hemoglobin, so called residual hemoglobin always remains bound to membranes in resulting erythrocyte ghosts (***Kostic et al., 2014***). The fraction of this so called residual hemoglobin, which cannot be easily eliminated from the system, significantly affects subsequent encapsulation process and encapsulated drug releasing profile (***Kostic et al., 2014***).

The overall presence of residual hemoglobin in the final suspensions of erythrocyte ghosts was primarily determined by cyanmethemoglobin assay (Figure 18). The concentration of residual hemoglobin was 7.21 and 1.76 g/L for porcine and human sample, respectively. This reflects the decrease in concentration of hemoglobin by 95% and 99% in the suspension of erythrocyte ghost comparing to the starting suspensions of porcine and outdated human erythrocytes, respectively. These amounts of residual hemoglobin in erythrocyte ghosts are consistent with the range reported in other studies (***Bernestein et al., 1938; Danon et al., 1956***). However, the localization of residual hemoglobin in the suspension still remains unknown.

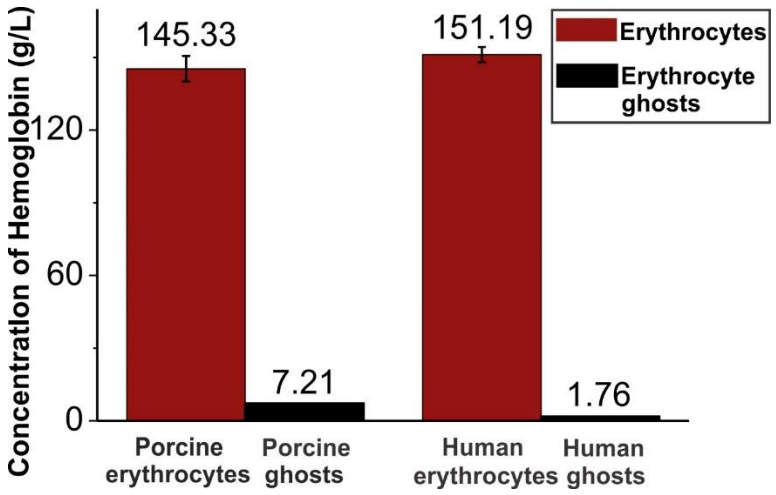

Figure 18. Concentration of hemoglobin in erythrocytes and their ghosts obtained by gradual hemolysis. The concentration was determined by spectrophotometric cyanmethemoglobin method.

Two photon excitation fluorescence microscopy as an advanced technique offers the possibility for non-invasive, label-free high resolution imaging of living cells and deep tissues by using the fluorescence emission from the endogenous fluorescent molecules (***Masters et al., 2008***). The near infrared radiation generates two photon excitation signals of endogenous fluorophores, such as tryptophan, riboflavines, nicotinamides, collagen, elastin etc., and thus provides rich morphological and biochemical information of biological systems (***Kolesová et al., 2016; Wang et al., 2006***). Less investigated and reported is intrinsic fluorescence of hemoglobin, the main intracellular component of erythrocytes, which emits strong Soret fluorescence with the peak at 438 nm upon two-photon excitation by femtosecond pulses in red and near infrared region (600-750 nm) (***Zheng et al., 2010***). Such optical properties of hemoglobin opened the possibility to use two photon excitation microscopy as a tool for label-free imaging of erythrocytes, even in vivo (***Li et al., 2011***).

Besides spatial distribution of hemoglobin in intact human and porcine erythrocytes, images of residual hemoglobin in erythrocyte ghosts also can be obtained by two photon excitation fluorescence microscopy (Figures 19 and 20, respectively). Intensity of two photon excitation signal depends on the concentration of the hemoglobin, but also on the pulse peak power, pulse duration, repetition rate, focal volume, excitation wavelength etc. In order to evaluate the local

change (i.e. decrease) in hemoglobin content after the hemolysis, we mixed the ghosts with intact erythrocytes. In this way we can evaluate local content of hemoglobin, i.e. distribution of hemoglobin across erythrocytes and ghosts, and not only average value for whole cell or suspension. From the image data we obtained variation of intensity along appropriately chosen representative lines, as depicted in Figures 19 and 20. The line is chosen in the way to intercept at least two erythrocytes and two ghosts which provide up to 8 representative points positioned in the proximity of membrane within the cells for comparison of two photon excitation signals. Note that the signals from the chosen points provide highly localized data for the comparison, just opposite to the cyanmethemoglobin assay, which is intrinsically averaging method. This ensures the same excitation parameters for both, erythrocytes and erythrocyte ghosts. The above procedure ensures that the peak ratio from the two photon excitation intensity profile is equal to the concentration ratio in the untreated erythrocyte(s) and the ghost(s). We emphasize that this simple step enables us to determine changes in the content of residual hemoglobin in ghosts relative to the starting content of hemoglobin in intact erythrocytes, but not the absolute concentration.

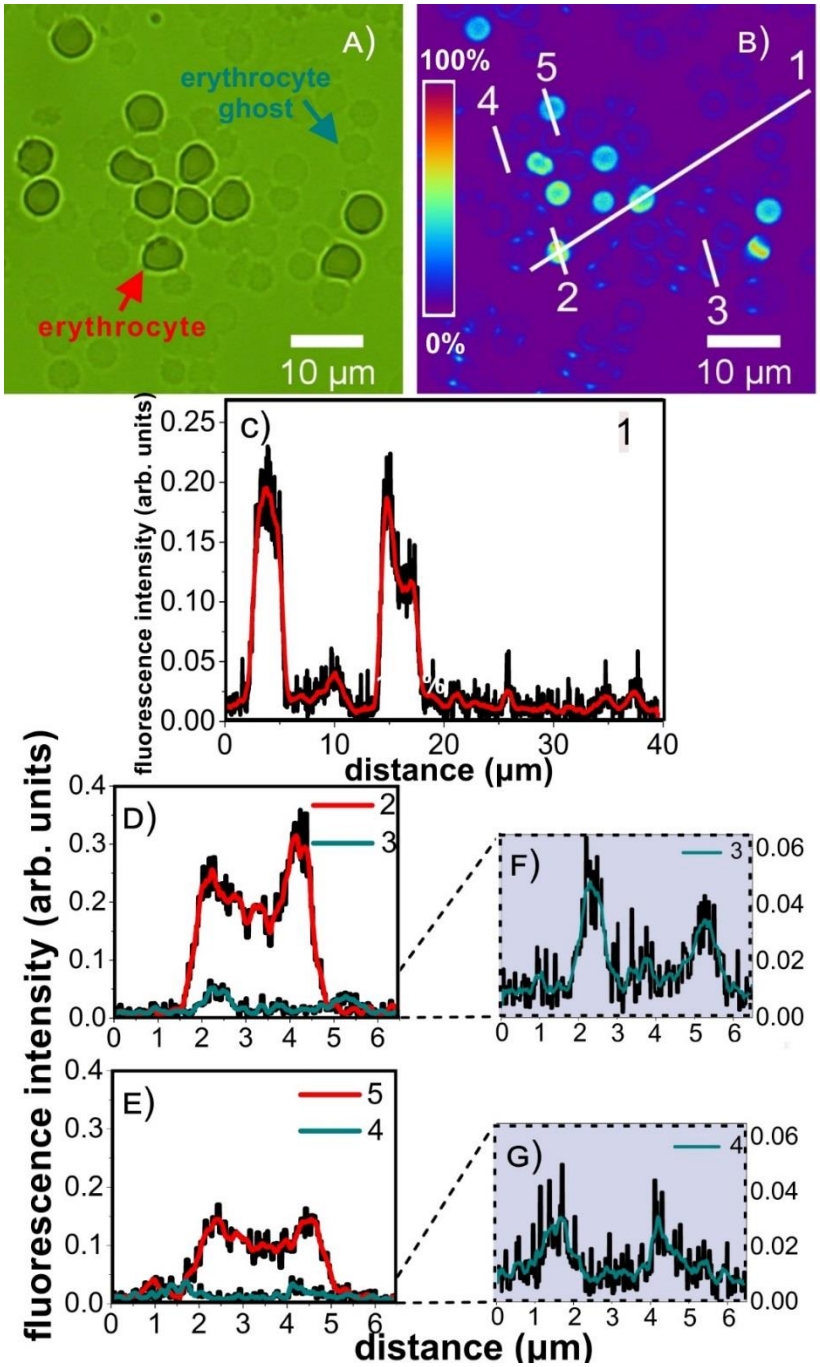

Figure 19. Mixed suspension of human erythrocytes and resulting erythrocyte ghosts: **(A)** bright field microscopy image; **(B)** two photon excitation microscopy image; **(C-G)** two photon excitation signal profiles along the corresponding lines at **(B)** image. Profiles 3 and 4 are given in magnified vertical scale in **(F)** and **(G)** graphs. Black curves are raw data plot, red and green curves are obtained upon adjacent points averaging.

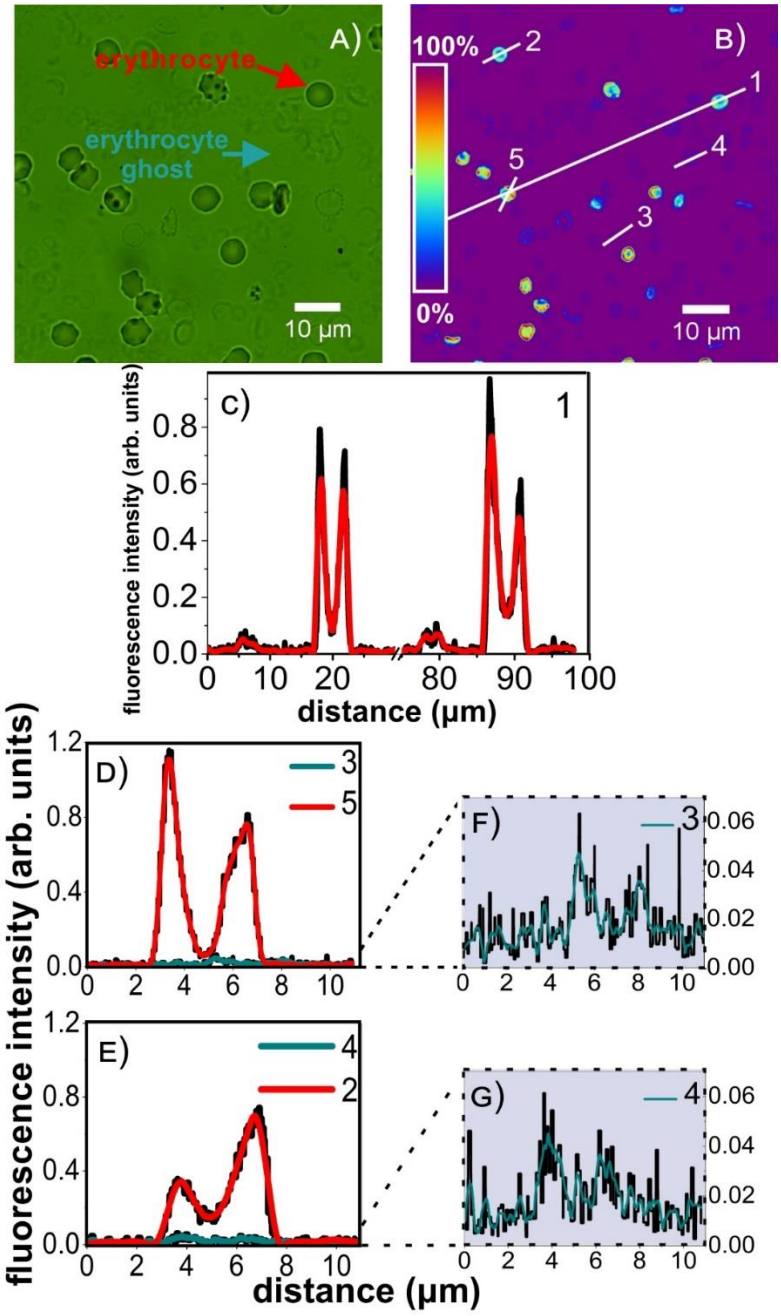

Figure 20. Mixed suspension of porcine erythrocytes and resulting erythrocyte ghosts: (a) bright field microscopy image; **(B)** two photon excitation microscopy image; **(C-G)** two photon excitation signal profiles along the corresponding lines at **(B)** image. Profiles 3 and 4 are given in magnified vertical scale in **(F)** and **(G)** graphs. Black curves are raw data plot, red and green curves are obtained upon adjacent points averaging.

As can be seen from the Figures 19 and 20, after the conversion of erythrocytes to empty erythrocyte membranes, fluorescence emission from hemoglobin significantly decreased, but was still detectable. Therefore, the applied process that we used allows the production of ghosts, however a certain amount of the hemoglobin always remains bound to the membrane. Comparing the peak values from graphs 19 (D) and (E) (red curves) to those in graphs 19 (F) and (G) one can estimate lower fluorescence emission for both porcine and human erythrocyte ghosts in comparison to respective erythrocytes. Our results suggest that residual hemoglobin in the suspension was localized on intracellular side of the ghost membranes. The two photon excitation signal in the internal volume of both, human and porcine erythrocyte ghosts is at the noise level, thus hemoglobin content is negligible.

These results supports already reported data on hemoglobin ability to bind to erythrocyte membrane via transmembrane protein, e.g. band 3 or some other cytoskeleton proteins via α globin chains (***Murakami et al., 2003***). This phenomenon that we have confirmed by two photon excitation microscopy could be used as valuable marker of inevitable oxidative damages (***Sharma et al., 2001***) emerged during *in vitro* storage and erythrocytes handling. The higher concentration of residual hemoglobin obtained in porcine ghosts relative to initial concentration, can be explained by specific membrane lipid composition and their high susceptibility to oxidative stress induced by reactive oxygen species (***Brzezińska-Slebodzińska, 2003***) related to lower level of enzymes protectants against oxidative damages (***Vodela et al., 1997***).

CONCLUSION

According to results obtained during the examination of two controlled drug delivery systems based on ordered mesoporous silica and erythrocyte ghosts following conclusions can be withdrawn:

- The ability of ordered mesoporous silica material (OMS) to improve biopharmaceutical performance of poorly soluble compound fenofibrate, was confirmed *in vitro*. *In vivo* study in dogs revealed pharmacokinetic profile of fenofibrate and its active metabolite fenofibric acid after oral administration of fenofibrate-OMS formulations. This study indicative of the potential of OMS-based formulations to improve bioavailability of fenofibrate, revealed good tolerability and satisfying safety level of the used dose (eq. 33.5 mg) of fenofibrate in this highly stable formulation and opened the possibility for its further in vivo testing in humans.
- The results of the clinical trial indicated that administration of an ordered mesoporous silica based formulation of fenofibrate resulted in an increased rate and extent of absorption in humans when compared to a marketed product. In addition, single doses of the ordered mesoporous silica based formulation were well tolerated by all volunteers. The present study is the first to demonstrate the bioavailability-enhancing potential of this novel formulation approach in man, and evidences the utility of this technique to overcome bioavailability problems associated with poor solubility.
- Although SD due to its surface active properties may bind to membranes and cause its disruption and solubilisation as in detergent-like way, under the applied process based on gradual hemolysis it was successfully encapsulated in erythrocyte ghosts. Despite its antihemolytic effect at lower concentrations, relatively high encapsulation efficiency was achieved. Comparing the two inexpensive, widely available materials-slaughterhouse porcine and outdated transfusion human blood, we demonstrated more preserved structure and functional properties of porcine erythrocytes related to the superior encapsulation and release of SD, and defined them as more promising candidate for the usage in SD encapsulation process on a large scale. However, obtained results indicate the necessity of further investigation in order to produce universal effective SD carrier

based on erythrocyte ghosts. These approaches depending of the administration route will include layering with different polymers (in order to mask the antigen determinants on the surface and to control relase more subtle), as well as examination of their behaviour in vivo.

The present study offers a potential solution for the problem of slaughterhouse waste disposal and on the other hand it contributes to the defining of the optimal formulation for diclofenac.

- Two-photon excitation fluorescence (2PE) microscopy can be used in analysis of spatial distribution of hemoglobin in erythrocytes and erythrocyte ghosts, at individual cell level. High-quality, label- and fixation- free visualization of hemoglobin can be achieved at 730nm excitation wavelength. The 2PE fluorescence signal from residual hemoglobin at representative points near the cell membrane in the ghosts was reported to have lower intensity than at the corresponding points in intact erythrocytes. Hemoglobin distribution in erythrocytes together with residual hemoglobin content and distribution in resulting erythrocyte ghosts can be directly and relatively easily estimated. The proposed method could be of significant importance for identifying different pathological or non-pathological conditions and application in material selection in biotechnological processes.

REFERENCES

Alba-Simionesco, C., Coasne, B., Dosseh, G., Dudziak, G., Gubbins, K., Radhakrishnan, R., Sliwinska-Bartkowiak, M., 2006. Effects of confinement on freezing and melting. J. Phys. Condens. Mat. 18, 15-68.

Andersson, J., Rosenholm, J., Areva, S., Linden, M., 2004. Influences of material characteristics on ibuprofen drug loading and release profiles from ordered micro- and mesoporous silica matrices. Chem. Mater. 16, 4160‑4167.

Azais, T., Tourne-Peteilh, C., Aussenac, F., Baccile, N., Coelho, C., Devoisselle, J.-M., Babonneau, F., 2006. Solid-state NMR study of ibuprofen confined in MCM-41 material. Chem. Mater. 18, 6382‑6390.

Altman, R., Bosch, B., Brune, K., Patrignani, P., Young, C., 2015. Advances in NSAID development: Evolution of diclofenac products using pharmaceutical technology. Drugs 75, 859-877.

Adriaenssens, K., 1976. Use of Enzyme-Loaded Erythrocytes in In Vitro Correction of Arginase Deficient Erythrocytes in Familiar Hyperargininemia. Clin. Chem. 22**,** 323–326.

Annese, V., Latiano, A., Rossi, L., 2005. Erythrocytes-mediated delivery of dexamethasone in steroid-dependent IBD patients – a pilot uncontrolled study. Am. J. Gastroenterol. 100, 1370-1375.

Attaulakhanov, F. I., Kulikova, E. V., Vitvitsky, V. M., 1996. Reversible binding of anthracycline antibiotics to erythrocytes treated with glutaraldexyde. Biotechnol. Appl. Biochem. 24, 241-244.

Alvarez, F. J., Jordan, J. A., Calleja, P., 1998. Cross-linking treatment of loaded erythrocytes increases delivery of encapsulated substance to macrophages. Biotechnol. Appl. Biochem. 27, 139-143.

Agnihotri, J., Saraf S., Singh S., Bigoniya P. 2015. Development and evaluation of anti-malarial bio-conjugates: artesunate-loaded nanoerythrosomes. Drug Deliv. and Transl. Res. 5, 489–497.

Brahmanker, D. M., Jaiswal, S. B., 2009. Biopharmaceutics and Pharmacokinetics: Pharmacokinetics, 2nd ed.Vallabh Prakashan, Delhi, pp. 399-401.

Boissere, C., Martines, M. A. U., Tokumoto, M., Larbot, A., Prouzet, E., 2003. Mechanisms of pore size control in MSU-X mesoporous silica. Chem. Mater. 15, 509-515.

Bimbo, L.M., Makila, E., Laaksonen, T., Lehto, V.P., Salonen, J., Hirvonen, J., Santos, H.A., 2011. Drug permeation across intestinal epithelial cells using porous silicon nanoparticles. Biomaterials 32, 2625‑2633.

Babonneau, F., Yeung, L., Steunou, N., Gervais, C., Ramila, A., Vallet-Regi, M., 2004. Solid state NMR characterisation of encapsulated molecules in mesoporous silica. J. Sol‑Gel Sci. Technol. 31, 219‑223.

Bird, J., Best, R., Lewis, D. A., 1983. The Encapsulation of Insulin in Erythrocytes. J. Pharm. Pharmacol. 35, 246–247.

Banz, A., Cremel, M., Rembert, A., 2010. In situ targeting of dendritic cells by antigen-loaded red blood cells: a novel approach to cancer immunotherapy. Vaccine. 28(17), 2965–2972.

Benatti, U., 1989. Enhanced Antitumor Activity of Adriamycin by Encapsulation in Mouse Erythrocytes Targeted to Liver and Lungs. Pharmacol. Res. 21, (suppl 2) 27–33.

Bird, J., Best, R., Lewis, D. A., 1983. The Encapsulation of Insulin in Erythrocytes. J. Pharm. Pharmacol. 35, 246–247.

Beutler, E., 1977. Enzyme Replacement Therapy in Gaucher’s Disease. Preliminary Clinical Trial of a New Enzyme Preparation. Proc. Natl. Acad. Sci. USA 74, 4620–4623.

Bukara, K., Schueller L., Rosier, J., Daems, T., Verheyden, L., Eelen, S., Martens, J., Van den Mooter, G., Bugarski, B., Kiekens, F., 2016. In Vivo Performance of Fenofibrate Formulated With Ordered Mesoporous Silica Versus 2-Marketed Formulations: A Comparative Bioavailability Study in Beagle Dogs. J. Pharm. Sci. 105, 2381-2385.

Brater, D. C., 2002. Anti-inflammatory agents and renal function. Semin. Arthritis Rheum. 32(3 Suppl 1), 33–42.

Bourgeaux, V., Lanao, J. M., Bax, B. E., Godfrin, Y., 2016. Drug-loaded erythrocytes: on the road toward marketing approval. Drug Design Development and Therapy 10, 665-676.

Cadot, J. M., 2009. In vitro-in vivo correlation: application to biotech product development, in Morishita, M., Park, K. (Eds.), Biodrug delivery systems: Fundamentals, Applications and Clinical development, CRC Press, Boca Raton, pp. 341-356.

Chen, Y., Lu, Y., Chen, J., Lai, J., Sun, J., Hu, F., Wu, W., 2009. Enhanced bioavailability of the poorly water-soluble drug fenofibrat by using liposomes containing a bile salt. Int. J. Pharm. 376, 153-160.

Corma, A., 1997. From microporous to mesoporous molecular sieve materials and their use in catalysis. Chem. Rev. 97, 2373-2420.

Corma, A., Kan, Q., Navarro, M. T., Perez-Pariente, J., Rey, F., 1997. Synthesis of MCM-41 with different pore diamaters without addition of auxiliary organics. Chem. Mater. 9, 2123-2126.

Charnay, C., Begu, S., Tourne-Peteilh, C., Nicole, L., Lerner., D. A., Devoisselle, J. M., 2004. Inclusion of ibuprofen in mesoporous templated silica drug loading and release property. Eur. J. Pharm. Biopharm. 57, 533-540.

Chiarantini, L., 1995. Modulated Red Blood Cell Survival by Membrane Protein Clustering. Mol. Cell Biochem. 144 (1), 53–59.

Chen, Y., Lu, Y., Chen, J., Lai, J., Sun, J., Hu, F., Wu, W., 2009. Enhanced bioavailability of the poorly water-soluble drug fenofibrat by using liposomes containing a bile salt. Int J Pharm. 376, 153-160.

Carson, J., Notis W. M., Orris E. S., 1990. Colonic ulceration and bleeding during diclofenac therapy. Engl J Med. 323-135.

Cooper, D. L., Harirforoosh S., 2014. Design and optimization of PLGA-based diclofenac loaded nanoparticles. Plos One 9.

Chambers, E., Mitragoni, S., 2004. Prolonged circulation of large polymeric nanoparticles by non-covalent adsorption on erythrocytes. J Control Release. 100, 111–19.

Colilla, M., Manzano, M., Vallet-Regí, M., 2008. Recent advances in ceramic implants as drug delivery systems for biomedical applications. Int J Nanomedicine. 3(4), 403-14.

Davies, N. M., Anderson, K. E., 1997., Clinical pharmacokinetics of diclofenac. Therapeutic insights and pitfalls. Clin Pharmacokinet. 33(3), 184–213.

Deloach, J. R., Ihler, G. M., 1977. A Dialysis Procedure for Loading of Erythrocytes with Enzymes and Lipids. Biochim. Biophys. Acta. 496, 136–145.

Doucet, J, Gao Z, MacLaren, L A, McAlister, V. C., 2004. Modification of xenoantigens on porcine erythrocytes for xenotransfusion. Surgery 135:178-186.

Dressman, J. B., Herbert, E., Wieber, A., Birk, G., Saal, C., Lubda, D., 2015.Mesoporous silica-based dosage forms improve release characteristics of poorly soluble drugs: case example fenofibrate. J Pharm Pharmacol. 1-12.

Deák, R., Mihály, J., Szigyártóa, I., Wacha, A., Lelkes, G., Bóta, A., 2015. Physicochemical characterization of artificial nanoerythrosomes derived from erythrocyte ghost membranes. Coll. Surf. B. 135, 225-234.

Deuticke, B., Kim, M., Zolinev, C., 1973. The Influence of Amphotericin - B on the Permeability of Mammalian Erythrocytes to Nonelectrolytes, anions and Cations. Biochim. Biophys. Acta. 318, 345–359.

Du, L., Song, H., Liao, S., 2009. Tuning the morphology of mesoporous silica by using various template combinations. Appl. Surf. Sci. 255, 9365-9370.

Deloach, J. R., 1982. Comparative Encapsulation of Cytosine Arabinoside Monophosphate in Human and Canine Erythrocytes with In Vitro Drug Efflux. J. Appl. Biochem. 4, 533–541.

Eichler, H. C., 1987. In Vitro Drug Release From Human Carrier Erythrocytes. Adv. Biosci. (series) 67, 11–15.

Eichler, H. G., 1986. In Vivo Clearance of Antibody-Sensitized Human Drug Carrier Erythrocytes. Clin. Pharmacol. Ther. 40, 300–303.

Fei, Y., Kostewicz, E. S., Sheu, M. T., Dressman, J. B., 2013. Analysis of the enhanced oral bioavailability of fenofibrate lipid formulations in fasting humans using an in vitro-in silico-in vivo approach. Eur. J. Pharm Sci. 85, 1274-1284.

Fowler, P. D., Shadforth, M. F., Crook, P. R., John, V. A., 1983. Plasma and synovial fluid concentrations of diclofenac sodium and its major hydroxylated metabolites during long-term treatment of rheumatoid arthritis. Eur. J. Clin. Pharmacol. 25(3), 389–394.

Field, W. N., Gamble, M. D., Lewis, D. A., 1989. A Comparison of Treatment of Thyroidectomized Rats with Free Thyroxin and Thyroxin Encapsulated in Erythrocytes. Int. J. Pharm. 51, 175–178.

Fraternale, A., Rossi, L., Magnani, M., 1996. Encapsulation, Metabolism, and Release of 2-Fluoro-Ara-AMP from Human Erythrocytes. Biochim. Biophys. Acta. 1291 (2), 149–154.

Fei, Y., Kostewicz E. S., Sheu, M. T., Dressman, J. B., 2013. Analysis of the enhanced oral bioavailability of fenofibrate lipid formulations in fasting humans using an in vitro-in silico-in vivo approach. Eur J Pharm Sci. 85, 1274-1284.

Fei, Y., Herbert, E., Wieber, A., Saal, C., Lubda, D., Kucera, S., Dressman, J. Evaluation of the dissolution behaviour of novel fenofibrate silica formulations in preprandial biorelevant media. AAPS Poster M1189, AAPS Annual Meeting, San Antonio, Texas 2013.

Fun, W., Yan, W., Hu, Z., Ni, H., 2012. Erythrocytes load of low molecular weight chitosan nanoparticles as a potential vascular drug delivery system. Colloids Surf B. 95, 258-265.

Flynn, G., McHale, L., McHale, A. P., 1994. Methotrexate-Loaded, Photosensitized Erythrocytes: A Photo-Activatable Carrier/Delivery System for Use in Cancer Therapy. Cancer Lett. 82 (2), 225–229.

Guay, D., 1993. Micronized fenofibrate: a new fibric acid hypolipidemic agent. Ann. Pharmacoter. 33(10), 1083-1103.

Genest, J. J., Nguyen, N. H., Theroux, P., Davignon, J., Cohn, J. S., 2000. Effect of micronized fenofibrate on plasma lipoprotein levels and hemostatic parameters on hypertrigliceridemic patients with low levels of high density lipoprotein cholesterol in the fed and fasted state. J. Cardiovasc. Pharmacol. 35(1), 164-172.

Grun, M., Unger, K. K., Matsumoto, A., Tsutsumi, K., 1999. Nowel pathways for the preparation of mesoporous MCM-41 materials: control of porosity and morphology. Micropor. Mesopor. Mater. 27, 207-216.

Gothoskar, A. V., 2004. Resealed erythrocytes: a review. Pharm. Tech. 140-158.

Gupta N., Patel B. Ahsan, F. 2014. Nano-Engineered Erythrocyte Ghosts as Inhalational Carriers for Delivery of Fasudil: Preparation and Characterization. Pharm Res. 31, 1553-1565.

Garin, M. I., 1996. Erythrocytes as Carriers for Recombinant Human Erythropoietin. Pharm. Res. 13, 869–874.

Horter, D., Dressman, B., 2001. Influence of physicochemical properties on dissolution of drugs in the gastrointestinal tract. Adv. Drug. Deliv. Rev. 46, 75-87.

Hens, B., Brouwers, J., Corsseti, M., Augustins, P., 2015. Gastrointestinal behavior of nano- and microsized fenofibrate: In vivo evaluation in man and in vitro simulation by assessment of the permeation potential. Eur. J. Pharm. Sci. 77, 40-47.

Heikkila, T., Salonen, J., Tuura, J., Kumar, N., Salmi, T., Murzin, D. Y., Hamdy, M. S., Mul, G., Laitinen, L., Kaukonen, A. M., Hirvonen, J., Lehto, V., 2007. Evaluation of mesoporous TCPSi, MCM-41, SBA-15 and TUD-1 materials as API carriers for oral drug delivery. Drug. Deliv. 14, 337-347.

Hu, Y., Zhi, Z., Zhao, Q., Wu, C., Zhao, P., Jiang, H., Jiang, T., Wang, S., 2012. 3D cubic mesoporous silica microsphere as a carrier for poorly soluble drug carvedilol. Microporous Mesoporous Mater. 147, 94‑101.

Hu, Y., Zhi, Z., Wang, T., Jiang, T., Wang, S., 2011. Incorporation of indomethacin nanoparticles into 3-D ordered macroporous silica for enhanced dissolution and reduced gastric irritancy. Eur. J. Pharm. Biopharm. 79, 544‑551.

Horcajada, P., Ramila, A., Perez-Pariente, J., Vallet-Regı, M., 2004. Influence of pore size of MCM-41 matrices on drug delivery rate. Microporous Mesoporous Mater. 68, 105‑109.

Ha, J.M., Hamilton, B.D., Hillmyer, M.A., Ward, M.D., 2009. Phase behavior and polymorphism of organic crystals confined within nanoscale chambers. Cryst. Growth Des. 9, 4766‑4777.

Hamidi, M., Tajerzadeh, H. 2003. Carrier Erythrocytes: An Overview, Drug Delivery. 10**,** 9–20.

Hamidi M., Azimi K., Mohammadi-Samani S., 2011. Co-encapsulation of a drug with a protein in erythrocytes for improved drug loading and release: Phenytoin and bovine serum album. J Pharm Pharmaceut 14, 46-59.

Hens, B., Brouwers, J., Corsseti, M., Augustins, P., 2015. Gastrointestinal behavior of nano- and microsized fenofibrate: In vivo evaluation in man and in vitro simulation by assessment of the permeation potential. Eur J Pharm Sci. 77, 40-47.

Ihler, G. M., 1983. Erythrocyte Carriers. Pharmacol. Ther. 20**,** 151–169.

John, C., Morten, C., 2002. The Science of Dosage Form Design, 2nd ed. Churchill Livingstone, pp. 290-300.

Jiang, H., Wang, T., Wang, L., Sun, C., Jiang, T., Cheng, G., Wang, S., 2012. Development of an amorphous mesoporous TiO2 nanosphere as a novel carrier for poorly water-soluble drugs: effect of different crystal forms of TiO2 carriers on drug loading and release behaviors. Microporous Mesoporous Mater. 153, 124‑130.

Jarvis, K.L., Barnes, T.J., Prestidge, C.A., 2011. Surface chemical modification to control molecular interactions with porous silicon. J. Colloid Interface Sci. 363, 327‑333.

Jaitely, V., 1995. Resealed Erythrocytes: Drug Carrier Potentials and Biomedical Applications. Indian Drugs 33**,** 589–594.

Jain, S., Jain, N. K., 1997. Engineered Erythrocytes as a Drug Delivery System. Indian J. Pharm. Sci. 59**,** 275–281.

Jain, S., Jain, S. K., Dixit, V. K., 1995. Erythrocytes Based Delivery of Isoniazid: Preparation and In Vitro Characterization," Indian Drugs 32, 471–476.

Jenner, D. J., 1981. The Effect of the Intravenous Administration of Corticosteroids Encapsulated in Intact Erythrocytes on Adjuvant Arthritis in the Rat. Brit. J. Pharmacol. 73, 212–213.

Jain, S., Jain, S. K., Dixit, V. K., 1995. Erythrocytes Based Delivery of Isoniazid: Preparation and In Vitro Characterization. Indian Drugs 32, 471–476.

Jain S. K., Vyas, S. P., 1994. Magnetically Responsive Diclofenac Sodium- Loaded Erythrocytes: Preparation and In Vitro Characterization. J. Microencapsul. 11 (2), 141–151.

Jammaer J., Aerts C. A., D'Haen J., Won Seob J., Martens J. 2009. Convenient synthesis of ordered mesoporous silica at room temperature and quasi-neutral pH. J Mater Chem 19, 8290-8293.

Kushal, M., Monali, M., Durgavati M., Mittal, P., Umesh, S., Pragna S., 2013. Oral controlled release drug delivery system: an overview. IRJP 4 (3), 70-76.

Kawabata, Y., Wada, K., Nakatani, M., Yamada, S., Onoue, S., 2011. Formulation design for poorly water-soluble drugs based on biopharmaceutics classification system: basic approaches and practical applications. Int. J. Pharm. 420, 1-10.

Kresge, C. T., Leonowicz, M. E., Roth, W. J., Vartuli, J. C., Beck, J. S., 1992. Ordered mesoporous molecular sieves synthetized by a liquid-crystal template mechanism. Nature 359, 710-712.

Kruk, M., Cao, L., 2007. Pore size tailoring in large pore SBA-15 silica synthesized in the presence of hexane. Langmuir 23, 7247-7254.

Kiekens, F., Eelen, S., Verheyden, L., Daems, T., Martens, J., Den Mooter, G.V., 2012. Use of ordered mesoporous silica to enhance the oral bioavailability of ezetimibe in dogs. J. Pharm. Sci. 101, 1136‑1144.

Kaukonen, A. M., Laitinen, L., Salonen, J., Tuura, J., Heikkila, T., Limnell, T., Hirvonen, J., Lehto, V. P., 2007. Enhanced in vitro permeation of furosemide loaded into thermally carbonized mesoporous silicon (TCPSi) microparticles. Eur. J. Pharm. Biopharm. 66, 348‑356.

Klibansky, C., 1959. PhD thesis, Hebrew University, Jerusalem, Israel.

Kostić, I., Ilić V., Đorđević, V., Bukara, K., Mojsilović, S., Nedović, V., Bugarski, D., Veljović, Đ., Mišić, D., Bugarski B., 2014. Erythrocyte membranes from slaughterhouse blood as potential drug vehicles: Isolation by gradual hypotonic hemolysis and biochemical and morphological characterization. Colloids Surf B 122, 250-259.

Ketan, S., Gajjar, A., Jignasa, S., 2012. Drug solubility: Importance and enhancement techniques. ISRN Pharm. 1-33.

Kiekens, F., Eelen, S., Verheyden, L., Daems, T., Martens, J., Van den Mooter, G., 2011. Use of ordered mesoporous silica to enhance the oral bioavailability of ezetimibe in dogs. J Pharm Sci. 101, 1136-1144.

Krajišnik, D., Daković, A., Malenović, A., Rakić, M. M., Dondur, V., Radulović, Ž., Milić J., 2013. Investigation of adsorption and release of diclofenac sodium by modified zeolite composites. Appl Clay Sci. 83-84, 322-326.

Kulkarni, A. R., Kumaresh, S., Soppimath Aminabhavi, T. M., 1999. Controlled release of diclofenac sodium from sodium diclofenac beads crosslinked with glutaraldehyde. Pharm Acta Helv. 74, 29-36.

Kozakevych, R. Z., Bolbykh, Y. M., Tertykh, V. A., 2013. Controlled release of diclofenac sodium from silica-chitosan composites. World Journal of nanoscience and engineering. 3, 69-78.

Kolesová, H., Čapek, M., Radochová, B., Janáček, J., Sedmera, D., 2016. Comparison of different tissue clearing methods and 3D imaging techniques for visualization of GFP-expressing mouse embryos and embryonic hearts. Histochem Cell Biol. 146(2), 141-152.

Kuo, Y. C., Wu, H. C., Hoang, D., Bentley, WE. ., D'Souza W. D., Raghavan S. Colloidal Properties of Nanoerythrosomes Derived from Bovine Red Blood Cells. Langmuir. 32: 171-179.

Kapoor, S., Hegde, R., Bhattacharyya, A.J., 2009. Influence of surface chemistry of mesoporous alumina with wide pore distribution on controlled drug release. J. Control. Release 140, 34‑39.

Kinnari, P., Makila, E., Heikkila, T., Salonen, J., Hirvonen, J., Santos, H.A., 2011. Comparison of mesoporous silicon and non-ordered mesoporous silica materials as drug carriers for itraconazole. Int. J. Pharm. 414, 148‑156.

Lee, V. H. L., 1987. Controlled drug delivery Fundamentals and Applications: Influence of drug properties on design, 2nd ed. Marcel Dekker, Inc New York, pp. 16-25.

Lu, Y., Park, K., 2013. Polymeric micelles and alternative nanonized delivery vehicles for poorly soluble drugs. Int. J. Pharm. 453, 198-214.

Limnell, T., Riikonen, J., Salonen, J., Kaukonen, A., Laitinen, L., Hirvonen, J., Lehto, V., 2007. Surface chemistry and pore size affect carrier properties of mesoporous silicon microparticles. Int. J. Pharm. 343, 141‑147.

Limnell, T., Santos, H.A., Makila, E., Heikkila, T., Salonen, J., Murzin, D.Y., Kumar, N., Laaksonen, T., Peltonen, L., Hirvonen, J., 2011. Drug delivery formulations of ordered and nonordered mesoporous silica: comparison of three drug loading methods. J. Pharm. Sci. 100, 3294‑3306.

Lewis, S. C., Langman, M.J., Laporte, J. R., Matthews, J. N., Rawlins, M. D., Wiholm, B. E., 2002. Dose-response relationships between individual nonaspirin nonsteroidal anti-inflammatory drugs (NANSAIDs) and serious upper gastrointestinal bleeding: a metaanalysis based on individual patient data. Br J Clin Pharmacol. 54(3), 320–326.

Lewis, D. A., 1984. Red Blood Cells for Drug Delivery. Pharm. J. 233**,** 384–385.

Lizano, C., Weissig, V., Torchilin, V. P., Sancho, P., Garcia-Perez, A. I., Pinilla, M., 2003. In vivo biodistribution of erythrocytes and polyethileneglycol-phosphatidilethanolamine micelles carrying the antitumor agent dequalinium. Eur. J. Pharm. Biopharm. 56, 153-157.

Lopes, L. B., Scarpa, M. V., Silva, G. V. J., Rodrigues, D. C., Santilli, C. V., Oliviera, A. G., 2004. Studies on the encapsulation of diclofenac in small unilamellar liposomes of soya phosphatidylcholine. Colloids Surf B. 39, 151-158.

Liu, D., Chen, L., Jiang, S., Zhu, S., Quian, Y., Wang, F., Li, R., Xu, Q., 2014. Formulation and characterization of hydrophilic drug diclofenac sodium-loaded solid lipid nanoparticles based on phospholipid complexes technology. J Liposome Res. 24, 17-26.

Li, D., Zheng, W., Zhang, W., The, S., Zeng, Y., Luo, Y., Qu, J., 2011. Time-resolved detection enables standard two-photon fluorescence microscopy for *in vivo* label-free imaging of microvasculature in tissue. Opt Lett. 36(14), 2638-2640.

Lejeune, A., Moorjani, M., Gicquaud, C., Lacroix, J., Poyet, P., Gaudreault, R., 1994. Nanoerythrosome, a new derivative of erythrocyte ghosts: Preparation and antineoplastic potential as drug carrier for daunorubicin. Anticancer Res. 14, 915-920.

Martinez, M., Rathbone, M., Burgess, D., Huynh, M., 2008. In vitro and in vivo considerations associated with parenteral sustained release products: a review based upon information presented and points expressed at the 2007 Controlled Release Society Annual Meeting. J. Control. Release 129, 79-87.

Ming-Thau, S., Ching-Min, Y., Sokoloski, T. D., 1994. Characterization and dissolution of fenofibrate solid dispersion systems. Int. J. Pharm. 103(2), 137-146.

Mellaerts, R., Houthoofd, K., Elen., K., Chen., H., Van Speybroeck, M., Van Humbeeck, J., Augustijns, P., Mullens, J., Van den Mooter, G., Martens., J. A., 2010. Aging behavior of pharmaceutical formulations of itraconasole on SBA-15 ordered mesoporous silica carrier material. Micropor. Mesopor. Mater. 130, 154-161.

Mellaerts, R., Jammaer, J.A.G., Van Speybroeck, M., Chen, H., Van Humbeeck, J., Augustijns, P., Van den Mooter, G., Martens, J.A., 2008a. Physical state of poorly water soluble therapeutic molecules loaded into SBA-15 ordered mesoporous silica carriers: a case study with itraconasole and ibuprofen. Langmuire 24, 8651-8659.

Mellaerts, R., Mols, R., Jammaer, J.A.G., Aerts, C.A., Annaert, P., Van Humbeeck, J., Van den Mooter, G., Augustijns, P., Martens, J.A., 2008. Increasing the oral bioavailability of the poorly water soluble drug itraconazole with ordered mesoporous silica. Eur. J. Pharm. Biopharm. 69, 223‑230.

Magnani, M., Rossi, L., Brandi, G., 1992. Targeting antiretroviral nucleoside analogues in phosphorylated form to macrophages: in vitro and in vivo studies. Proc Natl Acad Sci U S A., 89(14), 6477–6481.

Magnani, M., 1998. Erythrocyte Engineering for Drug Delivery and Targeting. Biotechnol. Appl. Biochem. 28, 1–13.

Muzykantov, V. R., 2010. Drug delivery by red blood cells: vascular carriers designed by Mother Nature. Expert Opin. Drug Deliv. 7 (4), 403-427.

Magnani, M., Rossi, L., D'Ascenzo, M., Panzani, I., Bigi, L., Zanella, A., 1998. Erythrocyte engineering for drug delivery and targeting. Biotechnol. Appl. Biochem. 26, 1-6.

Magnani, M., Rossi, L., Fraternale, A., 2002. Erythrocyte-mediated delivery of drugs, peptides and modified oligonucleotides. Gene. Ther. 9, 749-751.

Magnani, M., 1989. Acetaldehyde Dehydrogenase-Loaded Erythrocytes as Bioreactors for Removal of Blood Acetaldehyde, Alcoholism. Clin. Exp. Res. 13, 849–859.

Matherne, C. M., Satterfield, W. C., Gasparini, A., 1994. Clinical efficacy and toxicity of doxorubicin-encapsulated in glutaraldexyde-treated erythrocytes administered to dogs with lymphosarcoma. Am. J. Vet. Res. 55, 847-853.

Mellaerts R., Aerts C. A., Van Humbeeck J., Augustijns P., Van den Mooter G., Martens J., 2007. Enhanced release of itraconazole from ordered mesoporous SBA-15 silica materials. Chem Commun. 13, 1375-1377.

Mansouri, S., Merhi, Y., Winnik, F. M., Tabrizian, M., 2011. Investigation of layer-by-layer assembly of polyelectrolytes on fully functional human red blood cells in suspension for attenuated immune response. Biomacromolecules. 12, 585-592.

Masters, B. R., So P., 2008. Handbook of Biomedical Nonlinear Optical Microscopy. Oxford University Press.

Mellaerts, R., Mols, R., Jammaer, J. A. G., Aerts, A., Annaerts, P., Humbeeck, J. V., Van den Mooter, G., 2008. Increasing the oral bioavailability of the poorly water soluble drug itraconazole with ordered porous material. Eur J Pharm Biopharm. 69, 223-230.

Muzykantov, V. R., 2010. Drug delivery by red blood cells: Vascular carriers designed by mother nature. Expert Opin Drug Deliv. 7, 403–27.

Nicolau, C., Gersonde, K., 1979., Incorporation of Inositol Hexaphosphate into Intact Red Blood Cells, I: Fusion of Effector-Containing Lipid Vesicles with Erythrocytes. Naturwissenschaften 66 (11), 563–566.

Nangare, K., Powar, S., Payghan, S., 2016. Nanoerythrosomes: Engineered Erythrocytes as a Novel Carrier for the Targeted Drug Delivery. Asian Journal of Pharmaceutics. 10, 223-233.

Oddsson, E., Gudjonsson, H., Thjodleifsson, B., 1990. Endoscopic findings in the stomach and duodenum after treatment with enteric-coated and plain naproxen tablets in healthy subjects. Scand J Gastroenterol. 25, 231–234.

Pouton, C. W., 2006. Formulation of poorly water-soluble drugs for oral administration: physicochemical and physiological issues and the lipid formulation classification system. Eur. J. Pharm. Sci. 29, 278-287.

Patrono, C., Baigent, C., 2014. Nonsteroidal anti-inflammatory drugs and the heart. Circulation. 129(8), 907–16.

Phillips, K. A., Veenstra, D. L., Oren, E., Lee, J. K. Sadee, W., 2001. Potential role of pharmacogenomics in reducing adverse drug reactions: a systematic review. JAMA. 286(18), 2270-2279.

Patrono, C., Patrignani, P., Garcia, Rodriguez., LA., 2001. Cyclooxygenase - selective inhibition of prostanoid formation: transducing biochemical selectivity into clinical read-outs. J. Clin. Invest. 108(1), 7–13.

Riikonen, J., Makila, E., Salonen, J., Lehto, V.P., 2009. Determination of the physical state of drug molecules in mesoporous silicon with different surface chemistries. Langmuir 25, 6137‑6142.

Rengarajan, G.T., Enke, D., Steinhart, M., Beiner, M., 2011. Size-dependent growth of polymorphs in nanopores and Ostwald s step rule of stages. Phys. Chem. Chem. Phys. 13, 21367‑21374.

Rechsteiner, M. C., 1975. Uptake of Protein by Red Cells. Exp. Cell Res. 43, 487–492.

Rossi, L., Serafini, S., Cenerini, L., 2001. Erythrocyte-mediated delivery of dexamethasone in patients with chronic obstructive pulmonary disease. Biotechnol. Appl. Biochem. 33, 85-89.

Rossi, L., Castro, M., D'Orio, F., 2004. Low doses of dexamethasone constantly delivered by autologous erythrocytes slow the progression of lung disease in cystic fibrosis patient. Blood Cells Mol. Dis. 33, 57-63.

Rabasović, M., Pantelić, D., Jelenković, B., Ćurčić, S., Rabasović, M., Vrbica, M., Lazović, V., Ćurčić, B., Krmpot, K., 2015. J. Biomed. Opt. 20(1).

Scott, J., Wirnsberger, G., Stuckz, G. D., 2001. Mesoporous and mesostructured materials for optical applications. Chem. Mater. 13, 3140-3150.

Salonen, J., Laitinen, L., Kaukonen, A., Tuura, J., Bjorkqvist, M., Heikkila, T., Vahaheikkila, K., Hirvonen, J., Lehto, V.P., 2005. Mesoporous silicon microparticles for oral drug delivery: loading and release of five model drugs. J. Control. Release 108, 362‑374.

Song, S.W., Hidajat, K., Kawi, S., 2005. Functionalized SBA-15 materials as carriers for controlled drug delivery influence of surface properties on matrix drug interactions. Langmuir, 9568‑9575.

Salonen, J., Kaukonen, A.M., Hirvonen, J., Lehto, V.P., 2008. Mesoporous silicon in drug delivery applications. J. Pharm. Sci. 97, 632‑653.

Song, S.W., Hidajat, K., Kawi, S., 2005. Functionalized SBA-15 materials as carriers for controlled drug delivery influence of surface properties on matrix drug interactions. Langmuir, 9568‑9575.

Salvo, F., Fourrier-Reglat, A., Bazin, F., Robinson, P., Riera-Guardia, N., Haag, M., 2011. Cardiovascular and gastrointestinal safety of NSAIDs: a systematic review of meta-analyses of randomized clinical trials. Clin Pharmacol Ther. 89(6), 855–66.

Sinha, M., Gautam, L., Shukla, P. K., Kaur, P., Sharma, S., Singh, T. P., 2013. Current perspectives in NSAID-induced gastropathy. Mediat. Inflamm. 209-258.

Sprandel, U., 1987. Towards Cellular Drug Targeting and Controlled Release of Drugs by Magnetic Fields. Adv. Biosci. (series) 67**,** 243–250.

Schrier, S. L., 1975. Energized Endocytosis in Human Erythrocyte Ghosts, J. Clin. Invest. 56 (1), 8–22.

Sprandel, U., Hubbard, A. R., Chalmers, R. A., 1980. In Vivo Life Span of Resealed Rabbit Erythrocyte 'Ghosts'. Res. Exp. Med. (Berl) 177 (1), 13–17.

Skorokhod, O. A., Garmaeva, T., Vitvitsky, V. M., 2004. Pharmacokinetics of erythrocyte-bound daunorubicin in patients with acute leukemia. Med. Sci. Monit. 10, 55-64.

Sharma, D., Soni M., Kumar, S., Gupta G. D., 2009. Solubility enhancement—eminent role in poorly soluble drugs. Res J Pharm Tech. 2(2), 220–224.

Suwalsky, M., Manrique, M., Villena, F., Sotomayor, C. P., 2009. Structural effects in vitro of the antiinflamatory drug diclofenac on human erythrocytes and molecular models on cell membranes. Biophys Chem. 141, 34-40.

Sternberg, N., Georgieva, R., Duft, K., Baumler, H., 2011. Surface-modified loaded human red blood cells for targeting and delivery of drugs. 1-12.

Sayari, A., Yang, Y., Kruk, M., Jaroniec, M., 1999. Expanding the pore size of MCM-41 silicas: use of amines as expanders in direct synthesis and postsynthesis procedures. J. Phys. Chem. B 103, 3651‑3658.

Summers, M. P., 1983. "Recent Advances in Drug Delivery. Pharm. J. 230, 643–645.

Staels, B., Dallongeville, J., Auwerx, J., Schoonjans, K., Leitersdorf, E., Fruchart, J., 1998. Mechanism of Action of Fibrates on Lipid and Lipoprotein Metabolism. Cardiovascular Drugs. 98, 2088-2093.

Taguchi, A., Schuth, F., 2005. Ordered mesoporous materials in catalysis. Microporous. Mesoporous. Mater. 77, 1-45.

Tozuka, Y., Wongmekiat, A., Kimura, K., Moribe, K., Yamamura, S., Yamamoto, K., 2005. Effect of pore size of FSM-16 on the entrapment of flurbiprofen in mesoporous structures. Chem. Pharm. Bull. 53, 974‑977.

Todd, P. A., Sorkin, E. M., 1988. Diclofenac sodium. Drugs. 35(3), 244–285.

Torotra, G. J., Grabowski, S. R., 1993. The Cardiovascular System: The Blood, in Principles of Anatomy and Physiology, Harper Collins College Publishers, New York, NY, 7th ed., pp. 566–590.

Telen, M. J., 1993. The Mature Erythrocytes, in Winthrob's Clinical Hematology, R. Lee et al., Eds. Lea & Febiger, Philadelphia, PA, 9th ed., pp. 101–133.

Tsong, T. Y., Kinosita, K., 1985. Use of Voltage Pulses for the Pore Opening and Drug Loading, and the Subsequent Resealing of Red Blood Cells. Bibl Haematol. 51, 108–114.

Tajerzadeh, H., Hamidi, M., 2000. Evaluation of the Hypotonic Preswelling Method for Encapsulation of Enalaprilat in Human Intact Erythrocytes, Drug Dev. Ind. Pharm. 26, 1247–1257.

Tan, C., L-Asparaginase in Leukemia. Hosp. Pract. **7,** 99–103.

Tonetti, M., Astroff, A. B., Satterfield, W., De Flora, A., Benatti, U., DeLoach, J., R., 1991. Pharmacokinetic properties of doxorubicin encapsulated in glutaraldexyde-treated canine erythrocytes. Am. J. Vet. Res. 52, 1630-1635.

Todd P. A., Sorkin E. M., 1988. Diclofenac sodium. A reappraisal of its pharmacodynamics and pharmacokinetic properties and therapeutic efficiency. Drugs. 35, 244–285.

Takagi, T., Ramachandran, C., Bermejo, M.,Yamashita, S., Yu, L. X., Amidon, G. L., 2006. A provisional biopharamaceutical classification of the top 200 oral drug products in the United States, Great Britain, Spain and Japan. Mol. Pharm. 3, 631-643.

Updike, S. J., Wakamiya, R. T., 1983. Infusion of Red Blood Cell-Loaded Asparaginase in Monkey. J. Lab. Clin.Med. 101, 679–691.

Van Speybroeck, M., Mellaerts, R., Mols, R., Thi, T. D., Martens, J. A., Humbeeck, J. V., Annaert, P., Van den Mooter, G., Augustijns, P., 2010. Enhanced absorption of the poorly soluble drug fenofibrate by tuning its release rate from ordered mesoporous silica. Eur. J. Pharm. Sci. 41, 623-630.

Van Speybroeck, M., Barillaro, V., Thi, T.D., Mellaerts, R., Martens, J., Van Humbeeck, J., Vermant, J., Annaert, P., Van den Mooter, G., Augustijns, P., 2009. Ordered mesoporous silica material SBA-15: a broad-spectrum formulation platform for poorly soluble drugs. J. Pharm. Sci. 98, 2648‑2658.

Vialpando, M., Aerts, A., Persoons, J., Martens, J., Van Den Mooter, G., 2011. Evaluation of ordered mesoporous silica as a carrier for poorly soluble drugs: influence of pressure on the structure and drug release. J. Pharm. Sci. 100, 3411‑3420.

Vane, J. R., 1971. Inhibition of prostaglandin synthesis as a mechanism of action for aspirin-like drugs. Nat N Biol. 231(25), 232–2355.

Vyas, S. P., Khar, R. K., 2002. Resealed Erythrocytes in Targeted and Controlled Drug Delivery: Novel Carrier Systems, CBS Publishers and Distributors, India, pp. 87–416.

Van Assendelft, O. W., Holtz, A. H., Lewis, S. M. 1984. Recommended method for the determination of the haemoglobin content of blood, I. C. S. H. Publications, World Health Organization, 1. 4. 1.

Vialpando, M., Backhujis F., Martens, J. A., Mooter, G. V., 2012. Risk assessment of premature drug release during wet granulation of ordered mesoporous silica loaded with poorly soluble compounds itraconazole, fenofibrate, naproxen and ibuprofen. Eur J Pharm Biopharm. 81, 190-198.

Van Speybroeck, M., Bariallaro, V., Do Thi, T., Mellaerts, R., Martens, J., Van Humbeeck, J., Vermant, J., Annaert P., Van den Mooter, G., Augustijns, P., 2009. Ordered mesoporous silica material SBA-15: A broad spectrum formulation platform for poorly soluble drugs. J Pharm Sci. 98, 2648-2658.

Van Speybroeck, M., Mellaerts, R., Mols, R., Thi, T. D., Martens, J. A., Van Humbeeck, J., Annaert, P., Van den Mooter, G., Augustijns, P., 2010. Enhanced absorption of the poorly soluble drug fenofibrate by tuning its release rate from ordered mesoporous silica. Eur J Pharm Sci. 41, 623-630.

Vallet-Regi, M., Balas, F., Arcos, D., 2007. Mesoporous materials for drug delivery. Angew. Chem. 46, 7548-7558.

Wan, Y., Zhao, D., 2007., On the controllable soft-templating approach to mesoporous silicates. Chem. Rev. 107, 2821-2860.

Wang, F., Hui, H., Barnes, T.J., Barnett, C., Prestidge, C.A., 2010. Oxidized mesoporous silicon microparticles for improved oral delivery of poorly soluble drugs. Mol. Pharmacol. 7, 227‑236.

Witham, R. 1991. Voltaren (diclofenac-sodium)-induced ileocholitis. J Gastroenterol. 86, 246–247.

Wang, B., Koenig K., Riemann, I., Krieg, R., Halbhuber, K., 2006. Intraocular multiphoton microscopy with subcellular spatial resolution by infrared femtosecond lasers. Histochem Cell Biol. 126(4), 507-515.

Xu, W., Riikonen, J., Lehto, V., 2013. Mesoporous systems for poorly soluble drugs. Int. J. Pharm. 453, 181-197.

Xia, X., Zhou, C., Ballell, L., Garcia-Bennett, A.E., 2012. In vivo enhancement in bioavailability of atazanavir in the presence of proton-pump inhibitors using mesoporous materials. ChemMedChem 7, 43–48.

Xu, W., Gao, Q., Xu, Y., Wu, D., Sun, Y., Shen, W., Deng, F., 2009. Controllable release of ibuprofen from size-adjustable and surface hydrophobic mesoporous silica spheres. Powder Technol. 191, 13‑20.

Yun, Y. H., Lee, B. K., Park, K., 2015. Controlled drug delivery: Historical perspective for the next generation. J. Controlled Release 219, 2-7.

Yousaf, A. M., Kim, D. W., Oh, Y. K., Yong, C. S., Kim, Y. O., Choi, H. G., 2015. Enhanced oral bioavailability of fenofibrate using polymeric nanoparticulated systems: physicochemical characterization and in vivo investigation. Int. J. Nanomed. 10, 1819-1830.

Yu, Y., Ricciotti, E., Scalia, R., Tang, S. Y., Grant, G., Yu, Z., 2012. Vascular COX-2 modulates blood pressure and thrombosis in mice. Sci. Transl. Med. 4(132), 132-154.

Yousaf, A. M., Kim, D. W., Oh, Y. K., Yong, C. S., Kim, Y. O., Choi, H. G., 2015. Enhanced oral bioavailability of fenofibrate using polymeric nanoparticulated systems: physicochemical characterization and in vivo investigation. Int J Nanomed. 10, 1819-1830.

Zheng, F., Liang, L., Gao, Z., Sukamto, J. H., Aardahl, C. L., 2002. Carbon nanotube synthesis using mesoporous silica templates. Nano Lett. 2, 729-732.

Zhao, D., Sun, J., Li, Q., Stuckz, G. D., 2000. Morphological control of highly ordered mesoporous silica SBA-15. Chem. Mater. 12, 275-279.

Zhao, D., Feng, J., Huo, Q., Melosh, N., Fredrickson, G., Chmelka, B., Stucky, G., 1998. Triblock copolymer synthesis od mesoporous silica with periodic 50-300 A pores. Science 279, 548-552.

Zhao, Q., Wang, T., Wang, J., Zheng, L., Jiang, T., Cheng, G., Wang, S., 2012. Fabrication of mesoporous hydroxycarbonate apatite for oral delivery of poorly water-soluble drug carvedilol. J. Non-Cryst. Solids 358, 229‑235.

Zhao, P., Wang, L., Sun, C., Jiang, T., Zhang, J., Zhang, Q., Sun, J., Deng, Y., Wang, S., 2012b. Uniform mesoporous carbon as a carrier for poorly water soluble drug and its cytotoxicity study. Eur. J. Pharm. Biopharm. 80, 535‑543.

Zhang, Y., Wang, J., Bai, X., Jiang, T., Zhang, Q., Wang, S., 2012. Mesoporous silica nanoparticles for increasing the oral bioavailability and permeation of poorly water soluble drugs. Mol. Pharmacol. 9, 505‑513.

Zhang, Y., Zhi, Z., Jiang, T., Zhang, J., Wang, Z., Wang, S., 2010. Spherical mesoporous silica nanoparticles for loading and release of the poorly water-soluble drug telmisartan. J. Control. Release 145, 257‑263.

Zimmermann, U., Pilwat, G., Riemann, F., 1975. Preparation of Erythrocyte Ghosts by Dielectric Breakdown of the Cell Membrane. Biochim Biophys Acta. 375 (2), 209–219.

Zocchi, E., Guida, L., Benatti, U., 1987. Hepatic or splenic targeting of carrier erythrocytes: a murine model. Biotechnol Appl Biochem. 9(5), 423–434.

Zimmermann, U., 1973. Jahresbericht der Kernforschungsanlage Julich GmbH (Nuclear Research Center, Julich), pp. 55–58.

Zimmermann, U., 1983. Cellular Drug-Carrier Systems and Their Possible Targeting In Targeted Drugs, EP Goldberg, Ed. John Wiley & Sons, New York, pp. 153–200.

Zheng, W., Li, D., Zeng, Y., Luo, Y., Qu, J. Y. 2010. Two-photon excited hemoglobin fluorescence. Biomed Opt Express. 2, 71-79.

BIOGRAPHY

Katarina Bukara, master of pharmacy, was born on 23.02.1987. in Kraljevo, Serbia. After finishing elementary school ‘Sveti Sava’ in Kraljevo in 2002., she was enrolled in the Medical high school where she graduated in 2006. In both elementary and high school, she was awarded with ‘Vukova diploma’ for exceptional grades. In 2006/2007 she was enrolled at Faculty of Pharmacy, University of Belgrade and graduated in 2011. with average grade 9.37. She started her PhD in 2011/1012 at the Faculty of Technology and Metallurgy in Belgrade in the field of Biochemical engineering and Biotechnology under the supervision of dr Branko Bugarski, full professor. During her PhD studies she successfully passed all required exams according to the plan and program with average grade 10.00; and her final exam ’’Possibility of using erythrocyte membranes from slaughterhouse blood as carriers for biologically active molecules - an example of dexamethasone’’ was defended with grade 10.00.

Since 2011. she has been employed as a junior researcher in Innovation center of the Faculty of Technology and Metallurgy, University of Belgrade on the project ’’Development of new encapsulation enzyme technologies for the production of biocatalizators and biologically active components of food with an aim to improve its concurence, quality and safety’’ under the supervision of dr Branko Bugarski, full professor. During this period, she was actively involved in the collaboration with Institute for Medical Research, University of Belgrade and Institute for Physics, University of Belgrade. She spent one academic year (2015/2016) at the Faculty of Pharmaceutical, Biomedical and Veterinary sciences, University of Antwerp, Belgium as an exchange student and holder of the scholarship in the field of pharmaceutical technology provided by European Commission. Since 2016. she has been involved in the projects of pharmaceutical company Johnson & Johnson, Belgium, in the department for the research and development of parenteral and liquid dosage forms.

The list of published articles and reports

Articles published in the top-level scientific international journals **(M21):**

1. **Bukara K.**, Jovanic S., Drvenica I., Stancic A., Ilic V., Rabasovic M., Pantelic D., Jelenkovic B., Bugarski B., Krmpot A. (2017) Mapping of hemoglobin in erythrocytes and erythrocyte ghosts using two photon excitation fluorescence microscopy. J. Biomed. Opt. 22(2), doi: 10.1117/1.JBO.22.2.026003.

2. **Bukara K.**, Schueller L., Rosier J., Martens M. A., Daems T., Verheyden L., Eelen S., Van Speybroeck M., Libanati C., Martens J. A., Van Den Mooter G., Frérart F., Jolling K., De Gieter M., Bugarski B., Kiekens F. (2016) Ordered mesoporous silica to enhance the bioavailability of poorly water-soluble drugs: Proof of concept in man. Eur J Pharm Biopharm, IF=3.975, ISSN 0939-6411.

3. **Bukara K.**, Schueller L., Rosier J., Daems T., Verheyden L., Eelen S., Martens J. A., Van den Mooter G., Bugarski B., Kiekens F. (2016) In Vivo performance of fenofibrate formulated with ordered mesoporous silica versus two marketed formulations: A comparative bioavailability study in beagle dogs. J Pharm Sci, IF=2.59, ISSN 1520-6017.

4. Drvenica I., **Bukara K.**, Ilić V., Mišić D., Vasić B., Gajić R., Đorđević V., Veljović Đ., Belić A., Bugarski B. (2016) Biomembranes from slaughterhouse blood erythrocytes as prolonged release systems for dexamethasone sodium phosphate. Biotechnol Prog, IF=2.167, ISSN 1520-6033.

5. Kostić I., Ilić V., Đorđević V., **Bukara K.**, Mojsilović S., Nedović V., Bugarski D., Veljović Đ., Mišić D., Bugarski B. (2014) Erythrocyte membranes from slaughterhouse blood as potential drug vehicles: Isolation by gradual hypotonic hemolysis and biochemical and morphological characterization. Colloids Surf B Biointerfaces, IF=4.152, ISSN 0927-7765.

Articles published in the prominent scientific international journals **(M22):**

1. **Bukara K.**, Drvenica I., Ilić V., Stančić A., Mišić D., Vasić B., Gajić R., Vučetić D., Kiekens F., Bugarski B. (2016) J Biotechnol, Comparative studies on osmosis based encapsulation of sodium diclofenac in porcine and outdated human erythrocyte ghosts. IF=2.667, ISSN 0168-1656.

Articles published in the scientific international journals **(M23):**

1. Kostić I., Ilić V., **Bukara K.**, Mojsilović S., Đurić Z., Drašković P., Bugarski B. (2014) Flow cytometric determination of osmotic behaviour of animal erythrocytes toward their engineering for drug delivery, Hemijska industrija, IF 0.364, ISSN: 2217-7426.

Reports from the international meeting completely printed **(M33):**

1. Bukara K., Kostić I., Pravilović R., Kalušević a., Ilić S., Marković V., Bugarski B., Termoprotective effect of maltose on hemoglobin isolated from porcine slaughterhouseblood and outdated human red blood cells, IV International congress "Engineering, Environment and Materials in Processing Industry" Jahorina, Republic of Srpska, Bosnia and Herzegovina, 04th- 06th March 2015.
2. Kostić I., Bukara K., Pravilović R., Ilic V., Mojsilović S., Markovic S., Bugarski B., Morphological characterization of erythrocyte membranes derived from bovine and porcine slaughterhouse blood as dexamethasone sodium phosphate carriers, IV International congress "Engineering, Environment and Materials in Processing Industry" Jahorina, Republic of Srpska, Bosnia and Herzegovina, 04th-06th March 2015, ISBN 978-99955-81-17-6.

Reports from the international meetings printed as abstracts **(M34)**:

1. Bukara K., Vladkovic A., Kostic I., Stancic A., Ilic V, Rabasovic M., Pantelic D., Jelenkovic B., Krmpot A., Bugarski B., Two photon excitation fluorescence microscopy analysis of porcine erythrocytes and erythrocyte ghosts, The fifth

International School and Conference on Photonics-PHOTONICA 2015. 24-28. August 2015 Belgrade, Serbia. ISBN: 978-86-7306-131

2. Bukara K., Kostic I., Ilic V., Stančić A., Bugarski B., Usage of erythrocyte membranes from slaughterhouse blood as controlled drug delivery systems-example of dexamethasone, Belgrade International Molecular Life Science Conference for Students, 15-18 January 2015, Belgrade, Serbia.

3. Bukara K., Kostic I., Ilic V., Stančić A., Bugarski B., Solid state characterization of maltose-embedded hemoglobin from porcine slaughterhouse blood, Belgrade International Molecular Life Science Conference for Students, 15-18 January 2015, Belgrade, Serbia.
4. Bukara K., Kostić I., Ilić V., Marković S., Lazarević N., Bugarski B., Solid state characterization of maltose-embedded hemoglobin from porcine slaughterhouse blood, Thirteenth Young Researchers Conference – Materials Science and Engineering, December 10-12, 2014, Belgrade, Serbia. ISBN 978-86-80321-30-1
5. Kostić I., Bukara K., Ilić V., Veljović Đ., Bugarski B., Morphology and protein composition of porcine erythrocyte ghosts altered by different buffers,18th International Microscopy Congress, Prague, Czech Republic 7- 12 September, 2014 ISBN 978-80-260-6720-7
6. Kostić I., Bukara K., Ilić V., Ralević U., Bugarski B., Preparation of erythrocyte ghosts from slaughterhouse blood for AFM observation, 18th International Microscopy Congress, Prague, Czech Republic 7- 12 September, 2014 ISBN 978-80-260-6720-7.
7. Kostić I., Đorđević V., Ilić V., Bukara K., Nedović V., Bugarski B., Novel carriers of active substances derived from porcine slaughterhouse blood, COST ACTION FA 1001 WG1+WG2+WG3 meeting "The nano, micro, macro confluence in food structure for health, wellness and pleasure" Bucharest, Romania, 27-28 February 2014 Editura Academica, ISBN: 978-973-8937-80-2.
8. Kostić I., Bukara K., Ilić V., Bugarski B., Effect of bovine blood storage in slaughterhouses on parameters relevant to hemoglobin isolation, International 57th

Meat Industry Conference "Meat and meat products – perspectives of sustainable production" June 10-12, 2013, Belgrade ISBN 978-86-82547-07-5.

9. Kostić I., Bukara K., Ilić V., Mojsilović S., Đorđević V., Isailović B., Veljović Đ, Bugarski B., Scanning electron microscopy observation of erythrocyte ghosts isolated from slaughterhouse blood by gradual hemolysis, Microscopy Conference, 25-30 August 2013. University of Regensburg, Regensburg, Germany urn:nbn:de:bvb:355-epub-287343

Reports from the meetings of the national importance printed as abstracts **(M64):**

1. Kostić I., Bukara K., Ilić V., Šekularac G., Mišić D., Nedović V., Bugarski B., From meat industry waste to potential active substances carriers: Erythrocyte ghosts from slaughterhouse blood as dexamethasone sodium phosphate carriers, II International Congress of Food Technology, Quality and Safety (Food Tech Congress) Novi Sad, Serbia, 28-30 October 2014, ISBN 978-86 -7994 7994 -041 -4.

Прилог 1.

Изјава о ауторству

Потписани-а КАТАРИНА БУКАРА

број индекса 4005/2011

Изјављујем

да је докторска дисертација под насловом

Системи са контролисаним отпуштањем лекова засновани на мезопорозној силици и еритроцитним мембранама (Controlled drug delivery systems based on mesoporous silica and erythrocyte membranes)

- резултат сопственог истраживачког рада,
- да предложена дисертација у целини ни у деловима није била предложена за добијање било које дипломе према студијским програмима других високошколских установа,
- да су резултати коректно наведени и
- да нисам кршио/ла ауторска права и користио интелектуалну својину других лица.

Потпис докторанда

У Београду, 09.06.2017.

Катарина Букара

Прилог 2.

Изјава о истоветности штампане и електронске верзије докторског рада

Име и презиме аутора Катарина Букара

Број индекса 4005/2011

Студијски програм Биохемијско инжењерство и биотехнологија

Наслов рада Системи са контролисаним отпуштањем лекова засновани на мезопорозној силици и еритроцитним мембранама (Controlled drug delivery systems based on mesoporous silica and erythrocyte membranes)

Ментор Бранко Бугарски

Потписани/а

Изјављујем да је штампана верзија мог докторског рада истоветна електронској верзији коју сам предао/ла за објављивање на порталу **Дигиталног репозиторијума Универзитета у Београду.**

Дозвољавам да се објаве моји лични подаци везани за добијање академског звања доктора наука, као што су име и презиме, година и место рођења и датум одбране рада.

Ови лични подаци могу се објавити на мрежним страницама дигиталне библиотеке, у електронском каталогу и у публикацијама Универзитета у Београду.

У Београду, 09.06.2017.

Потпис докторанда

Катарина Букара

Прилог 3.

Изјава о коришћењу

Овлашћујем Универзитетску библиотеку „Светозар Марковић“ да у Дигитални репозиторијум Универзитета у Београду унесе моју докторску дисертацију под насловом:

Системи са контролисаним отпуштањем лекова засновани на мезопорозној силици и биоразградивим нанокомпозитима
(Controlled drug delivery systems based on mesoporous silica and biodegradable nanocomposites)

која је моје ауторско дело.

Дисертацију са свим прилозима предао/ла сам у електронском формату погодном за трајно архивирање.

Моју докторску дисертацију похрањену у Дигитални репозиторијум Универзитета у Београду могу да користе сви који поштују одредбе садржане у одабраном типу лиценце Креативне заједнице (Creative Commons) за коју сам се одлучио/ла.

1. Ауторство

2. Ауторство - некомерцијално

3. Ауторство – некомерцијално – без прераде

4. Ауторство – некомерцијално – делити под истим условима

5. Ауторство – без прераде

6. Ауторство – делити под истим условима

(Молимо да заокружите само једну од шест понуђених лиценци, кратак опис лиценци дат је на полеђини листа).

Потпис докторанда

У Београду, 09.06.2017.

Катарина Вуцић